Abrading the enigma of the wound healing process: Modeling the inflammation, proliferation, and maturation stage

by

AMANDA PATRICK

Presented to the Faculty of the Graduate School of
The University of Texas at Arlington in Partial Fulfillment
of the Requirements
for the Degree of

DOCTOR OF PHILOSOPHY

THE UNIVERSITY OF TEXAS AT ARLINGTON
August 2022

ACKNOWLEDGEMENTS

I would like to thank Dr. Chen-Charpentier who provided guidance and supported me throughout this research process. I would also like to thank Dr. Korzenowski for his guidance and contribution, and Dr. Roy for his role in my further studies in differential equations and continued support throughout my last processes at the university. I would also like to thank Dr. Kojouharov, Dr. Gornet, Dr. Atkosun, and Dr. Aambartsoumian who gave me opportunities to apply my skills and leadership. In addition, I would like to thank my fellow graduate students and some who are already graduated, who contributed with help and encouragement through this journey.

August 9, 2022

ABSTRACT

Abrading the enigma of the wound healing process: Modeling the inflammation, proliferation, and maturation stage

Amanda Patrick, Ph.D.

The University of Texas at Arlington, 2022

Supervising Professor: Dr. Chen-Charpentier

Wound healing encompasses a group of processes categorized into overlapping stages known as the inflammation, proliferation, and maturation/remodeling stage. The dynamics of these processes are important in studying outcomes of wound care and determining factors that contribute to certain wound outcomes. A system of ordinary differential equations is constructed for the inflammation, proliferation, and remodeling stage. Parameter sets for this model are investigated based on output dynamics according to the literature and based on experimental data. A bifurcation analysis is conducted to determine sudden changes that can occur in the inflammation system. Fourier Amplitude Sensitivity Test (FAST) is implemented to investigate sensitivity in regard to each mechanism considered. Next, the system is turned into a stochastic differential equation to analyze possible realizations that result from biological random fluctuations.

TABLE OF CONTENTS

CHAPTER 1

INTRODUCTION

A wound is a depletion of the integrity of living tissue in the body. The mechanisms in which the body repairs a wound are organized into the overlapping stages of wound healing, namely, homeostasis, inflammation, proliferation, and remodeling. Within minutes blood clots are formed and the bleeding stops. This is the first provisional matrix formed for the wound while the focus of the mechanisms implemented will be to remove pathogens and debris in the inflammation stage. The turnover of the provisional matrix proceeds in the proliferation and remodeling stages. Elucidating mechanisms in wound healing is of interest in improving wound care and determining causes of diseases.

Mathematical modeling provides a means to help provide framework and implement theories that may not be feasible to test under experimentation. Ordinary differential equation models are useful when studying dynamics over time in a nonspecific unit of space. Previous studies incorporated this methodology to study wound healing phenomena such as the recovery after a myocardial infarction [34], keloid and hypertorphic scarring [8], relationship between transforming growth factor β and tissue tension [53], and acute wound healing [50], just to name a few.

CHAPTER 2

LITERATURE REVIEW

2.1 Wound Healing

According to MedilinePlus by the United States National Library of Medicine, wounds are "injuries that break the skin or other body tissues" and can include "cuts, scrapes, scratches, and punctured skin." The formation of a wound involves a disruption in skin and tissue integrity. Where and how this integrity of the body composition and function is disrupted is what characterizes the type of wound and what can elucidate the overall pathology to be diagnosed. Some types of wounds include those caused by mechanical stress. Examples of these types of wounds are penetrating wounds, blaunt force trauma wounds (i.e., abrasions, lacerations, skin tears), closed wounds (i.e., contusions, mematoma), ecetera. Mechanisms that cause chronic wounds are another import type of wound to elucidate since these types of wounds can lead to amputation and death. Nussbaum et al. [55] points out that individuals who are at risk are elderly, disabled, or in general, individuals who cannot care from themselves and individuals with pre-existing skin or immunological conditions.

In addition to being involved in the before mentioned wounds, the wound healing process is involved in cardiovascular issues. For example, when blood does not circulate properly in the myocardium, oxygen is not able to be distributed to cells. Heart cells undergo necrosis and tissues die, hence the sequence of phenomena

that characterizes what is known as mycardium infarction (i.e., heart attack). This context of wound healing has been of interest due to this repair process leading to adverse after effects. The dynamics of this process have been studied by methods incorporating experimental data and differential equation modeling such as in [34].

The dynamical processes of wound healing is not just important for treating wounds but in addressing economical related conserns. Research by Nussbaum et al. [55] conducted a retrospective analysis of the cost of chronic wound care. Some prevalent wound types among Medicare beneficiaries were surgical infections, diabetic infections, traumatic wounds, skin disorders, and venous infections. Data from 2014 revealed that there was a high prevalence amount individuals who were 75 years or older, and total Medicare expenditure estimates reached between 3 billion and 96.8 billion dollars where surgical wounds were one of the most expensive.

2.1.1 Neutrophils

After the onset of the injury or wound, one of the first types of white blood cells to infiltrate the wound is the neutrophil. Neutrophils are a relatively abundant type of circulating leukocyte at the site of the wound but are short lived [6]; Bratton and Henson describe their lifespan to be in hours. Regardless if the wound is pathogen abundant or not, these cells will be recruited to the site of the wound via chemotactic factors. In the context of an infected wound, neutrophils will phagocyotize pathogens and will release substances such as reactive oxygen species (ROS) and antimicrobial peptides.

The main means of removal of neutrophils is by a another leukocyte known as the macrophage. After neutrophils reach the end of their lifecycle they commit cell programmed death. This is a process known as apoptosis. Hence, afterwords

they become apoptotic neutrophils. These apoptotic neutrophils can release signals called 'find-me' or 'eat-me' signals to influence this phagocytosis. In Bratton and Henson [6], the abundance of neutrophils is described to be be greater than the abundances of macrophages and apoptotic neutrophils, but after neutrophils peak, the transient dramatically go down. This contrasts with modeling research including those by Cooper et al. [9, 70] and Torres et al. [70], where in Cooper assumptions and simulations resulted in lower density of neutrophils. In Torres [70] experimental data and the optimized solution show an equal abundance with M1 macrophages and the decrease is not that dramatic when compared with the macrophages. In fact, if M1 macrophages and M2 macrophages were combined, they would be of greater abundance than the measured data of neutrophils corroborating the research by Cooper. As Bratton and Henson note, however, much of the dynamical evidence and phenomena have been observed either by *in vitro* studies or by experimental methods on mice which will have some extent of difference to the expected phenomena in human health. For studies involving mice vs humans see [25, 69, 73].

The mechanisms that effect the removal of apoptotic neutrophils are important as the removal of these neutrophils serve to decrease the debris and constituents released and exposed to the remaining healthy tissue. In addition, this phogocytosis by macrophages can effect the anti-inflammatory vs inflammatory properties of macrophages. As a result, some immunological issues can occur can be caused by an overabundance of neutrophils or a low rate of removal.

Dovi et al. [16] note that activated neutrophils release substances such as reactive oxygen species, cationic peptides, and proteases that help combat pathogens, but these substances also can degrade components of the extracellular matrix. It is also

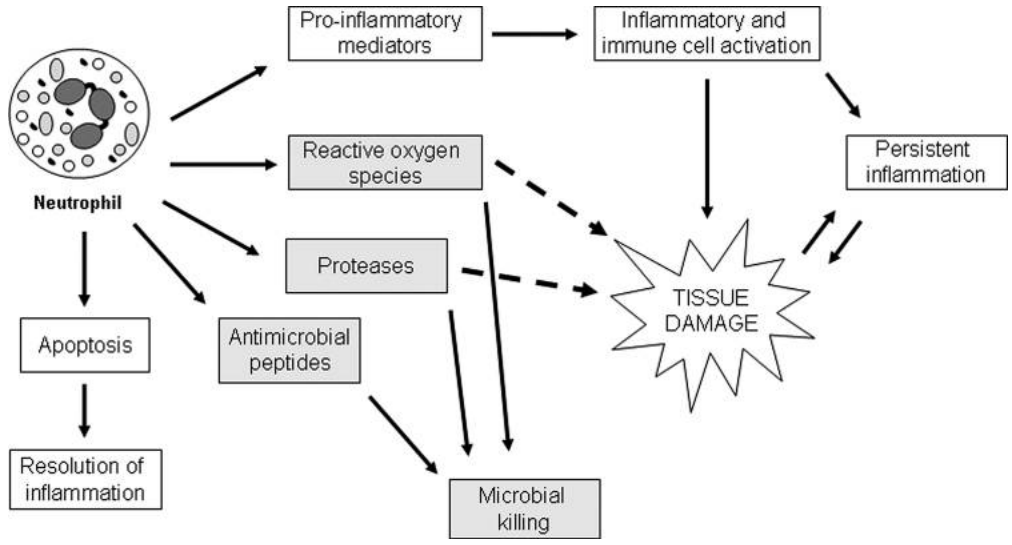

Figure 2.1: Neutrophil byproducts [75]

noted that neutrophils also have a high oxygen requirement to produce reactive oxygen intermediates.

2.1.2 Macrophages

Macrophages play a critical role in the wound healing process; they are involved in clearing debris and pathogens, as well as coordinating tissue repair. The roles of macrophages are complex in that there is a spectrum of different macrophage phenotypes, some in which contribute more to the inflammatory process and some contribute more the proliferation process [37, 48, 51, 52].

Classically activated and alternatively activated macrophages, also referred to as M1 macrophages, M2 macrophages, respectively, are classified according to their cell surface markers, function, and cytokine production. For example, M2 macrophages are primarily responsible for the production of a cytokine known as TGF-β. According to Krzyszczyk et al. [40], in mice, monocyte-derived macrophages begin to be systemically recruited in approximately 24 hrs and these monocytes differentiate in either M1 or

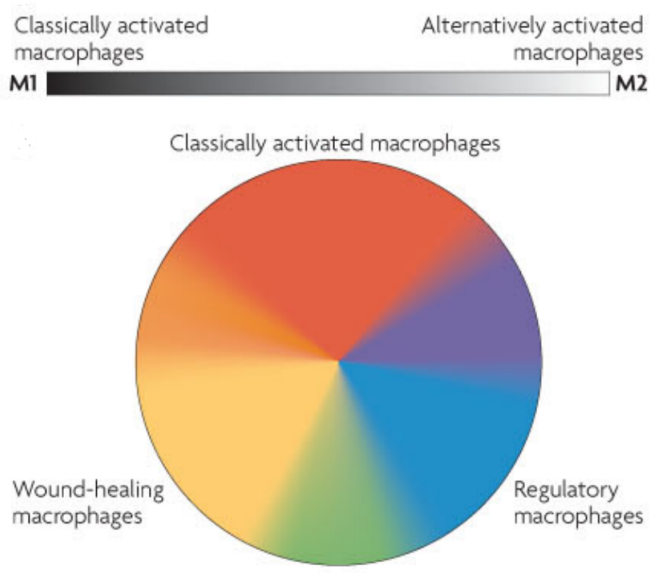

Figure 2.2: Polarization of Macrophages [51]

M2 macrophages. In particular, monocytes that differentiate to M1 macrophages are more abundant than those that differentiate to M2 macrophages.

2.1.3 Metalloproteinases and Tranforming Growth Factor-β

As white blood cells such as neutrophils, M1 macrophages, and M2 macrophages are present in the cell, they release proteases and cytokines that have an affect on the proliferation and remodeling stages of wound healing, two major substances being metalloproteinases (MMPs) and tranforming growth factor-β (TGF-β). MMPs are proteases which whose main function is to break down protiens. MMPs are modulated by tissue inhibitors of MMPs (TIMPs). They inhibit the activities of MMP [62]. TGF-β is a cytokine responsible to the chemoattraction of a major type of cell in the proliferation stage, fibroblasts. They are also associated with an increased production of TIMPS [47].

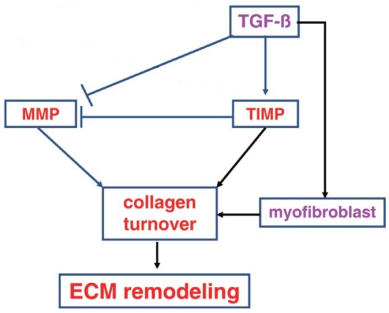

Figure 2.3: Dynamic between TIMPs, MMPs, and TGF-β [43]

2.1.4 Fibroblasts and Myofibroblasts

As M2 macrophages are present in the wound they release TGF-β which attract fibroblasts to the site of the wound. After these cells migrate to the cell they release more TGF-β and MMPs. Fibroblasts are able to differentiate to a more specialized cell known as myofibroblasts. The interaction of present fibroblasts and TGF-β can accelerate this differentiation. Fibrobasts and myofibrobasts affect one of the final productions of the the wound healing process which is the production of collagen.

2.1.5 Previous ODE Models

There are several types of models of healing. Ordinary differential equations models do not model change in space, but concentrate on change over time for a determined unit of space. Several models have been presented.

Reynolds et al. [61] focused on inflammation and anti-inflammation with their state variables being activated phagocytes, tissue damage, and anti-inflammatory mediators. Activated phagocytes are representative of inflammation and include neutrophils and macrophages. The anti-inflammatory variable is representative of mediators including cortisol and interleukin-10 (IL-10). Here subsystems based

on mass action kinetics are presented and the quasi-steady state assumption is implemented on the local response and resting phagocytes. Subsequent to model construction, different scenarios of pathogen growth rate and initial conditions are presented in scenarios where the wound is under circumstances that result in a healthy outcome, aseptic death, and septic death.

Cooper et al. [9] built a model expanding on Reynolds. The inflammation state variable replaced by more specialized inflammatory variables, neutrophils and macrophages. Estrogen and cortisol inhibition and enhancement factors are also implemented. A set of parameters that result in dynamical assumptions are simulated, the assumptions being that neutrophils peak between 0.75 and 2.75 days; the peak for macrophages is between 2.75 and 6.25 days; and that macrophage levels dropped below 0.1 by day 20.

For some of the state variables, the rates per cell units were adapted from Reynolds. More specifically, pathogen carrying capacity was chosen as 10^6 cells per unit space per unit time which, in order for the model to be well defined, sets P-units for the state variable P to be the same. The units for these cells are important when comparing results to experimental conditions, when combining results from different experiments, or when comparing parameters from different model experiments. For the Cooper study the purpose was to simulate general behavior, so units for some state variables such as debris were set to be arbitrary.

Torres et al. [70] utilizes these cell dynamics with experimental results. For pathogens, neutrophils, M1 and M2 macrophages, units are chosen to be 10^7 units. Note that the interaction mechanisms such as phagocytation and activation which has units pathogen units per inflammation cell units per time and cells per pathogen

units per time, respectively, will be affected by these chosen units. For example, the background immune defense parameter, k_{bp}, activation of local background immune response by pathogen, value would change when switching from 10^6 P-units to 10^7 P-units.

Some studies that modeled the proliferation and remodeling stage are Jin et al. [34] and Segal et al. [66]. Jin et al. incorporates macrophages, MMP-9, TGF-β, fibroblasts, and collagen to model the healing process after a myocardial infarction. They assume inhibition of MMP-9 by TGF-β due to the induced presence of TIMP-1. Subsequent to model formation they validate their model and parameter values by comparing model output to experimental data.

Segal et al. [66] constructs a model incorporating inflammation, pathogens, fibroblasts, and collagen. They include three types of fibroblasts (proliferating fibroblasts, migrating fibroblasts, and active fibroblasts). The collagen state variable is chosen to be a percentage where 0 represents the wound not being filled and 1 being the wound being filled. Values are allowed to go above 1 to account for scarring. They also include both inhibition of collagen deposition and degradation influenced by the current amount of collagen fibers formed. It is assumed the closer the wound is from being filled, the less need for fibroblasts which reduces amount of collagen being deposited. Moreover, they assume that inflammation cells can release enzymes that degrade collagen. To determine values for their parameters experimental data for collagen where scaled so that the highest values was a little above one. Subsequently, the resulting model was tested using low and high values of pathogen that resulted in high collagen deposition and low collagen disposition, respectively.

2.2 Modeling the Wound Healing Process

A system of ordinary differential equations is constructed to measure the dynamics over time between the different components in the inflammation, proliferative, and remodeling phase of the wound healing process. Main dynamics of previous ODE models are taken under consideration to form basic structures of the equations. Some mechanisms for pathogens, debris, neutrophils, and macrophages were adopted from Reynolds al. [9], Cooper et al. [2], and Torres et al. [11]. Some of the proliferative and remodeling mechanisms from Jin et al. [34] and Segal et al. [66] are accounted for. Certain mechanisms that effect and degradation terms where updated according to the literature (see Table 4.1).

2.2.1 Statement of Purpose

The purpose of this study is to construct a model of the wound healing system that incorporates dynamics from all three stages, incorporate of collagen turnover, and analyze this model in regard to parameter vs output dynamics.

CHAPTER 3

INFLAMMATION MODEL CONSTRUCTION

A system of ordinary differential equations was constructed to measure the dynamics over time between the different components in the inflammation, proliferative, and remodeling phase of the wound healing process. In this chapter, we concentrate on the inflammation stage. Growth terms for neutrophils and macrophages where constructed by using the quasi-steady state assumption with resting neutrophils and monocytes, respectively; the differentiation of neutrophils and monocytes are assumed to happen rapidly so that the rate of each of these can be assumed to be approximately zero. Some of the structures of the equations for pathogens, debris, neutrophils, and macrophages were adopted from Reynolds et al. [61], Cooper et al. [9], and Torres et al. [70].

3.1 Source Terms for Neutrophils and Macrophages

Let X_0 represent the predicesor cell and X_d represent the differentiated cell. Then the set of reactions is represented by the following

$$* \xrightarrow{s_x} X_0$$

$$X_0 \xrightarrow{R_x} X_d$$

$$X_d \xrightarrow{\mu_x} \quad .$$

These reactions have an associated set of differential equations. That is,

$$\frac{dX_0}{dt} = s_x - R_x X_0 - \mu_x X_0$$

$$\frac{dX_d}{dt} = R_x X_0.$$

If we assume quasi-steady state assumption then we get

$$\frac{dX_0}{dt} \approx 0$$

$$\implies X_0 \approx \frac{s_x}{R_x + \mu_x}$$

which gives us

$$\frac{dX_d}{dt} = R_x \frac{s_x}{R_x + \mu_x}.$$

which is comparable to the Michealis - Menten dynamics where if we let $R_x \longrightarrow \infty$ then $\frac{dX_d}{dt} \longrightarrow s_x$, the rate at which the predecessor cell enters the system, and if we let $R_x = 0$, $\frac{dX_d}{dt} = 0$.

3.2 Inflammatory Phase

3.2.1 Pathogens

Pathogens are assumed to proliferate logistically, where the growth rate is denoted by k_{pg} and the carrying capacity is denoted by p_∞. Upon initiation of the wound, the body utilizes a set of natural defenses even before phagocytes like

neutrophils and macrophages are introduced. These defenses will be categorized as the non-specific local immune response and include defensins and non-specific antibodies [56, 60, 61]. Hence, the next term will incorporate another term formed from quasi-steady state assumption on pathogens and the local non-specific immune response where s_b is the rate at which the non-specific response enter the system, k_{pb} is the destruction of pathogen per unit of non-specific response per time, μ_b is the intrinsic decay of the non-specific response, and k_{bp} is the activation of the non-specific response by pathogen. Incorporating these mechanisms, we get the following

$$\frac{dP}{dt} = k_{pg}P(1 - \frac{P}{p_\infty}) - \frac{k_{pb}s_bP}{\mu_m + k_{bp}P.} \tag{3.1}$$

As Reynolds et al. [61] pointed out, the solution P(t) = 0 model is asymptotically stable under the condition that

$$k_{pg} < \frac{k_{mp}s_m}{\mu_m}.$$

When this condition is not met, under certain corresponding initial conditions the end behavior of P(t) may tend toward some $P^* > 0$ which is indicative that the wound will remain infected if other mechanisms are not initiated. Hence, the following terms will incorporate the other means of defense against pathogens which are neutrophils and macrophages. Incorporating phagocytation by M1 macrophages, M2 macrophages, and neutrophils with the effect of estrogen we get

$$\frac{dP}{dt} = k_{pg}P(1 - \frac{P}{P_\infty}) - \frac{k_{pb}s_bP}{\mu_b + k_{bp}P} - k_{pn}PN(1 + k_{en}E) - k_{pm}P(M_1 + M_2)(1 + k_{em}E),$$

where k_{pn} and k_{pm} are the parameters associated with the rate that the pathogen and neutrophil and macrophage will interact and the act of phagocytation will occur, respectively. k_{en} and k_{em} are the amounts corresponding to how much per estrogen unit will enhance the phagocytation process.

3.2.2 Debris

Upon initiation of the wound, the consequence to the body introduced is the physical obstruction of tissue. These dead cells and possibly outside debris must also be removed. Moreover, during the inflammation process, the inflammatory mechanisms triggered are aimed at removing the pathogens and this can cause the introduction of more dead tissue and a release of cellular debris when apoptotic cells are not phagocytotized or removed from the area [6]. The equation for debris is as follows.

$$\frac{dP_t}{dt} = \mu_{an}A_N - k_{ptn}P_tN - k_{ptm1}P_tM_1 - k_{ptm2}P_tM_2 - \mu_{pt}P_t,$$

where $\mu_{an}A_N$ denotes debris introduced from unsuccessful efferocytosis; $k_{ptn}P_tN$, $k_{ptm1}P_tM_1$, and $k_{ptm2}P_tM_2$ denote the removal of debris via phagocytation by neutrophils, M1 macrophages, and M2 macrophages, respectively; and $\mu_{pt}P_t$ denotes the intrinsic/non specific removal of debris. In Cooper et al. [9] estrogen is assumed to promote phagocytization. Incorporting this enhancement to this model, it becomes

$$\frac{dP_t}{dt} = \mu_{an}A_N - k_{ptn}P_tN(1 + k_{en}E) - k_{ptm1}P_tM_1(1 + k_{em}E) - k_{ptm2}P_tM_2(1 + k_{em}E) - \mu_{pt}P_t.$$

3.2.3 Neutrophils

The first phagocytic cells introduced to the wound during the inflammation stage are neutrophils. Neutrophils phagocytize pathogens and debris and afterwards commit apoptosis. The equation for neutrophils is as follows:

$$\frac{dN}{dt} = R_N\frac{S_{nr}}{\mu_{nr} + R_N} - k_{an}N,$$

where R_N is the rate of activation of resting neutrophils; S_{nr} is the number of resting neutrophils that enter the system per unit time; μ_{nr} is the rate at which resting neutrophils exit the system; and $k_{an}N$ is the number of neutrophils that commit apoptosis per unit time. The rate at which resting neutrophils are activated is influenced by mechanisms triggered by existing neutrophils, macrophages, debris, pathogens, and apoptotic neutrophils. R_N is consequently

$$R_N = k_{npt}P_t + k_{np}P + k_{nan}A_N.$$

Adding the modulation effects of estrogen from Cooper et al. [9] the equation becomes

$$\frac{dN}{dt} = R_N\frac{S_{nr}}{\mu_{nr} + R_N}\frac{1}{(1 + \frac{E}{E_{ninf}})^2} - k_{an}N, \;\; R_N = k_{npt}P_t + k_{np}P + k_{nan}A_N.$$

3.2.4 Apoptotic Neutrophils

The state of neutrophils being in an apoptotic state can influence some critical parts of the wound healing process, namely, the continuation of the inflammation stage [21,39], the resolution of debris removal [14,21,38], and the polarization between M_1 macrophages and M_2 macrophages [3]. Neutrophils are assumed to commit apoptosis at a rate represented by the parameter k_{an}. After apoptosis, the apoptotic neutrophils can then be phagocytized by M1 macrophages and M2 macrophages which are represented by the mass action terms $k_{anm1}A_N M_1$ and $k_{anm2}A_N M_2$, respectively. Apoptotic neutrophils that are not removed by efferocytosis can then decay and leave the system. The proportion of those that release debris is represented by the term $d_{an}A_N$ and those that do not release debris is represented by the term $\mu_{an}A_N$. The apoptotic neutrophils equation is as follows:

$$\frac{dA_N}{dt} = k_{an}N - k_{anm1}A_N M_1 - k_{anm2}A_N M_2 - k_{ann}N - d_{an}A_N - \mu_{an}A_N,$$

Adding the effect of estrogen the equation becomes

$$\frac{dA_N}{dt} = k_{an}N - k_{anm1}A_N M_1(1+k_{em}E) - k_{anm2}A_N M_2(1+k_{em}E) - k_{ann}N(1+k_{en}E) - d_{an}A_N - \mu_{an}A_N.$$

3.2.5 M1 and M2 Macrophages

Macrophages have diverse functions in wound healing. There is spectrum of macrophage types. For our application, we will choose to categorize macrophages with more pro-inflammatory functions as M1 macrophages and macrophages with more anti-inflammatory functions as M2 macrophages. The equation for M1 macrophages is as follows:

$$\frac{dM_1}{dt} = R_{M1}\frac{s_{mr}}{\mu_{mr} + R_{M1} + R_{M2}} - k_{m1m2}A_N M_1 + k_{m2m1}M_2 - \mu_{m1}M_1$$

$$\frac{dM_2}{dt} = R_{M2}\frac{s_{mr}}{\mu_{mr} + R_{M1} + R_{M2}} + k_{m1m2}A_N M_1 - k_{m2m1}M_2 - \mu_{m2}M_2,$$

where R_{M1} and R_{M2} are the rate that monocytes differentiate into M1 macrophages and M2 macrophages, respectively; $k_{m1m2}A_N M_1$ is the amount of M1 macrophages that turn into M2 macrophages per unit time (a factor which has increased stimulation caused by efferocytosis); $k_{m2m1}M_2$ is the amount of M2 macrophages that turn into M1 macrophages per unit time; and μ_{m1} and μ_{m2} are the proportion of M1 macrophages and M2 macrophages that leave the wound site per unit time, respectively. The rate at which monocytes differentiate into M1 Macrophages is effected by the debris, pathogens, other M1 macrophage, and apoptotic neutrophils [9, 70]. With the inhibition effect of estrogen the rate is

$$R_{M1} = k_{mpt}P_t + k_{m1p}P + k_{m1n}N + \frac{k_{m1m1}M_1}{1 + (\frac{E}{E_{M\infty}})^2} + k_{m1an}A_N.$$

And the rate at which monocytes differentiate into M2 macrophages is assumed to be affected by other M2 macrophages and a background source k_c. So we have

$$R_{M2} = k_{m2m2}M_2 + k_c.$$

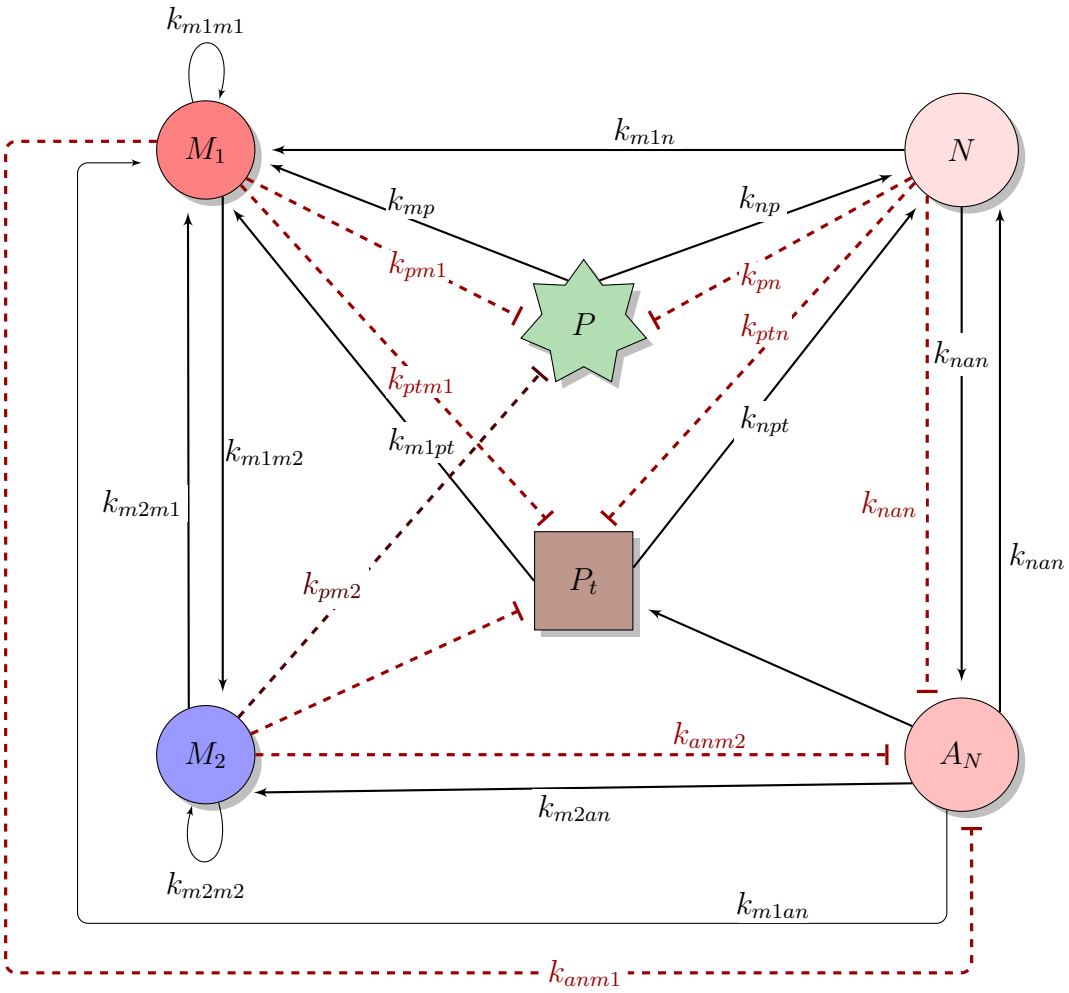

Figure 3.1: Inflammation Model Schematic. Dynamics of inflammatory system and parameters involved in each corresponding transition where arrows, $\rightarrow$, indicate upregulation, and bars, $\dashv$, indicate inhibition. Phenomena involved with upregulation include release of substance that promotes differentiation of a predecessor or proliferation of the state variable, release of substance that adds to the state variable, or the starting state variable becoming the following state variable. The phenomenon involved with inhibition is phagocytosis.

CHAPTER 4

INFLAMMATION MODEL ANALYSES AND RESULTS

4.0.1 Final Inflammation Model

The full inflammation model is given by the following where definitions and units for each parameter is given in Table 4.1, and a schematic of the relationship between each state variable is provided in Figure 3.1.

$$
\begin{aligned}
\frac{dP}{dt} &= k_{pg}P(1-\frac{P}{P_\infty}) - \frac{k_{pb}s_bP}{\mu_b + k_{bp}P} - k_{pn}PN(1+k_{en}E) - k_{pm}P(M_1+M_2)(1+k_{em}E) \\
\frac{dP_t}{dt} &= \mu_{an}A_N - k_{ptn}P_tN(1+k_{en}E) - k_{ptm1}P_tM_1(1+k_{em}E) \\
&\quad - k_{ptm2}P_tM_2(1+k_{em}E) - \mu_{pt}P_t \\
\frac{dA_N}{dt} &= k_{an}N - k_{anm1}A_NM_1(1+k_{em}E) - k_{anm2}A_NM_2(1+k_{em}E) - k_{ann}N(1+k_{en}E) \\
&\quad - d_{an}A_N - \mu_{an}A_N \\
\frac{dN}{dt} &= R_N\frac{S_{nr}}{\mu_{nr}+R_N}\frac{1}{(1+\frac{E}{E_{ninf}})^2} - k_{an}N, \;\; R_N = k_{npt}P_t + k_{np}P + k_{nan}A_N \\
\frac{dM_1}{dt} &= R_{M1}\frac{s_{mr}}{\mu_{mr}+R_{M1}+R_{M2}} - k_{m1m2}A_NM_1 + k_{m2m1}M_2 - \mu_{m1}M_1, \\
&\quad R_{M1} = k_{mpt}P_t + k_{m1p}P + k_{m1n}N + \frac{k_{m1m1}M_1}{1+(\frac{E}{E_{M\infty}})^2} + k_{m1an}A_N \\
\frac{dM_2}{dt} &= R_{M2}\frac{s_{mr}}{\mu_{mr}+R_{M1}+R_{M2}} + k_{m1m2}A_NM_1 - k_{m2m1}M_2 - \mu_{m2}M_2, \\
&\quad R_{M2} = k_{m2m2}M_2 + k_c.
\end{aligned}
\tag{4.1}
$$

4.0.2 Parameters

Parameter bounds were estimated based on the literature. These bounds were used to find an estimate that resulted in an output that met overall conditions based on the literature. And another method of finding parameters based on experimental data was implemented. The first method was based on the following assumptions:

1. Neutrophils peak around day 1 day post injury (dpi)
2. M1 macrophages peak between 2 - 3 dpi
3. M2 macrophages peak at least 1 dpi after M1 macrophages peak and once M2 macrophages peak they are the dominant macrophages present.

Initial conditions where assumed to be $P_0 = 1$ and $Pt_0 = 2$. which has a higher starting pathogen densisity then in in Cooper et al. [9] to simulate a wound with more pathogenic insult. A working set was found based on the parameter constraints in Table 4.1. The found parameter values are under "Estimation based on general dynamics". The simulations with varying initial conditions are shown in Figure 4.3 with the initial conditions defined in Figure 4.1.

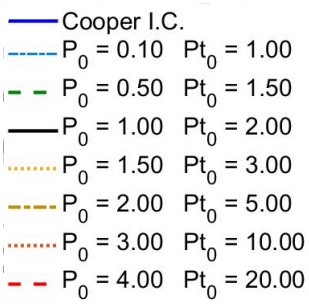

Figure 4.1: Initial conditions for general simulation results

For the method utilizing data, parameters were found that minimized the output from experimental data (Torres et al., [70]). In Torres, the experiment captures wound dynamics under the conditions that there is pathogen, but minimal debris. Pathogen starts small, but due to increase in carrying capacity the pathogen density increases causing the onset of the inflammation process. For the initial conditions we assume $P_t = 0.001$ and let P_0 be an optimization argument. Due to the nature of the experiment, another state variable B for broth was included. To account how the broth affects the carrying capacity, another parameter $k_{kbp\infty}$ was included. The inflammation dynamic from this experiment is modeled by system 4.1 with a modification on the logistic growth term for pathogens and with the inclusion of a new equation for broth which is the following:

$$\frac{dB}{dt} = -k_{bp}BP.$$

The pathogen equation was modified to the following:

$$\frac{dP}{dt} = k_{pg}P(1-\frac{P}{P_\infty + k_{kbp\infty}B})-\frac{k_{pb}s_bP}{\mu_b + k_{bp}P}-k_{pn}PN(1+k_{en}E)-k_{pm}P(M_1+M_2)(1+k_{em}E).$$

The fmincon MATLAB function was used to fit the solution to the data using the following equation weighted least squares function:

$$\min_p \sum_{i=1}^{n}(\frac{y_i - y(t_i, p_i)}{\sigma_i})^2. \tag{4.2}$$

Table 4.1: Parameter Descriptions. Chosen units for P, M, N and A_N are 10^7 cells

Pathogen Equation						
Parameter	Description	Range / Conditions for optimization	Estimation based on general dynamics	Estimation based on data	Unit	Reference / Reasoning
k_{pg}	Growth rate of pathogen		14.4	34.99	$\frac{1}{day}$	Depends on pathogen; chosen value
p_∞	Carrying capacity of pathogen		2	0.00450	$P\text{-}units$	Depends on pathogen and environment; chosen value
k_{pb}	Destruction of pathogen by local background response	$10 \leq k_{pb} \leq 20$	19.945	15	$\frac{\frac{1}{M-units}}{day}$	Range chosen around value from [61]
s_b	Source of background local response	$0.01 \leq s_b \leq 0.2$	0.141	0.0722	$\frac{M-units}{day}$	Range chosen around value from [61].
μ_b	Intrinsic decay of local response	$0.03 \leq \mu_b \leq 0.06$	0.052	0.0243	$\frac{1}{day}$	Range chosen around value from [61]. Note this was based on reported half-lives of non-specific antibodies such as immunoglobulins G and A; original references [33, 83]
k_{bp}	Activation of local background immune response by pathogen	$1.5 \leq k_{bp} \leq 2.5$	2.0	2.030	$\frac{\frac{1}{days}}{P-units}$	Range chosen around one from [61]. Units were updated from $P-units = 10^6 Pcells$ to $P-units = 10^7 Pcells$.
k_{pn}	Destruction of pathogen by neutrophils	$0 \leq k_{pn} \leq 100$	0.00128	0.00594	$\frac{\frac{1}{N-units}}{day}$	
k_{en}	Estrogen increase in the phagocytic abilities of neutrophils	$0 \leq k_{en} \leq 8.11$	0.347	4.915	$\frac{1}{E-units}$	Value was set to be no more than the mean +std of the working values found in Cooper [9]
k_{pm}	Destruction of pathogen by macrophages	$0 \leq k_{pm} \leq 100$	7.519	1.668	$\frac{\frac{1}{M-units}}{day}$	
k_{em}	Estrogen increase in the phagocytic abilities of macrophages	$0 \leq k_{em} \leq 7.87$	3.867	2.665	$\frac{1}{E-units}$	Value was set to be no more than the mean + std. of the working values found in Cooper [9]

Debri and Apoptotic Neutrophil Equations						
Parameter	Description	Range / Conditions for optimization	Estimation based on general dynamics	Estimation based on data	Unit	Reference / Reasoning
d_{an}	Debris released by apoptotic neutrophils	$0 \leq \mu_{an} \leq 100$	4.382	3.989	$\frac{1}{day}$	
k_{ptn}	Destruction of debris by neutrophils	$0 \leq k_{ptn} \leq 100$	0.048	8.624	$\frac{1}{\frac{N-units}{day}}$	
k_{ptm1}	Destruction of debris by M1 macrophages	$0 \leq k_{ptm1} \leq 100$ 6.531 $k_{ptm2} \geq k_{ptm1}$	0.191	13.214	$\frac{1}{\frac{M-units}{day}}$	
k_{ptm2}	Destruction of debris by M2 macrophages	$0 \leq k_{ptm2} \leq 100$	6.643	18.430	$\frac{1}{\frac{M-units}{day}}$	
μ_{pt}	Intrinsic decay of debris	$0.0019 \leq \mu_{pt} \leq 1.04$	11.187	1.002	$\frac{1}{day}$	Half-life of debris is assumed to be no shorter than 16 hrs. and no longer than 365 days which is a more generous assumption than the 33.27 hrs. assumed in Cooper [9]
k_{an}	Apoptosis rate of neutrophils	$1.0397 \leq k_{an} \leq 11.09$ $k_{an} > \mu_{m1}, \mu_{m2}$ $k_{an} \leq \mu_{nr}$	0.712	1.252	$\frac{1}{day}$	Half-lives of neutrophils are between 1.5 and 16 hrs. [58, 77] and are shorter than the half-lives of M1 and M2 macrophages; half-lives of resting neutrophils are shorter than the half-lives of neutrophils
k_{anm1}	Destruction of apoptotic neutrophils by M1 macrophages	$0 \leq k_{anm1} \leq 100$ $k_{anm1} \leq k_{anm2}$	15.409	10.507	$\frac{1}{\frac{M-units}{day}}$	Alternative macrophages are more effecient at efferocytosis [6]
k_{anm2}	Destruction of apoptotic neutrophils by M2 macrophages	$0 \leq k_{anm2} \leq 100$	51.403	51.192	$\frac{1}{\frac{M-units}{day}}$	
k_{ann}	Destruction of apoptotic neutrophils by neutrophils	$0 \leq k_{ann} \leq 100$	15.877	14.759	$\frac{1}{\frac{N-units}{day}}$	
u_{an}	Secondary necrosis of apoptotic neutrophils	$0 \leq u_{an} \leq 100$	3.623	8.978	$\frac{1}{day}$	

Neutrophil Equation						
Parameter	Specific Description	Range for optimization / Conditions	Estimation based on general dynamics	Estimation based on data	Unit	Reference / Reasoning
s_{nr}	Source of resting neutrophils	$s_{nr} > s_{mr}$	0.205	3.0474	$\frac{N-units}{day}$	
k_{npt}	Activation of neutrophils by debris	$0 \leq k \leq 100$	74.954	0.0211	$\frac{1}{\frac{M-units}{day}}$	
k_{np}	Activation of neutrophils by pathogens	$0 \leq k \leq 100$	1.027	14.910	$\frac{1}{\frac{P-units}{day}}$	
k_{nan}	Activation of neutrophils by apoptotic neutrophils	$0 \leq k_{nan} \leq 100$	27.378	9.0955	$\frac{1}{\frac{A_N-units}{day}}$	
μ_{nr}	Decay rate of resting neutrophils	$1.0397 \leq \mu_{nr} \leq 33.271$	12.976	1.406	$\frac{1}{day}$	Resting neutrophils are assumed to have shorter half-lives than activated neutrophils resting neutrophils, but lower bound on the half life is assumed to be no smaller than 0.5 hrs.
$E_{n\infty}$	Estrogen's effect on the inhibition of neutrophil production	$5.01 \leq E_{n\infty} \leq 100$	6.838	7.716	$E\text{-}units$	Value assumed to be no less than the mean - std. in Cooper [9]

Macrophage Equations						
Parameter	Specific Description	Range / Conditions for optimization	Estimation based on general dynamics	Estimation based on data	Unit	Reference / Reasoning
s_{mr}	Source of resting fixed tissue monocytes	$s_{mr} > s_{nr}$	0.2025		$\frac{M-units}{day}$	
k_{mpt}	Activation of M1 macrophages by debris	$0 \leq k_{mpt} \leq 100$	28.033	3.0409	$\frac{\frac{1}{P_t-units}}{day}$	
k_{m1p}	Activation of M1 macrophages by pathogens	$0 \leq k_{m1p} \leq 100$	99.123	44.947	$\frac{\frac{1}{P-units}}{day}$	
k_{m1n}	Activation of M1 macrophages by neutrophil byproducts	$0 \leq k_{m1n} \leq 100$	0.007	0.00121	$\frac{\frac{1}{N-units}}{day}$	
k_{m1m1}	Activation of M1 macrophages by their associated cytokines	$0 \leq k_{m1m1} \leq 100$	0.0775	0.00150	$\frac{\frac{1}{M-units}}{day}$	
k_{m1an}	Activation of M1 macrophages by apoptotic neutrophils	$0 \leq k_{m1an} \leq 100$	1.803	0.00364	$\frac{\frac{1}{A_N-units}}{day}$	
$E_{m\infty}$	Estrogen's effect on the inhibition of M1 macrophage production by other M1 macrophages	$2.06 \leq E_{m\infty} \leq 100$	8.742	6.113	$E\text{-}units$	Value chosen to be no less than the mean - std. from the values in Cooper [9]
μ_{mr}	Decay rate of resting tissue monocytes	$\mu_{mr} > \mu_{m1}, \mu_{m2}$	12.975	1.261	$\frac{M-units}{day}$	
k_{m2m2}	Activation of M2 macrophages by their associated cytokines	$0 \leq k_{m2m2} \leq 100$	0.00151	0.00160	$\frac{\frac{1}{M-units}}{day}$	
k_c		$0 \leq k_c \leq 1$	0.025	0.993	0.00111	
k_{m1anm2}	Transition of M1 macrophages to M2 macrophages affected by phagocytosis of apoptotic neutrophils	$0 \leq k_{m1anm2} \leq 100$	2.1	0.0505	3.969	
k_{m1m2}	Transition of M1 macrophages to M2 macrophages	$0 \leq k_{m1m2} \leq 100$	1.146	14.993	$\frac{\frac{1}{A_N-units}}{day}$	
k_{m2m1}	Transition of M2 macrophages to M1 macrophages	$0 \leq k_{m2m1} \leq 100$	0.117	0.183	$\frac{M-units}{day}$	
μ_{m1}	Decay rate of M1 macrophages	$0 \leq \mu_{m1} \leq 11.09$	0.602	1.245	$\frac{M-units}{day}$	Half-lives of M1 macrophages are assumed to be greater than 1.5 hrs.
μ_{m2}	Decay rate of M2 macrophages	$0 \leq \mu_{m2} \leq 11.09$	0.612	1.244	$\frac{M-units}{day}$	Half-lives of M2 macrophages are assumed to be greater than 1.5 hrs.

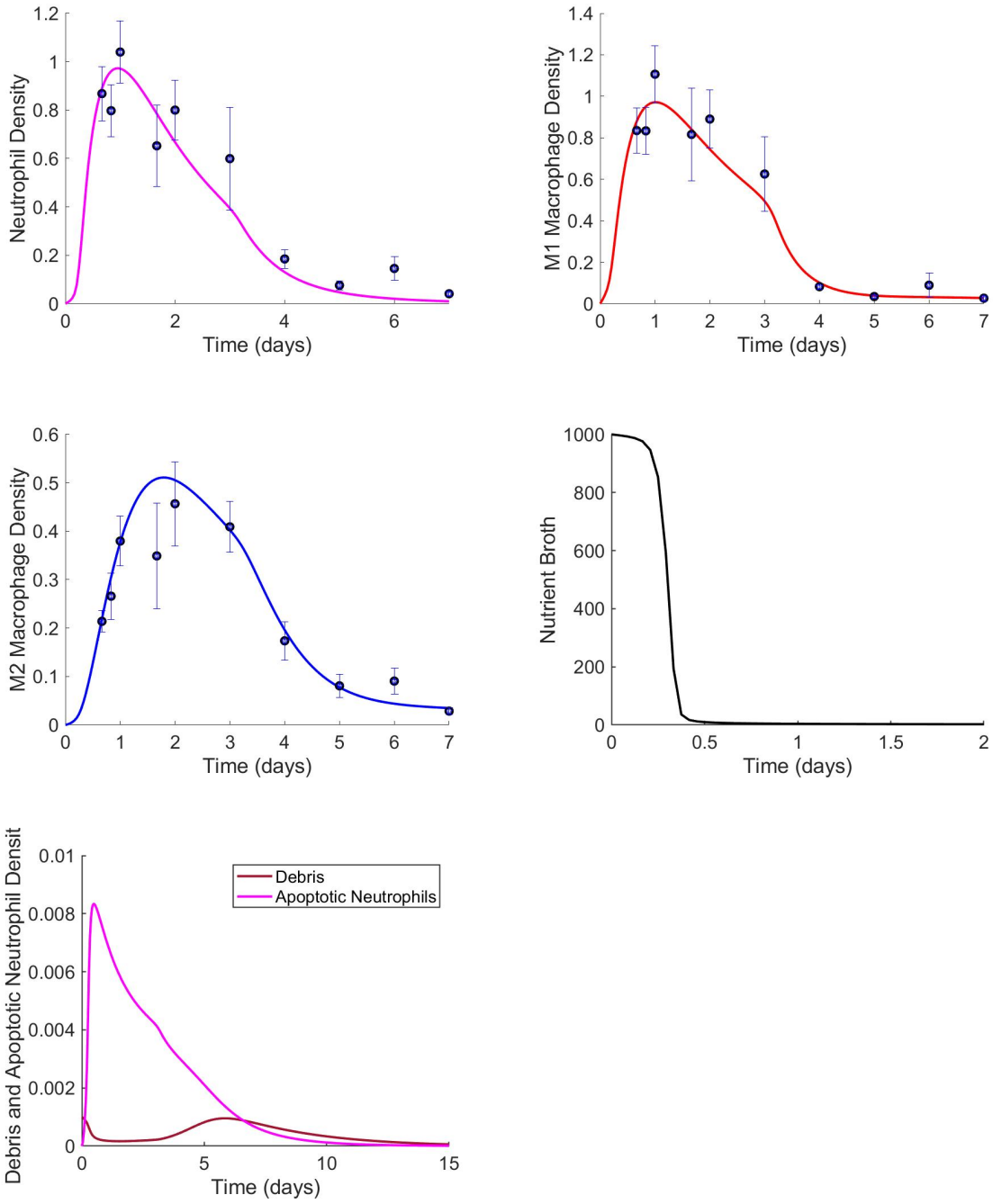

Figure 4.2: Output of resulting parameter set optimized from experimental data

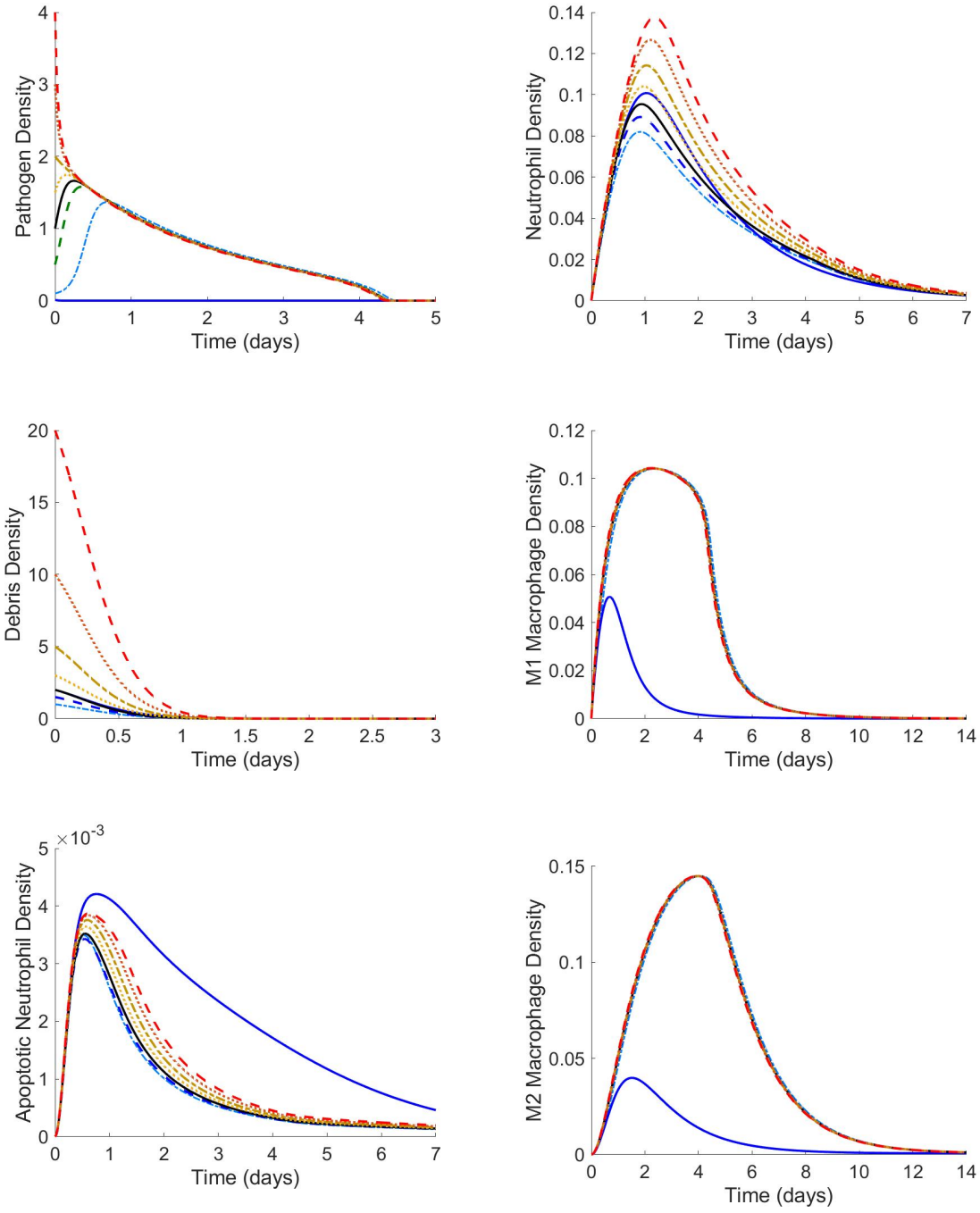

Figure 4.3: Transients resulting from assumptions based on literature with varying initial conditions

4.0.3 Bifurcation Analysis Pathogen Growth and Carrying Capacity

To analyze the model behavior in regard to the parameters, a bifurcation analysis was conducted in XPPAUTO. The following are analyses conducted for pathogen growth and carrying capacity.

Bifurcation analysis was conducted with respect to kpg, the growth rate of the pathogen. XPPAUTO indicated bifurcation points in three main locations: between 15 and 16, at 54.956, and a Hopf bifurcation at 15.446 (Table 4.2). The AUTO program was subsequently ran from the periodic solutions from the Hopf points, which resulted in unstable solutions shown by the blue circles (Figure 4.4). Different kpg values where tested around the bifurcation points (Figure 4.5). For high enough pathogen and debris initial conditions, kpg = 20 and kpg = 80 resulted in an unhealthy outcome indicated by the high end behavior for M1 and M2 macrophages. An example simulation of when kpg = 15.446 is provided in Figure 4.6 where the behavior oscillates.

Table 4.2: XPPAUTO Results for varying Growth Rate of Pathogens, kpg

TY	kpg	P^*	Pt^*	AN^*	N^*	$M1^*$	$M2^*$
BP	15.111	0.2671	0.00	0.00	0.00	0.0015	0.0221
BP	15.521	0.5913	0.00	0.001	0.0100	0.1007	0.1568
BP	15.526	0.6611	0.00	0.0002	0.0105	0.1016	0.1569
LP	15.526	0.6623	0.00	0.0002	0.0105	0.1016	0.1568
HB	15.446	0.3614	0.00	0.0001	0.0079	0.0935	0.1527
BP	54.956	0.00	0.00	0.00	0.00	0.0015	0.0221

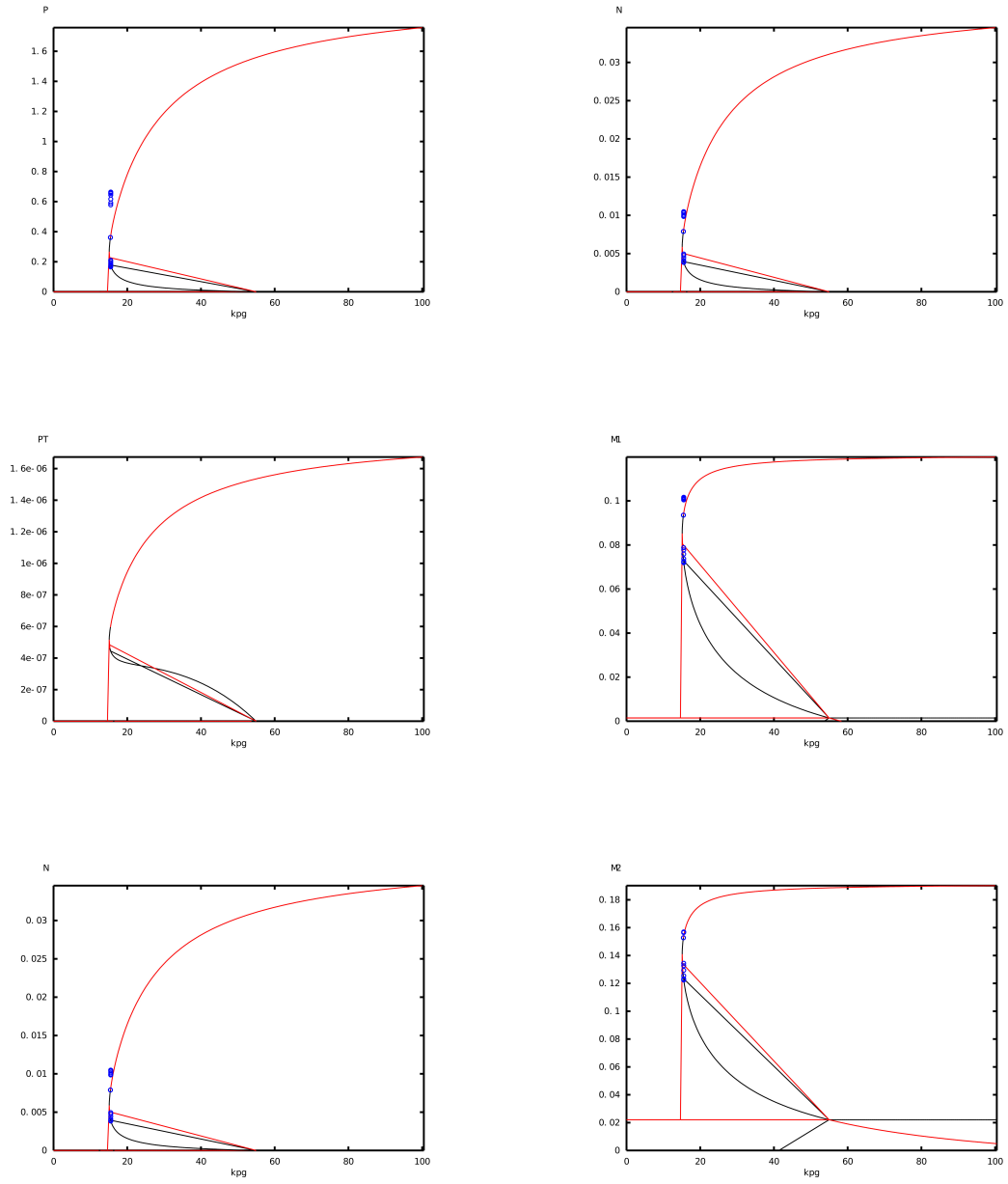

Figure 4.4: Bifurcation Diagrams with varying kpg (Pathogen Growth Rate). Red lines indicated stable steady states. Black indicates unstable steady states. Blue circles represent unstable periodic solutions.

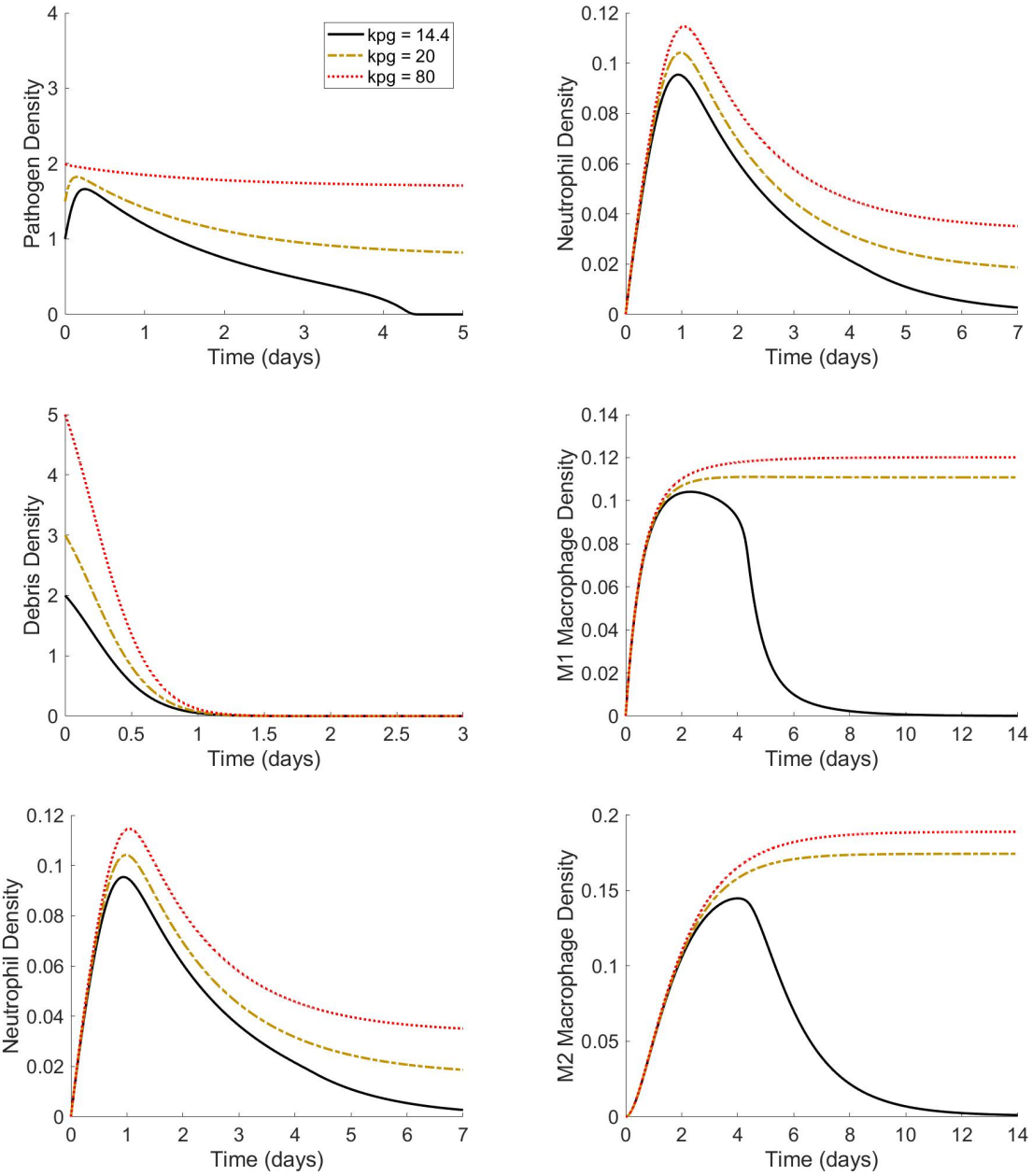

Figure 4.5: Simulations with varying kpg (pathogen growth rate)

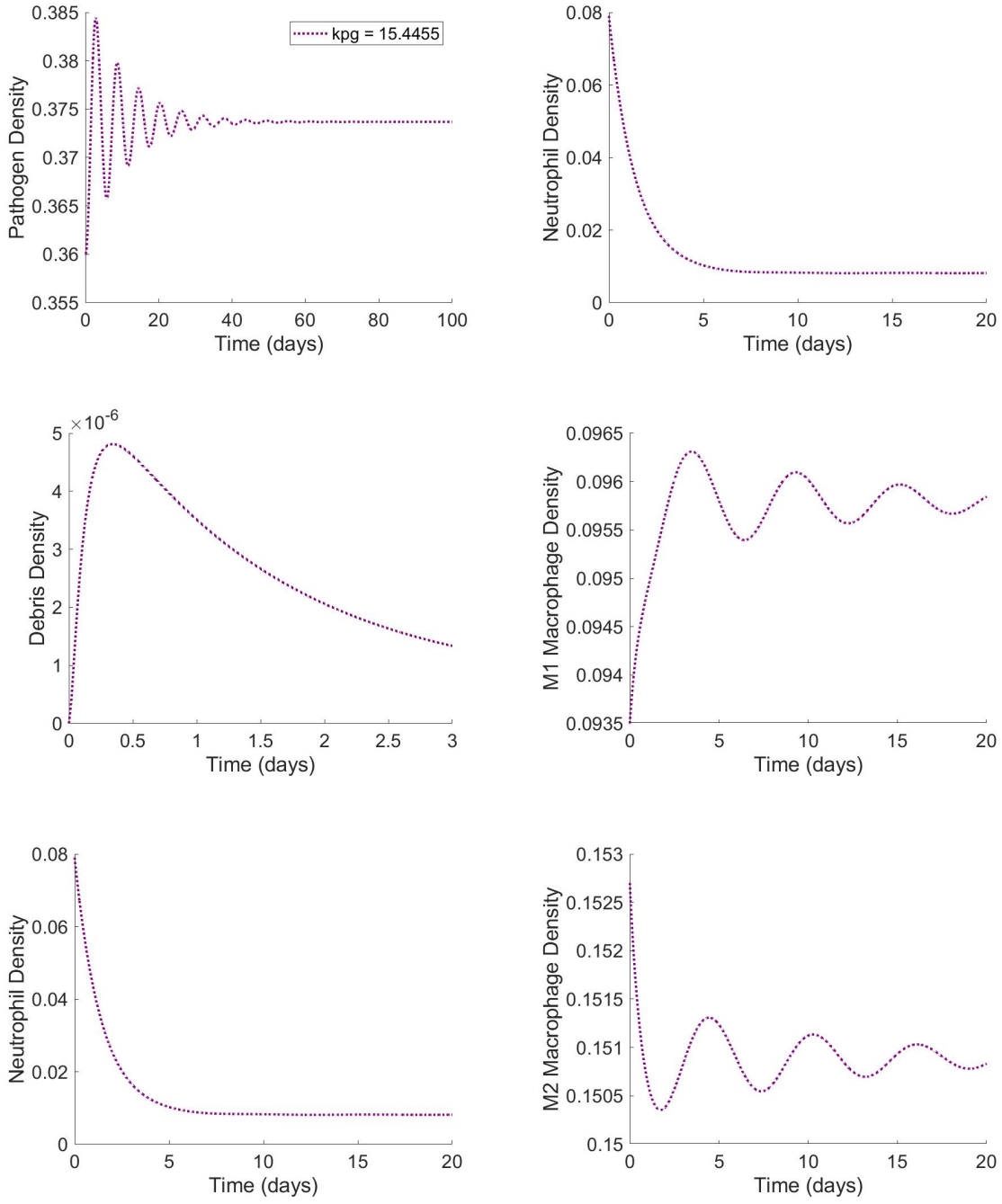

Figure 4.6: Example simulation with kpg (pathogen growth rate) at the Hopf bifurcation point

For kpb, the source of background local response, there where two bifurcation points found: a Hopf bifurcation at kpb = 16.215 and at kpb = 17.57 (Table 4.3). Bifurcation digrams in Figure 4.3 show that for low values of kpb the steady state is relatively high for all state variables and this is further elucidated in Figure 4.7 where the transient end behaviors are high. Figure 4.9 shows an example of oscillatory behavior when kpb = 16.215.

Table 4.3: XPPAUTO results for destruction of pathogen by local background response, kpb

TY	kpb	P*	Pt*	AN*	N*	M1*	M2*
BP	4.992	0.00	0.00	0.00	0.00	0.0015	0.0221
HB	16.215	0.3303	0.00	0.0001	0.0072	0.0911	0.1493
BP	17.57	0.2384	0.00	0.0001	0.0053	0.0819	0.1362

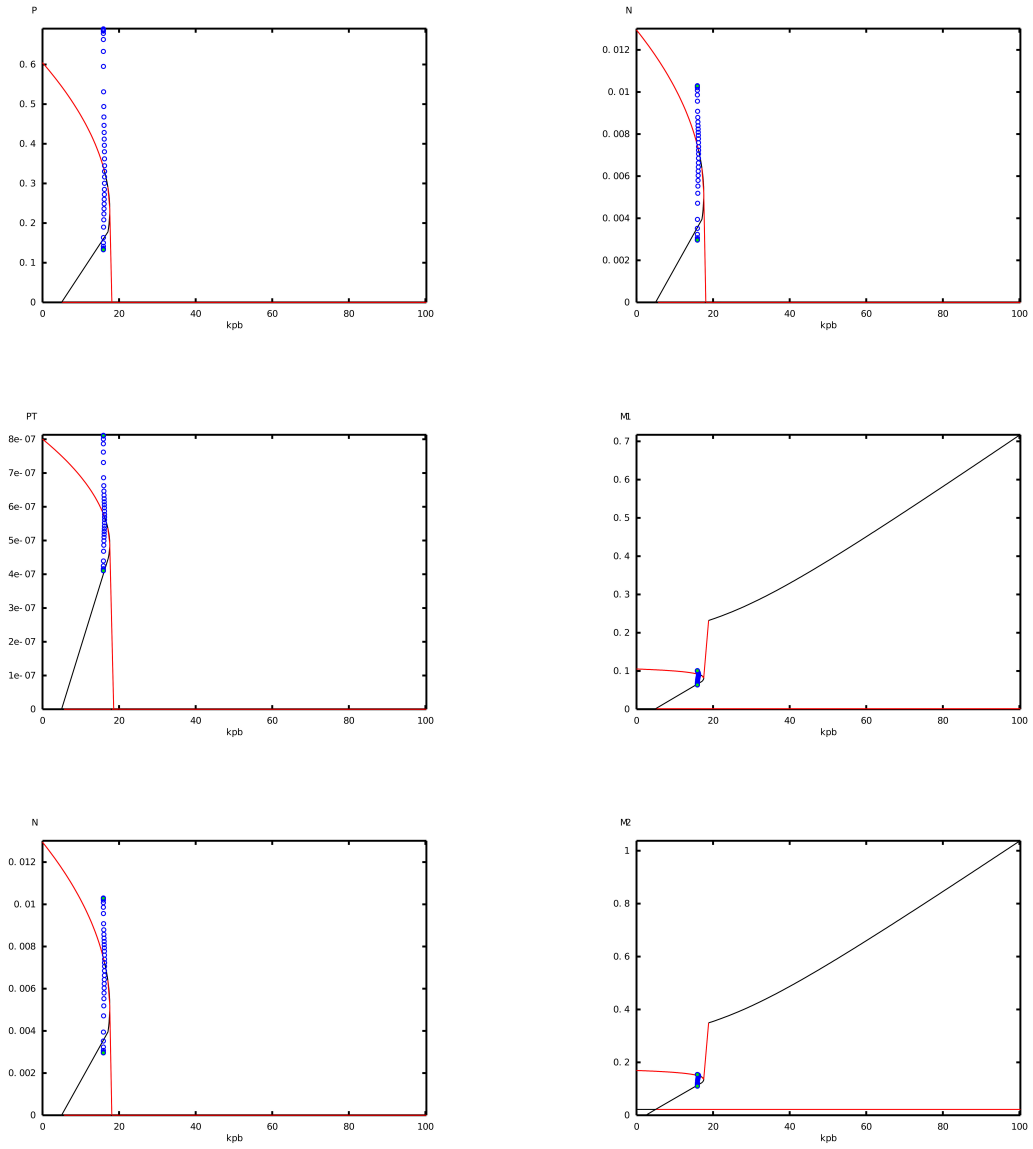

Figure 4.7: Bifurcation diagrams with varying kpb (destruction of pathogen by local background response)

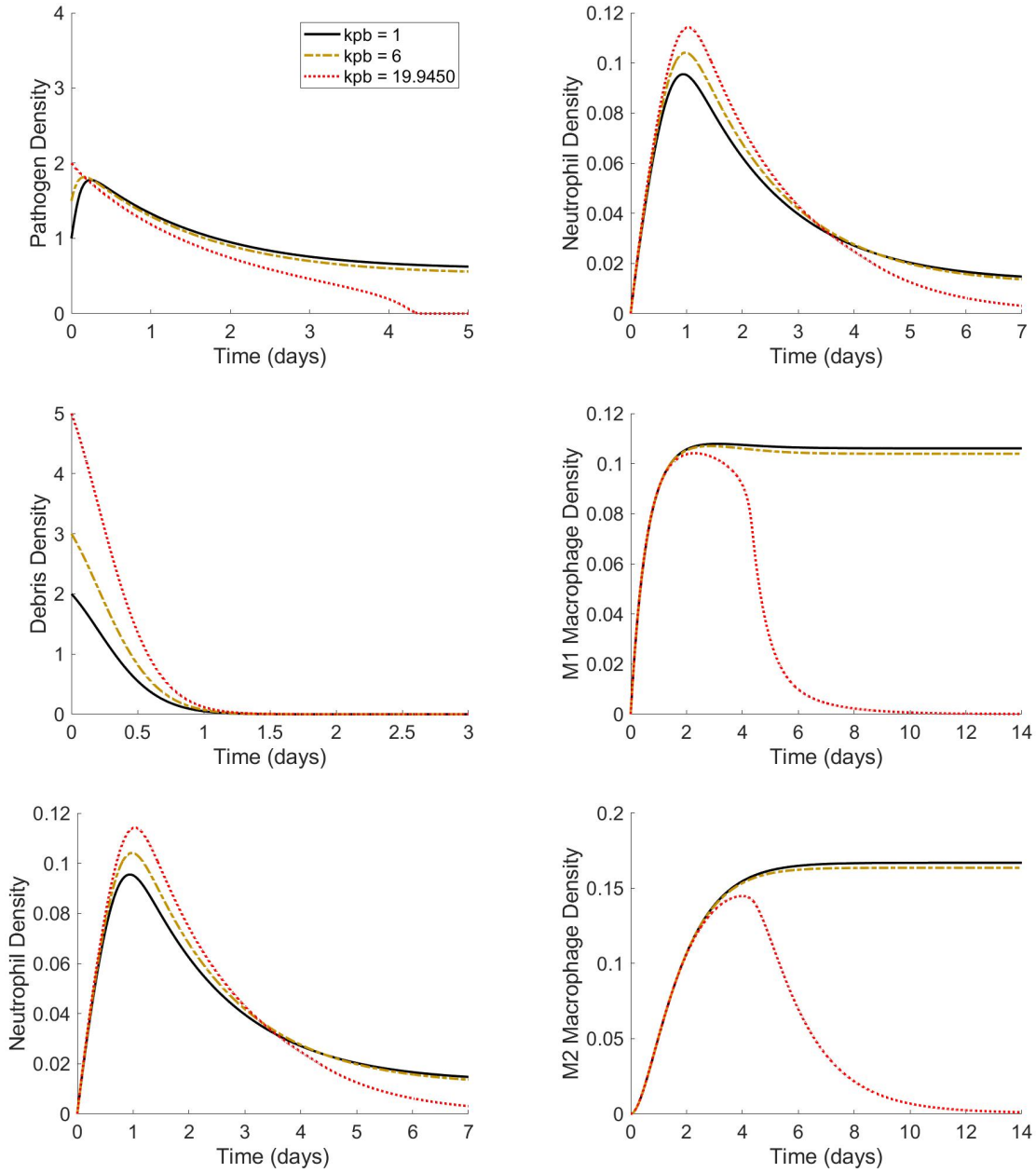

Figure 4.8: Simulations with varying kpb (destruction of pathogen by local background response)

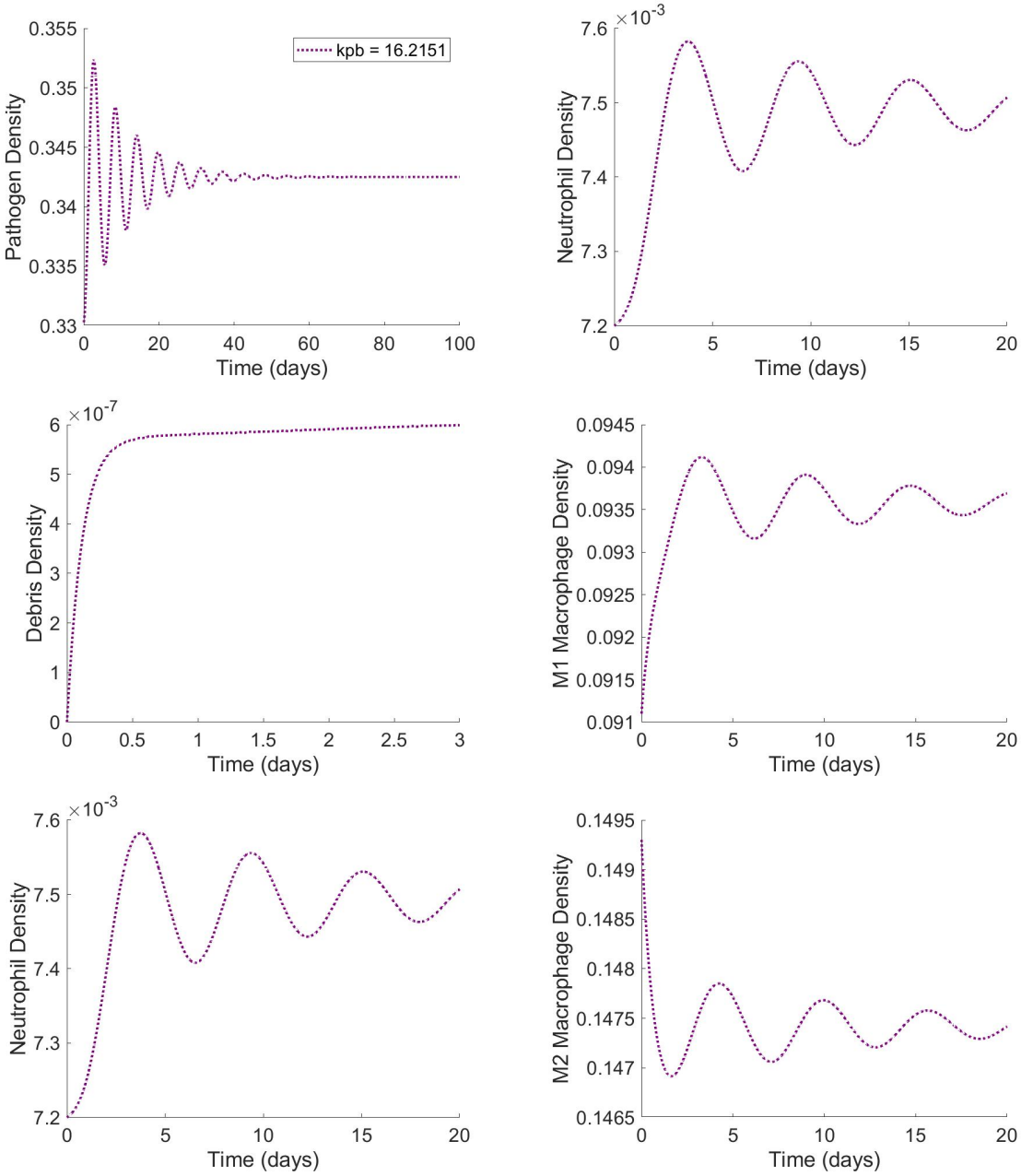

Figure 4.9: Example simulation with kpb (destruction of pathogen by local background response) at the Hopf bifurcation point

For ub, the intrinsic decay of local response, there where two bifurcation points found: at ub = 0.2085 and at a Hopf bifurcation ub = 0.1748 (Table 4.4). As ub

increases the steady state of each variable steadily increases but after a high enough value this steady state does not change much (Figure 4.4). Figure 4.11 shows the different transient end behavior for different values around the bifurcation point, and Figure 4.12 shows oscillatory behavior in apoptotic neutrophils.

Table 4.4: XPPAUTO results for varying intrinsic decay of local response, ub

TY	ub	P^*	Pt^*	AN^*	N^*	$M1^*$	$M2^*$
BP	0.2085	0.0000	0.00	0.00	0.00	0.0015	0.0221
LP	0.1178	0.2016	0.00	0.0001	0.0045	0.0768	0.1290
HB	0.1748	0.3046	0.00	0.0001	0.0067	0.0889	0.1462

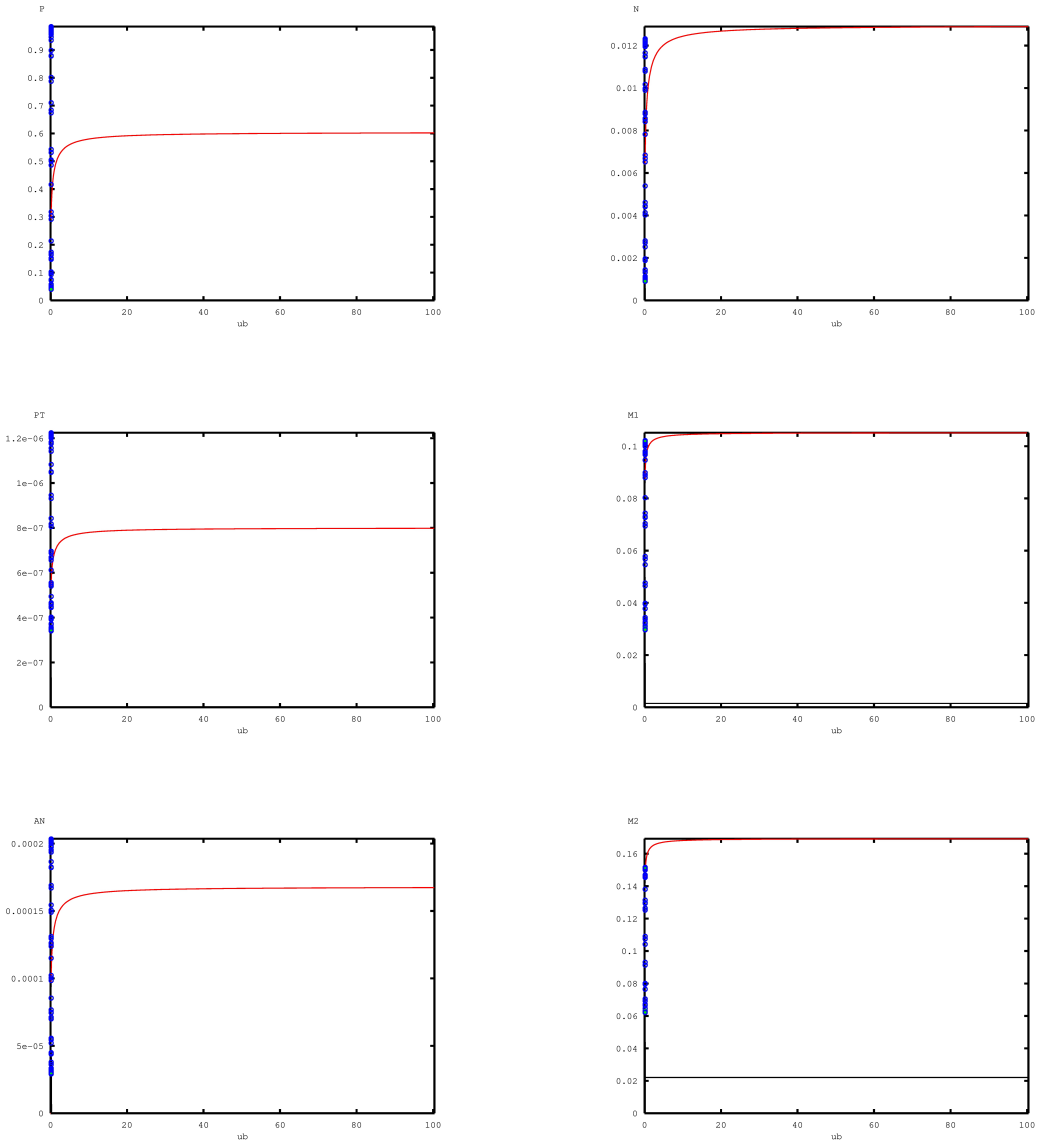

Figure 4.10: Bifurcation diagrams with varying ub (intrinsic decay of local response)

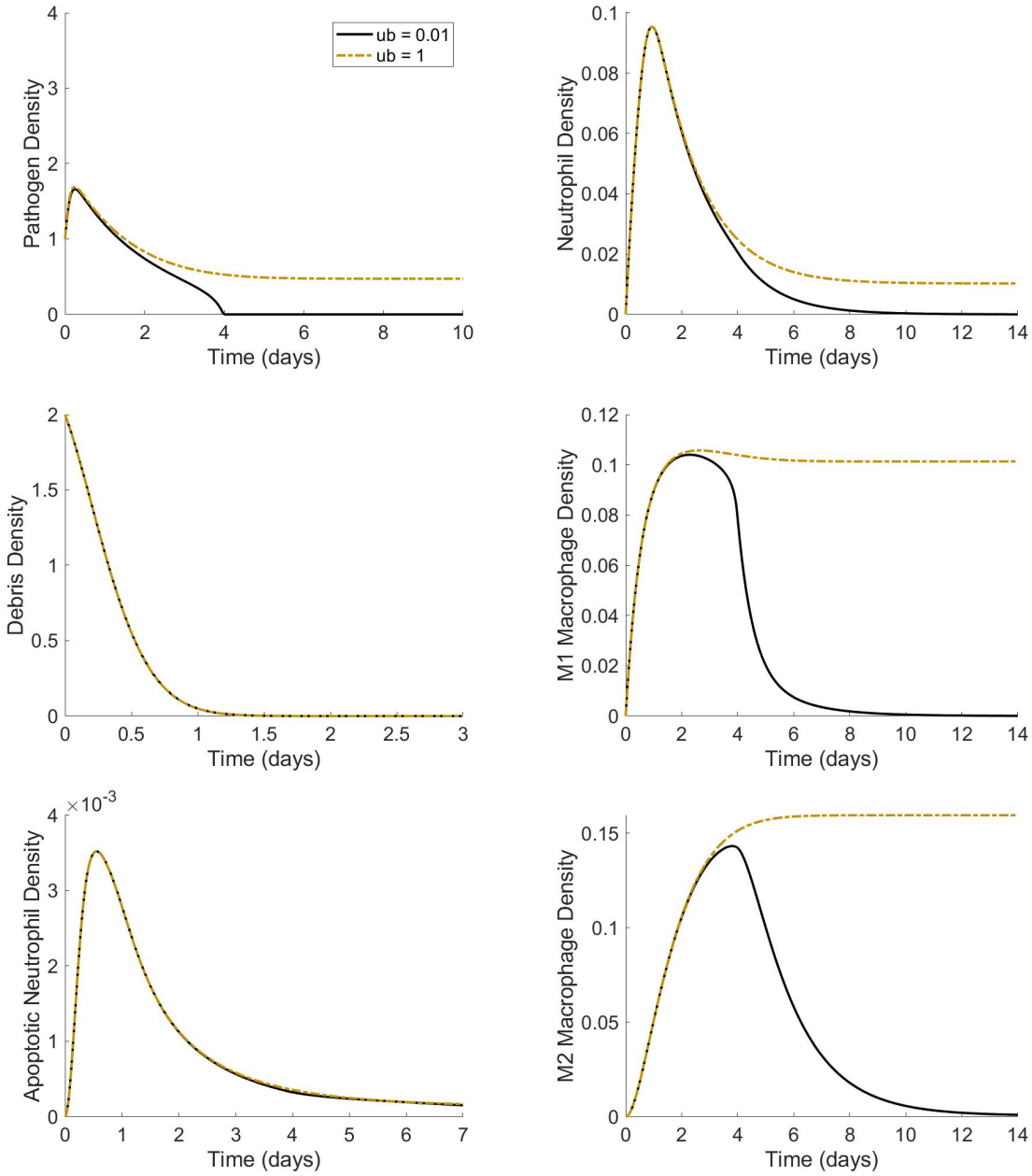

Figure 4.11: Simulations with varying ub (intrinsic decay of local response)

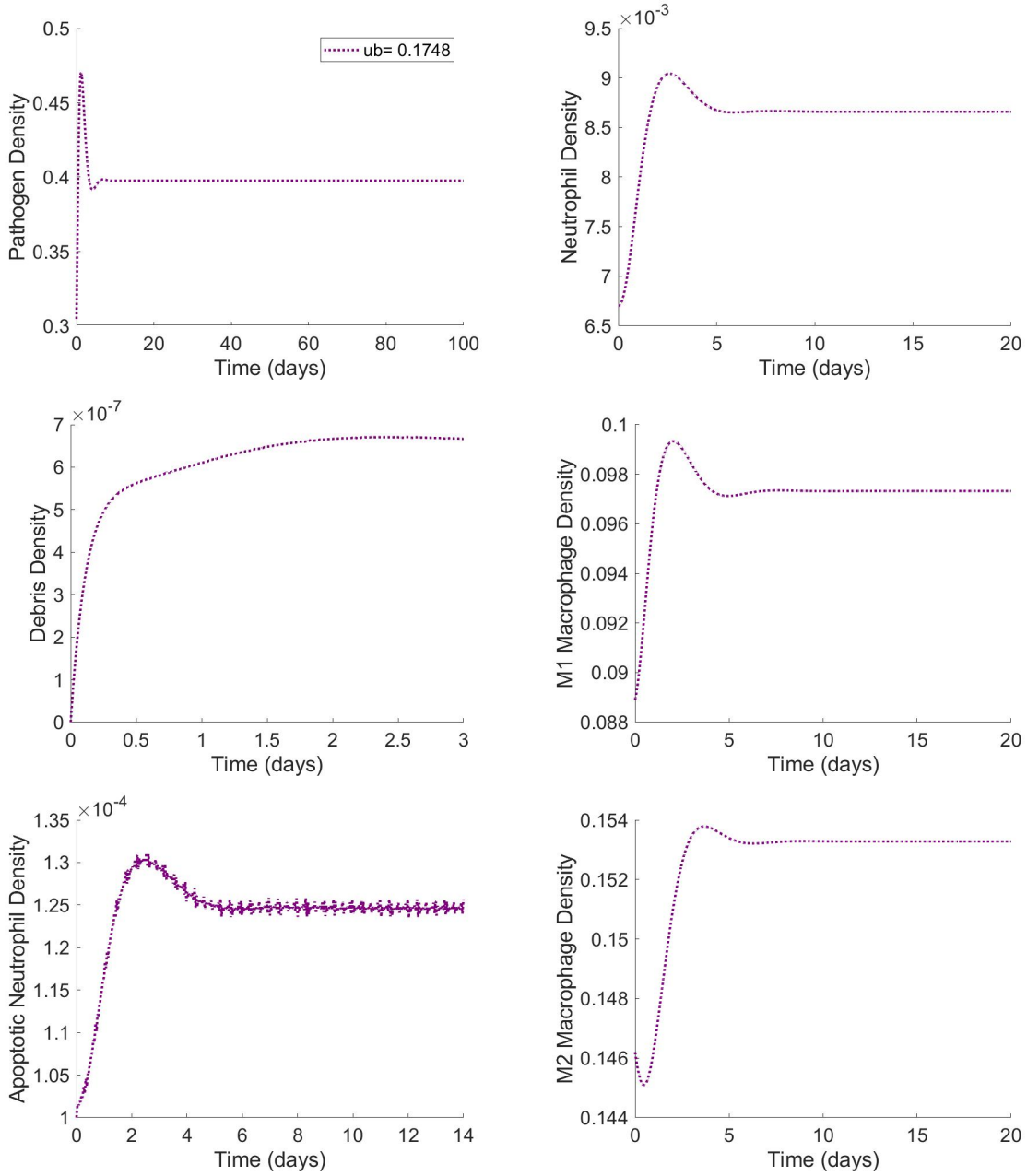

Figure 4.12: Example simulation with ub (intrinsic decay of local response) at the Hopf bifurcation point

For snr, the source of resting neutrophils, there was one bifurcation point found at snr = 4.222 (Table 4.5). The bifurcation diagrams in Figure 4.13 show that for

small snr, the steady state for debris, apoptotic neutrophils, M1 macrophages, and M2 macrophages the steady state is relatively high and it goes down as snr increases. In the diagram for neutrophils, after snr is big enough the steady state starts increasing a steady rate and for the other state variables except pathogens the steady state remains relatively higher. Figure 4.14 shows different transient behavior for varying snr values.

Table 4.5: XPPAUTO results for varying source of resting neutrophils, snr

TY	snr	P^*	Pt^*	AN^*	N^*	$M1^*$	$M2^*$
BP	4.222	0.00	0.00	0.00	0.00	0.0015	0.0221

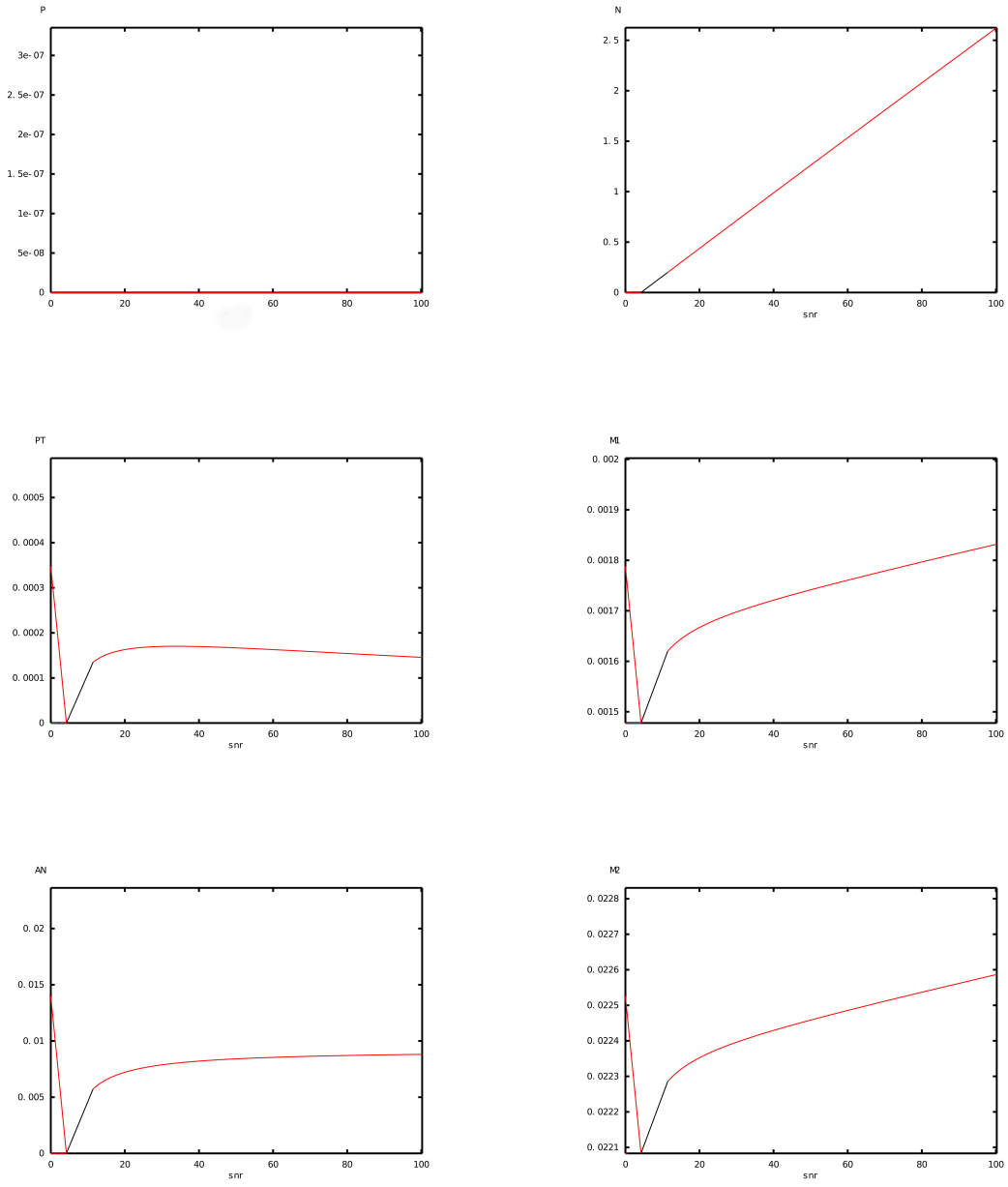

Figure 4.13: Bifurcation diagrams with varying snr (source of background resting neutrophils)

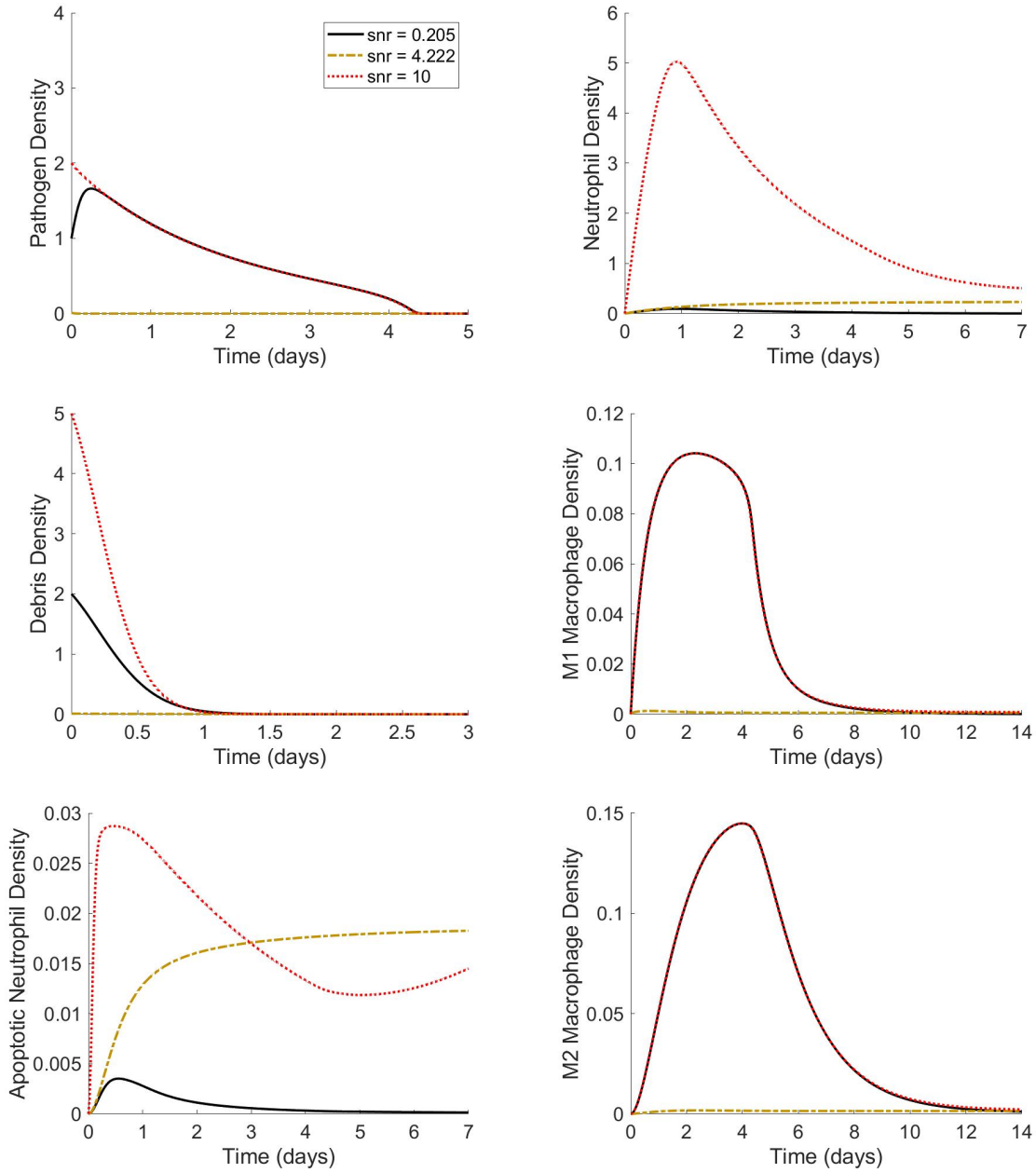

Figure 4.14: Simulations with varying snr (intrinsic decay of local response)

4.1 Sensitivity analysis around parameters estimated from general dynamics

The working set found that resulted in output for general dynamic assumptions were used to test ranges of values around the found parameter value. A range of 15 units for each parameter intersection with its biological bounds in Table 4.1 was chosen as the multidimensional parameter space. Pathogen growth rate (kpg), carrying capacity (p_∞), and estrogen concentration was chosen to be $[0, 50]$, $[0, 1000]$, and $[0, 50]$, respectfully. The chosen sensitivity analysis method used was the Fourier Amplitude Sensitivity Test (FAST). This was implemented within the SAFE package in MATLAB. The FAST method is a variance based method that implements ANOVA decomposition and uses the Fourier series to estimate the total model variance. The Fourier transform is used to decompose the variance of the model output described by each parameter. The sensitivity indices are the proportion of the variance attributable to the factor of interest over the total variance and has a range between 0 and 1. This method was chosen since it is computationally efficient and can be used for non-linear, non-monotonic models [81]. This analysis is conducted utilizing each state variable as the output, and afterwords the average of all the state variables as the output.

After each of the parameter sets are sampled, the resulting output is recorded. Figure 4.15 a shows the resulting outputs for pathogens for each sample parameter set. Figure 4.15 b shows the mean and standard deviation of these simulations. For pathogens the mean trajectory is downward trend. The trajectories start with the same initial condition, so the standard deviation starts at value zero and increase until around day one where it is more consistent. The output was analyzed according to each parameter. The FAST indices for each parameter is provided in Figure 4.16. For pathogens the parameters that reulted in the higest sensitivity indices were smr (source of monocytes), kpm (destruction of pathogens by macrophages), and kpg

(growth rate of pathogens). Estrogen related parameters that had higher sensitivity indices were kem (the enhancement of estrogen on macrophage phagocytosis) and E (estrogen concentration). The indices mean over 15 days is provided in Figure 4.17. The solid color bar indicate that the index value over time stays consistent.

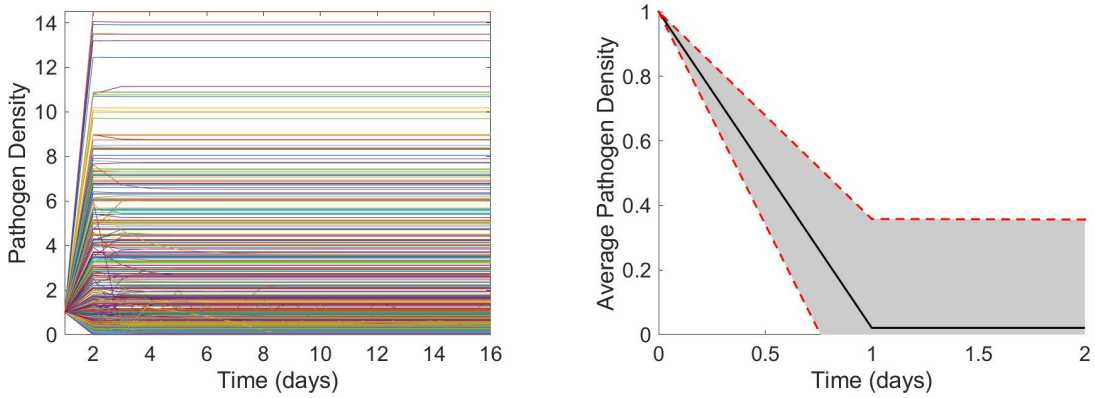

(a) Simulations

(b) Mean and Standard Deviation

Figure 4.15: Simulations of pathogen density after sampling and the average pathogen density of the simulations

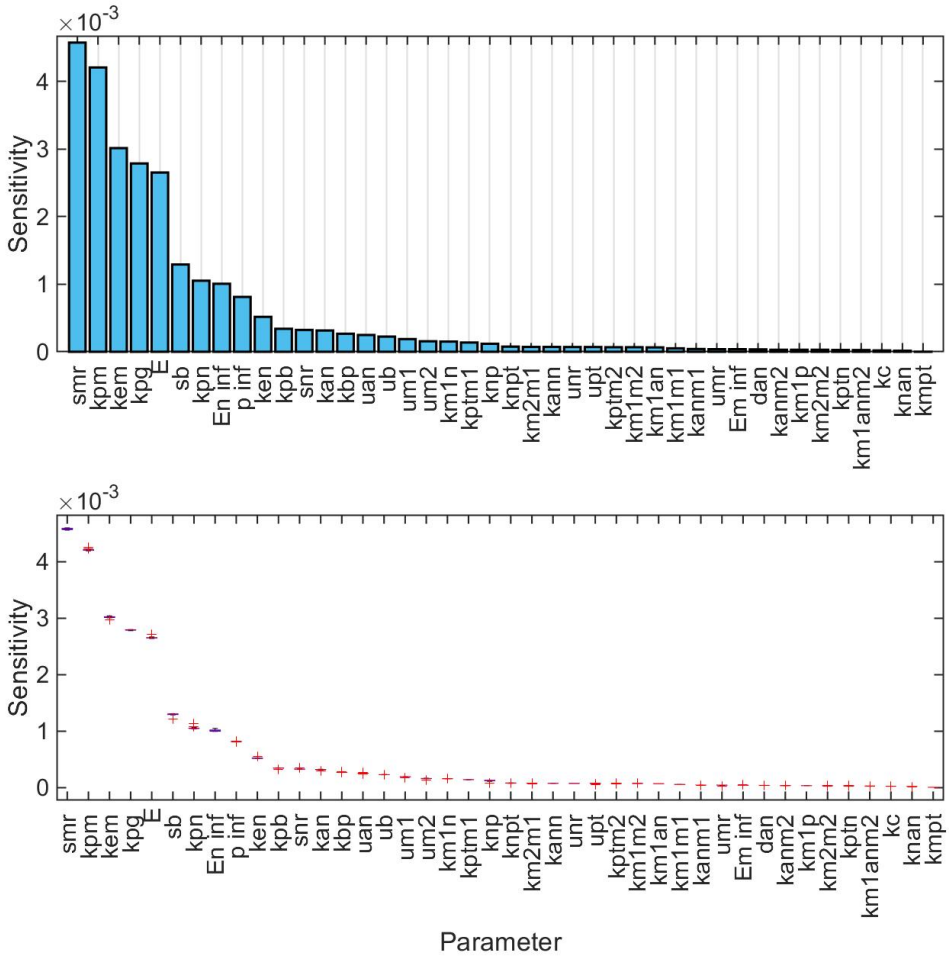

Figure 4.16: FAST global sensitivity analysis results: Mean and box plot of sensitivity for pathogen density over time

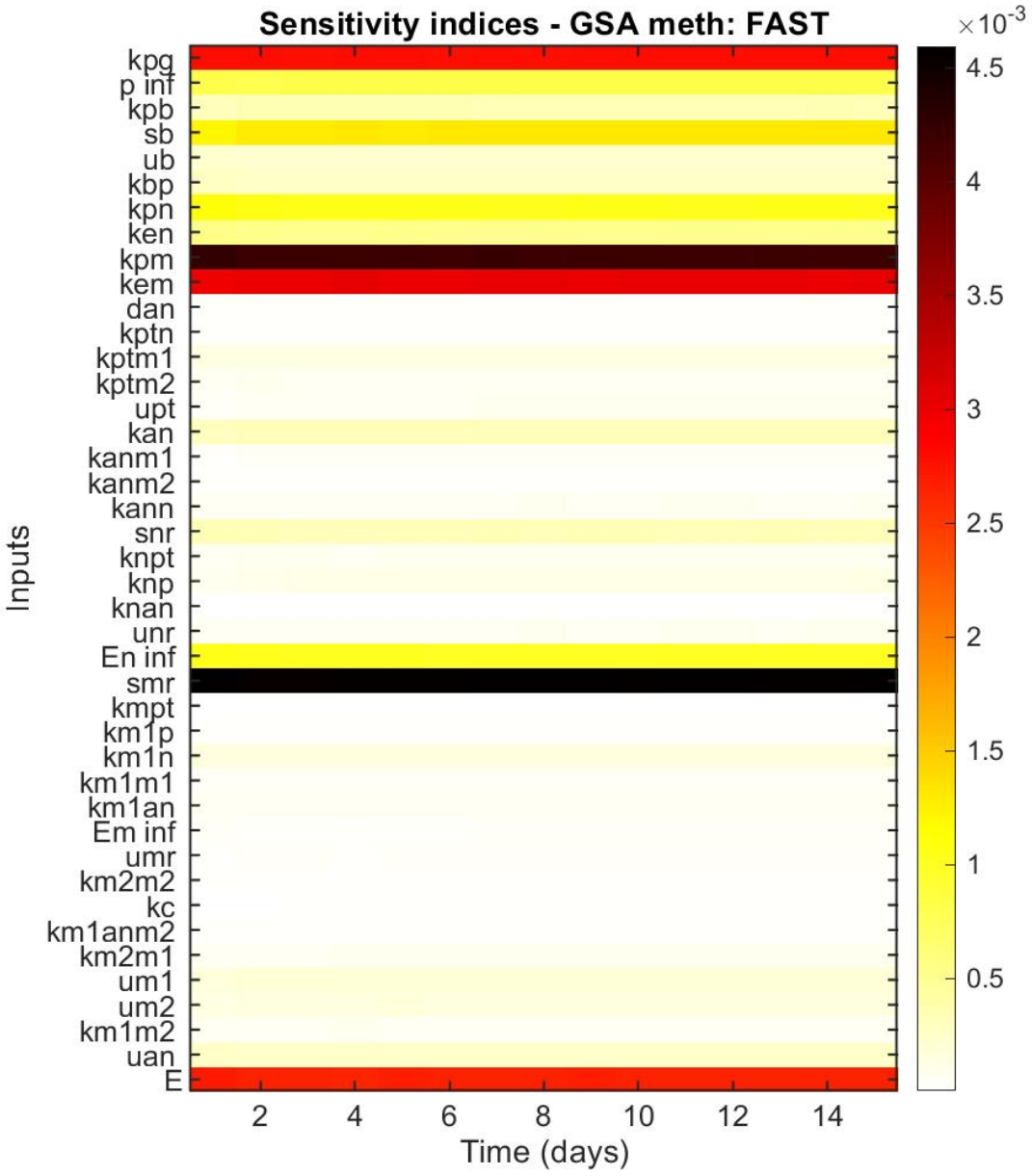

Figure 4.17: FAST global sensitivity analysis results: Sensitivity indices with respect to pathogens over 15 days

For debris the mean trajectory of the output is downward trend (Figure 4.18). Parameters that had higher sensitivity indices were smr (source of monocytes) and estrogen concentration (Figure 4.19 and 4.20). The sensitivity index for smr did not have as much variation with respect to time.

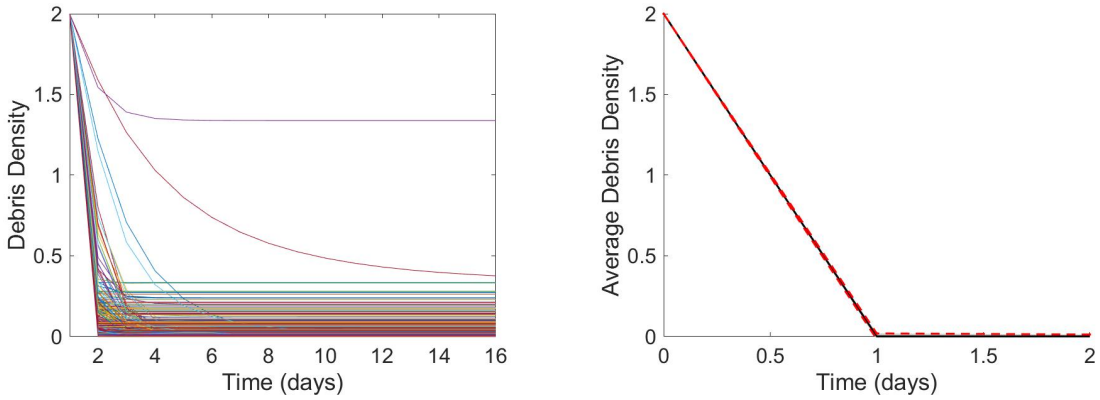

(a) Simulations (b) Mean and Standard Deviation

Figure 4.18: Simulations of debris density after sampling and the average pathogen density of the simulations

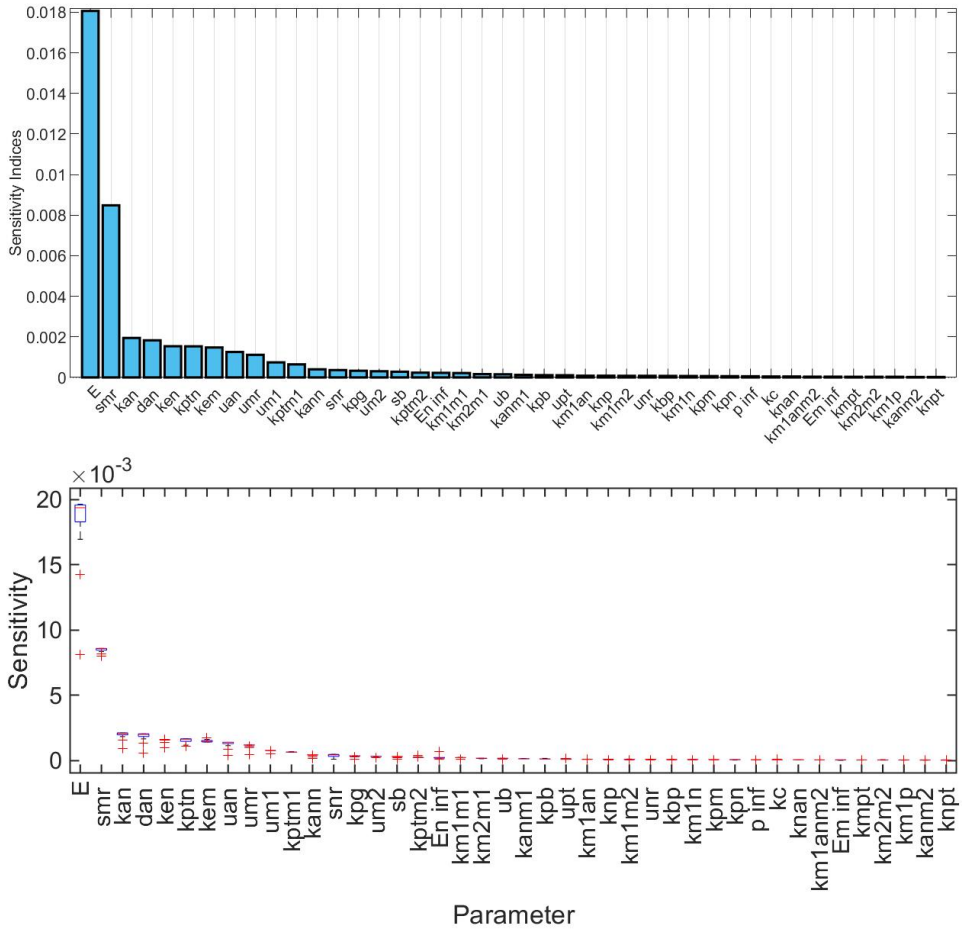

Figure 4.19: FAST global sensitivity analysis results: Mean and box plot of sensitivity for debris density over time

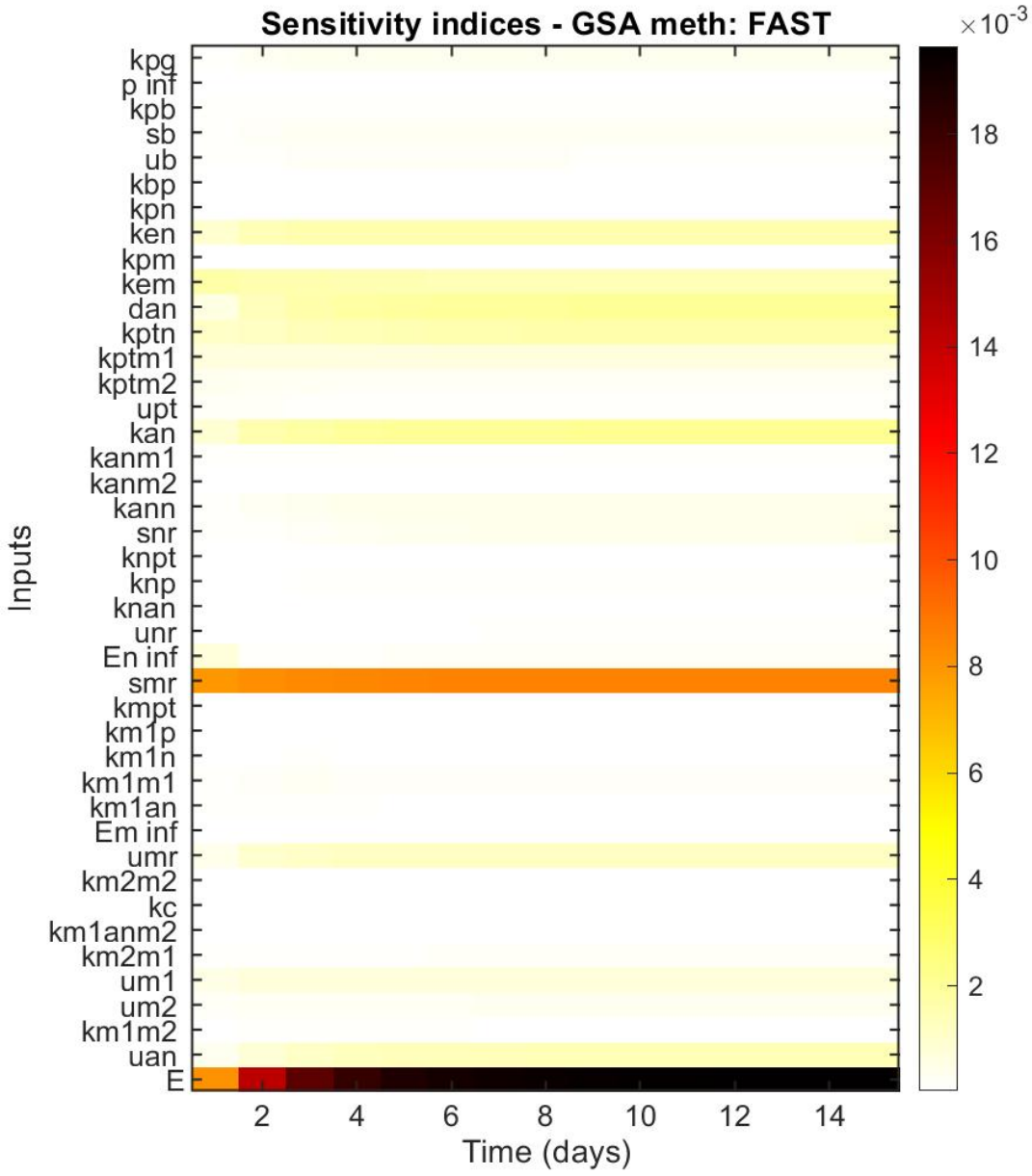

Figure 4.20: FAST global sensitivity analysis results: Sensitivity indices for Debris Density over 15 Days

For apoptotic neutrophils the mean trajectory increases steadily and is more steady after day 1 (Figure 4.21). Similarly to the results for debris, the parameters that resulted in higher sensitivity indices were the source of monocytes and estrogen concentration (Figure 4.22). However the indices for estrogen does not vary as much over time (Figure 4.23).

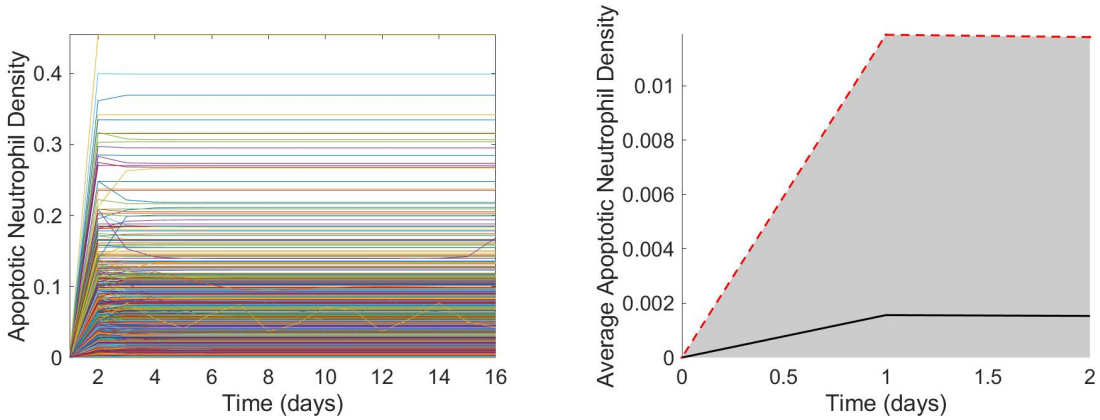

(a) Simulations

(b) Mean and Standard Deviation

Figure 4.21: Simulations of apoptotic neutrophil density after sampling and the average pathogen density of the simulations

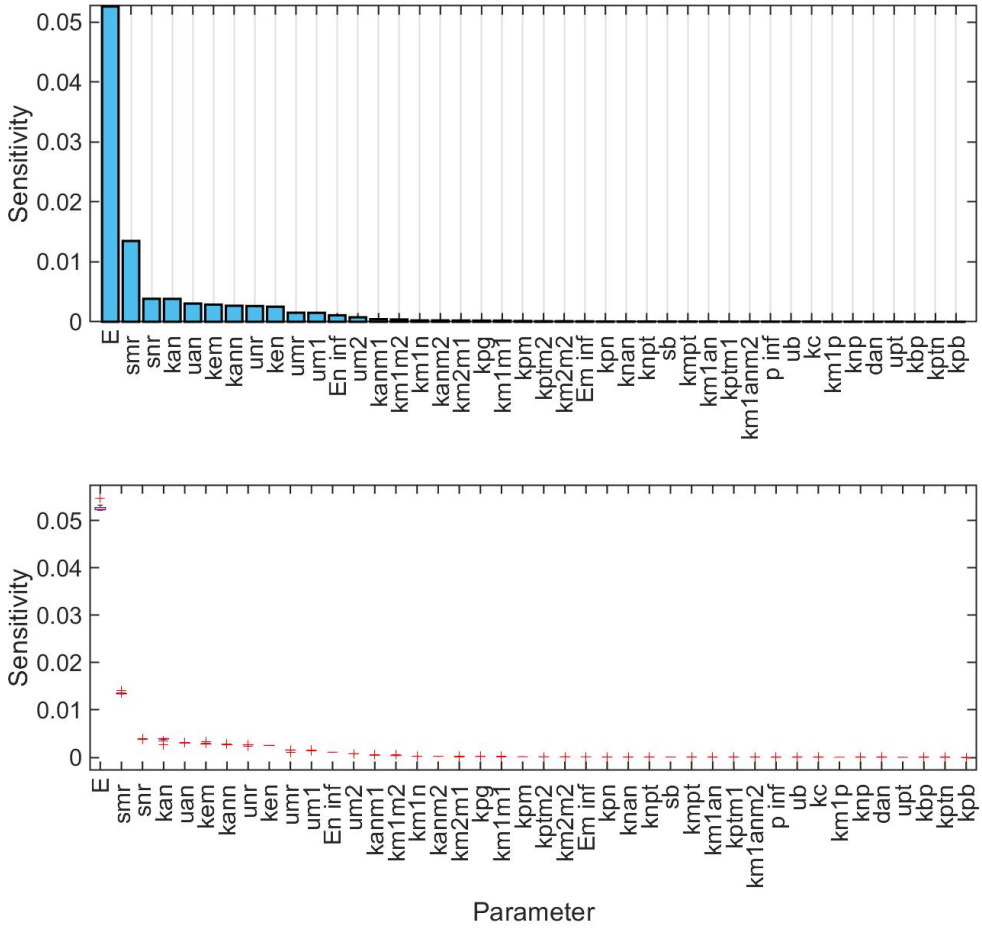

Figure 4.22: FAST global sensitivity analysis results: Mean and box plot of sensitivity for Apoptotic Neutrophil Density over Time

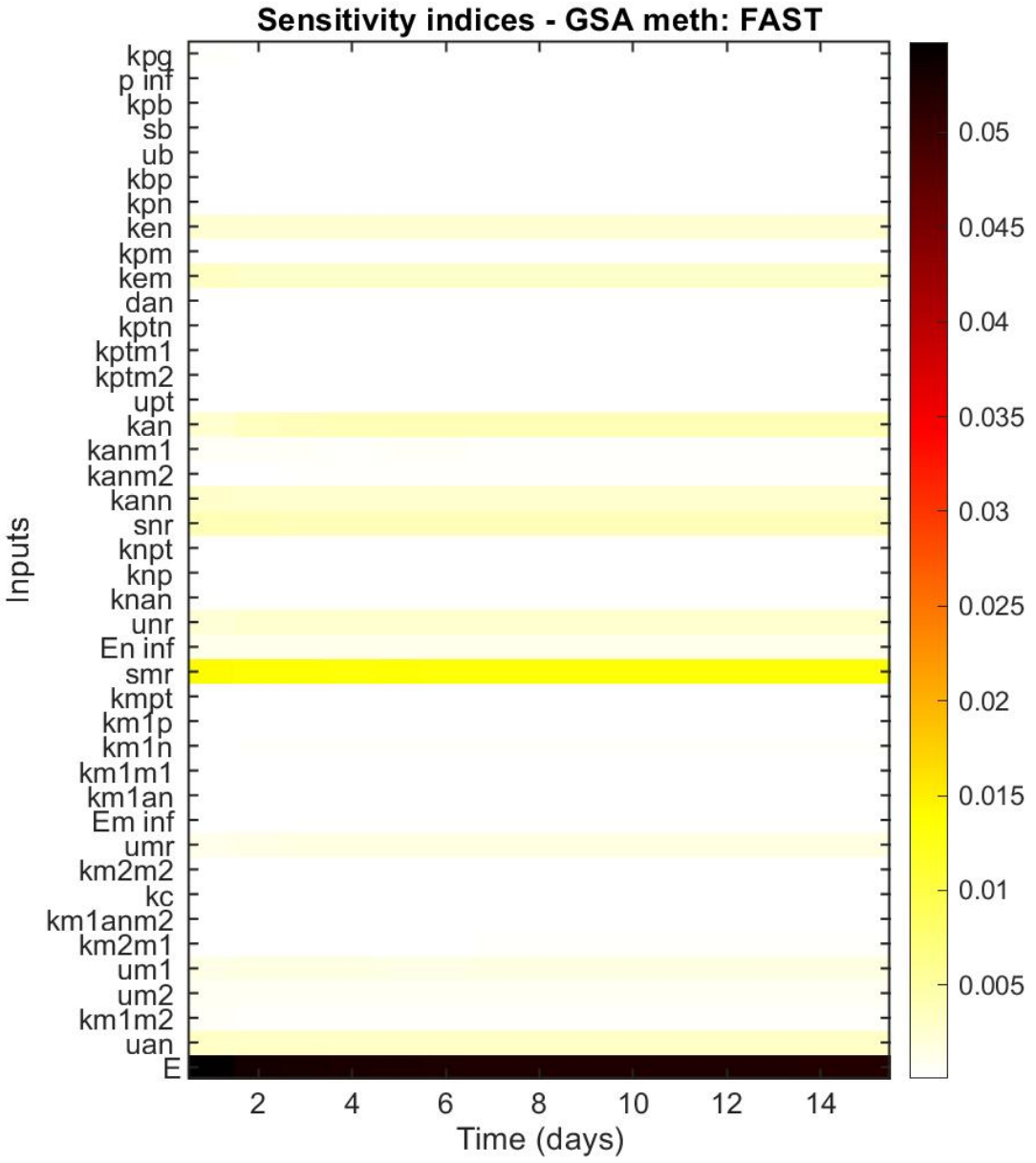

Figure 4.23: FAST global sensitivity analysis results: Sensitivity indices for apoptotic neutrophil density over 15 days

For neutrophils the mean trajectory has a slight peak around day 1 and steadily goes down (Figure 4.24). The non-estrogen related parameters that results in higher sensitivity indices were unr (decay of resting neutrophils), smr (source of monocytes), kan (apoptosis rate of neutrophils), and snr (source of resting neutrophils). The estrogen related parameter that had higher indices was estrogen concentration (Figure 4.25 and 4.26).

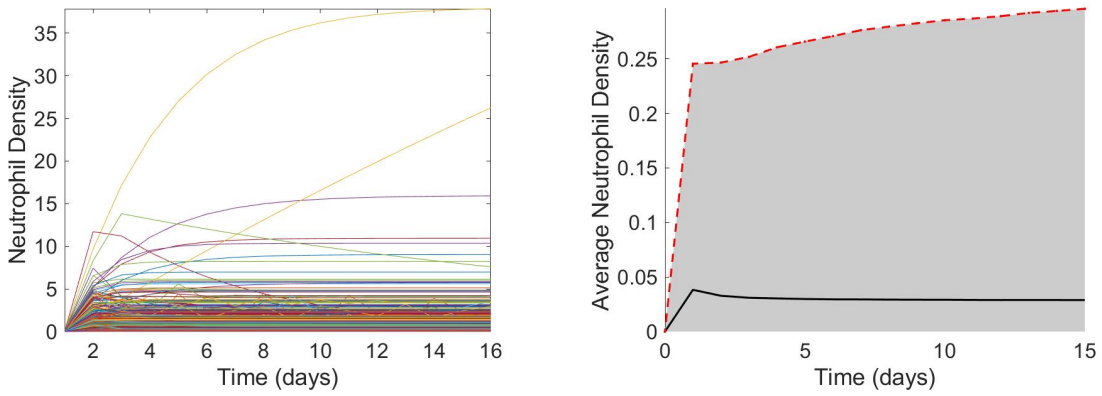

(a) Simulations (b) Mean and Standard Deviation

Figure 4.24: Simulations of Neutrophil Density after Sampling and the Average Pathogen Density of the Simulations

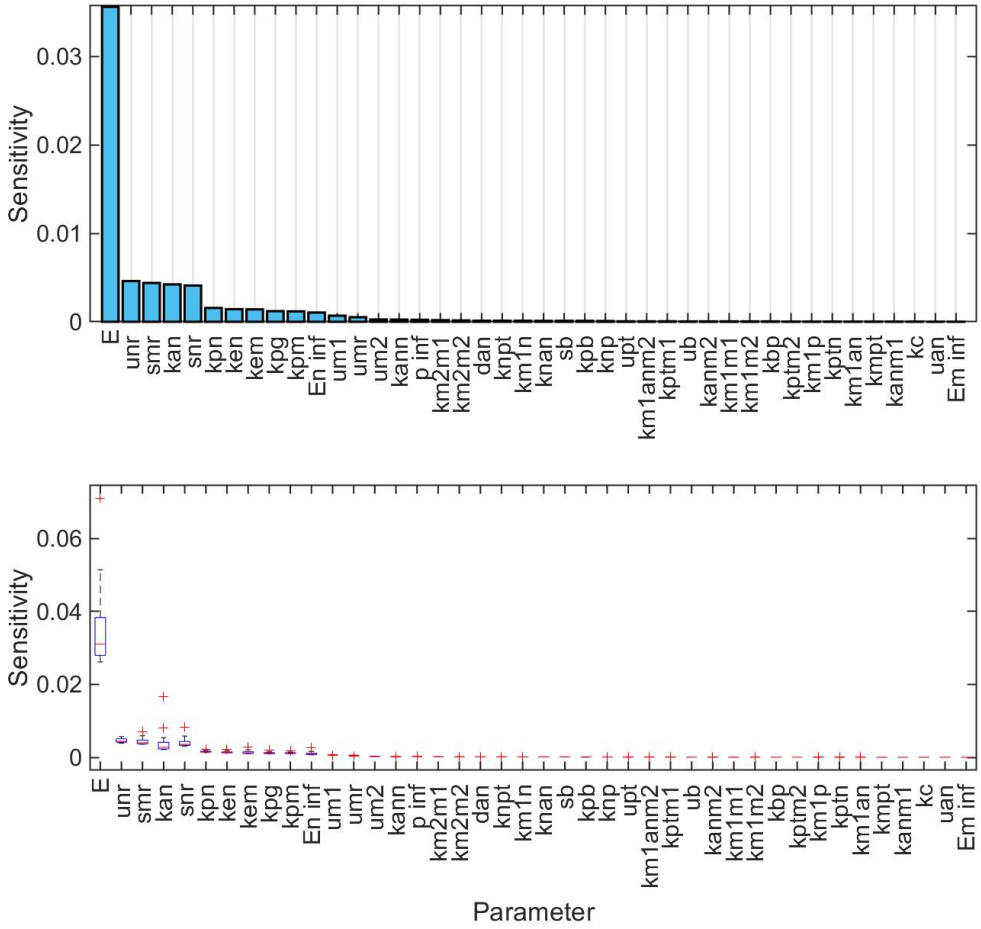

Figure 4.25: FAST global sensitivity analysis results: Mean and box plot of sensitivity for neutrophil density over time

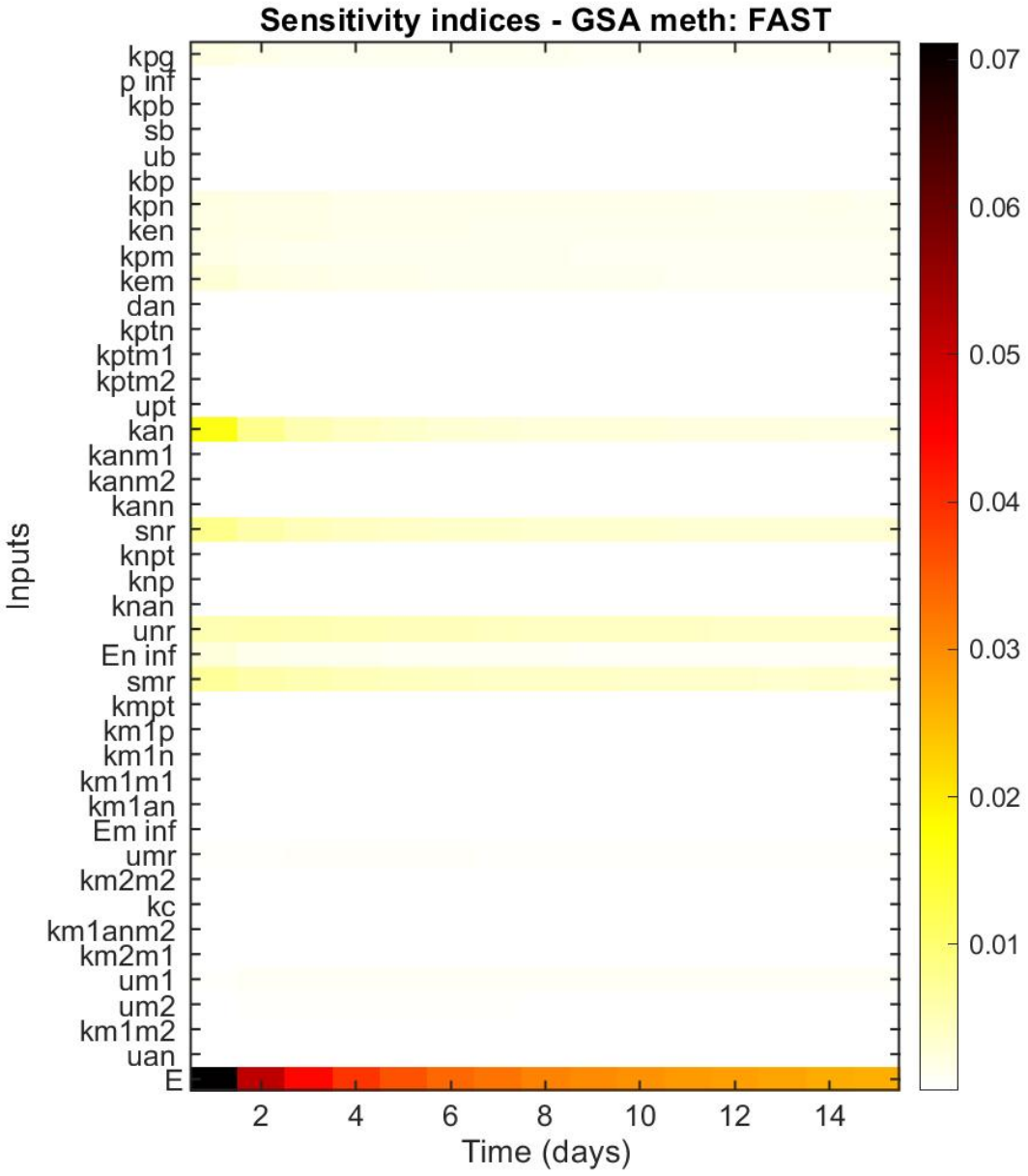

Figure 4.26: FAST global sensitivity analysis results: Sensitivity indices for Neutrophil Density over 15 Days

For M1 macrophages the mean trajectory increases and the increase slows before day 5 (Figure 4.27). The parameters that resulted in a higher sensitivity index were um1 (decay rate of M1 macrophages), smr (source of monocytes), umr (decay rate of monocytes), and um2 (decay rate of M2 macrophages) (Figure 4.28 and 4.32).

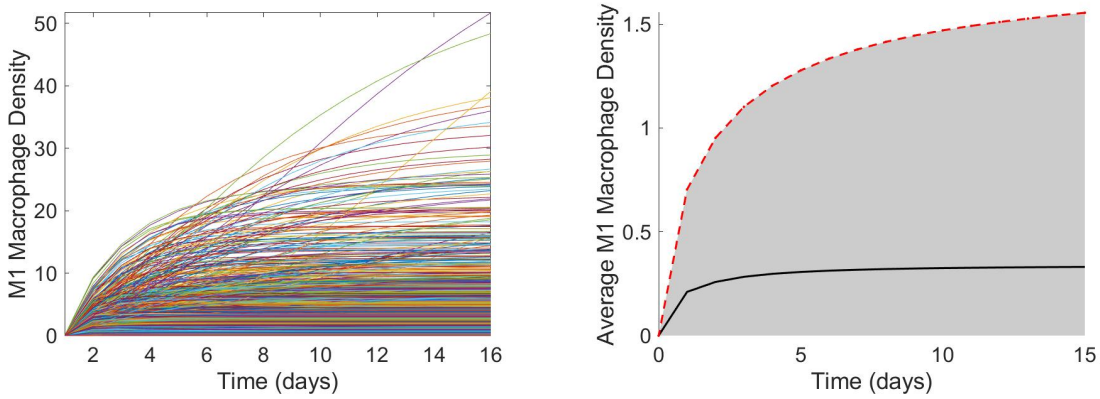

(a) Simulations

(b) Mean and Standard Deviation

Figure 4.27: Simulations of M1 Macrophages Density after Sampling and the Average Pathogen Density of the Simulations

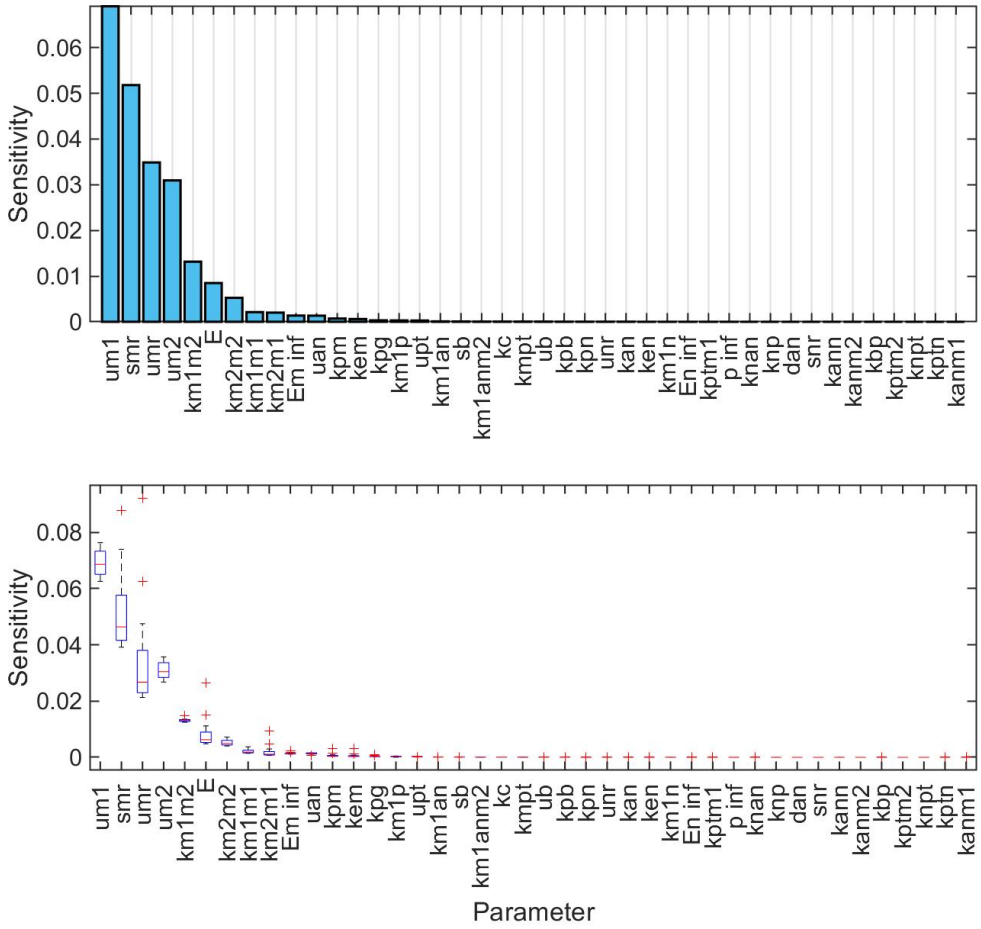

Figure 4.28: FAST global sensitivity analysis results: Mean and box plot of sensitivity for M1 Macrophage Density over Time

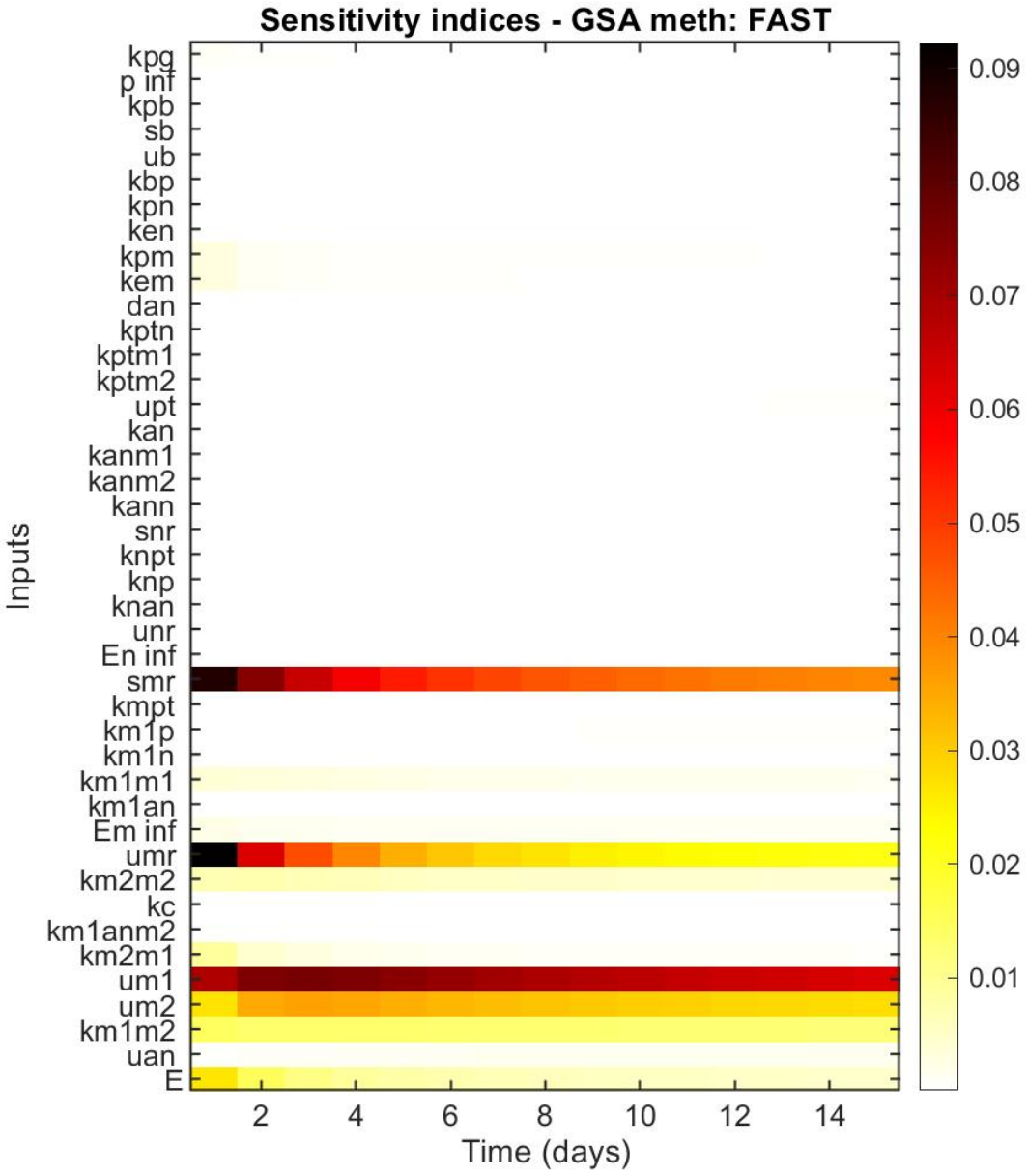

Figure 4.29: FAST global sensitivity analysis results: Sensitivity indices for M1 macrophage density over 15 days

For M2 macrophages the mean trajectory increases and this rate of increase decreases around day 1 (Figure 4.30). The parameters that had higher sensitivity indices were um2 (decay rate of M2 macrophages), smr (source of monocytes), km2m1 (transition of M2 macrophages to M1 macrophages), and umr (decay rate of monocytes) (Figure 4.31 and Figure 4.32).

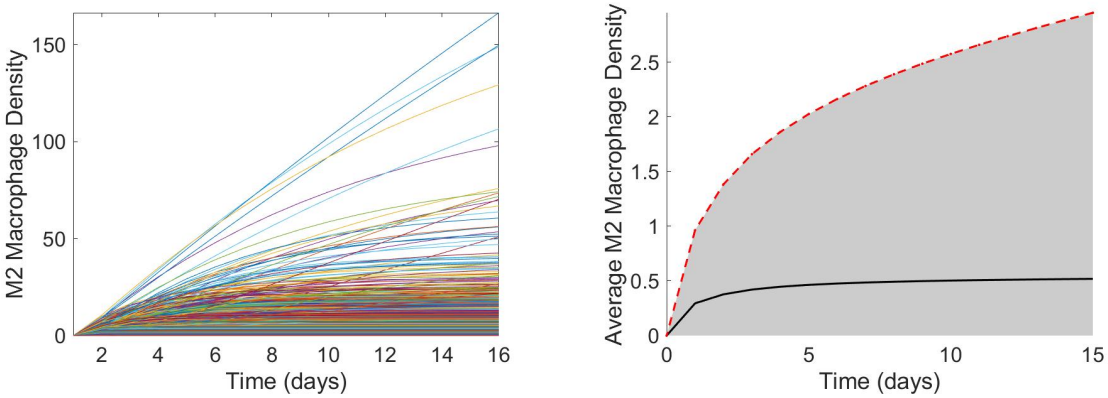

(a) Simulations

(b) Mean and Standard Deviation

Figure 4.30: Simulations of M2 macrophage density after sampling and the average pathogen density of the simulations

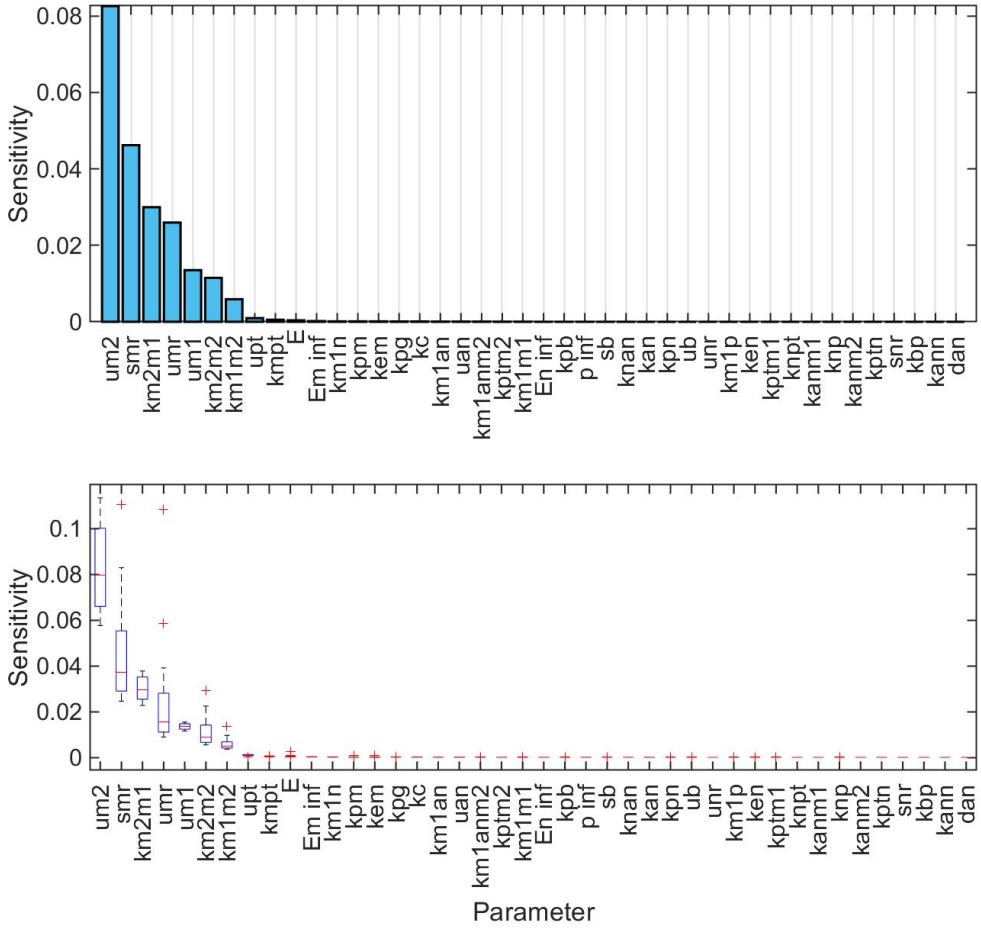

Figure 4.31: FAST global sensitivity analysis results: Mean and box plot of sensitivity for M2 Macrophage Density over Time

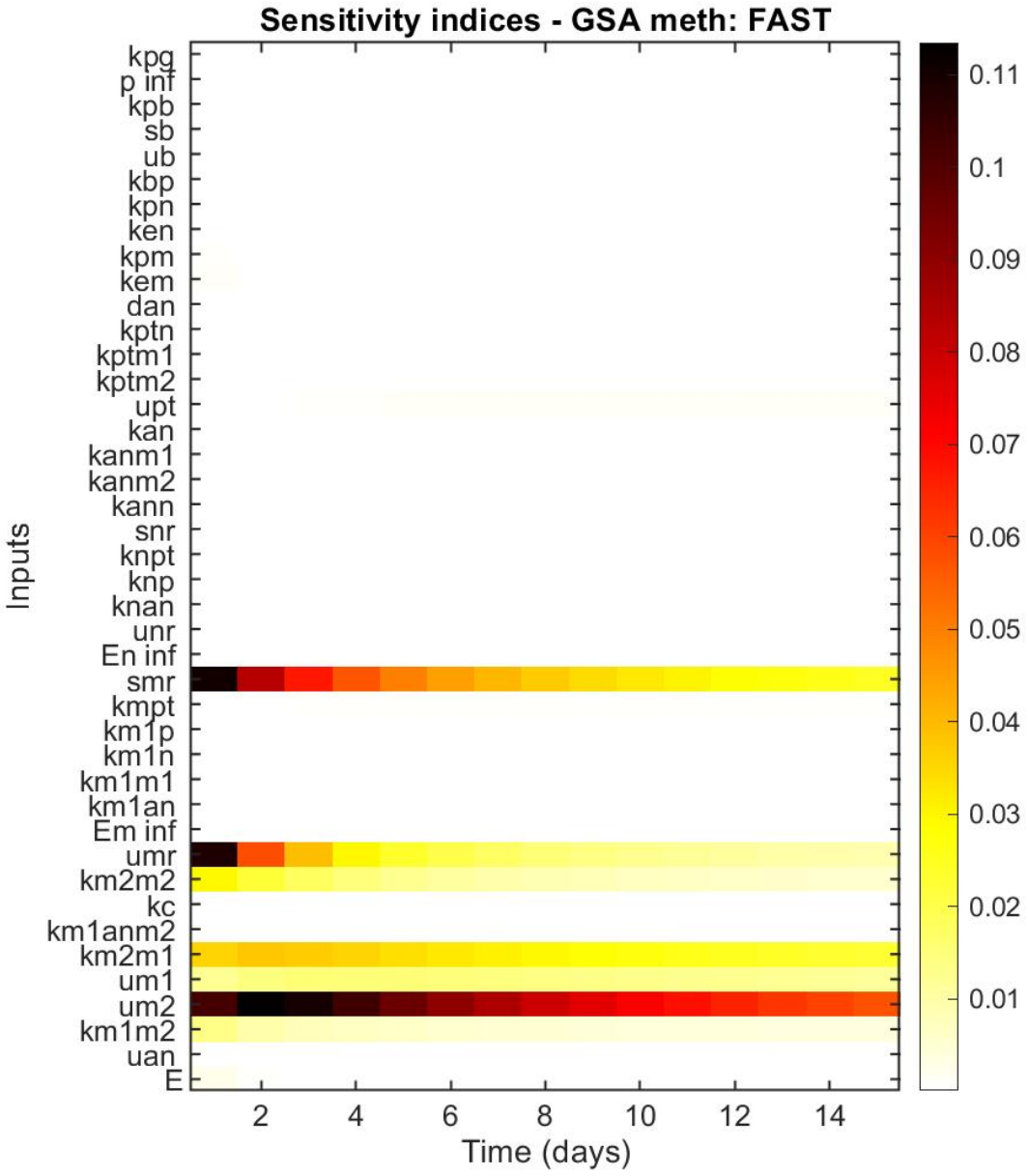

Figure 4.32: FAST global sensitivity analysis results: Sensitivity indices for M2 macrophages over 15 Days

4.2 Sensitivity Analysis with respect to the average

Next the sensitivity analysis was implemented for the output being the average of the state variables. The parameters that had higher sensitivity indices were kpm (the destruction of pathogen by macrophages), estrogen concentration, smr, kem (estrogen increase in the phagocytic abilities of macrophages), kpg (growth rate of pathogen), En_∞ (estrogen's effect of the inhibition of M1 macrophage production causes by existing M1 macrophages), and p_∞ (pathogen carrying capacity).(Figure 4.33). The indices remain around the same value as time increases (Figure 4.32).

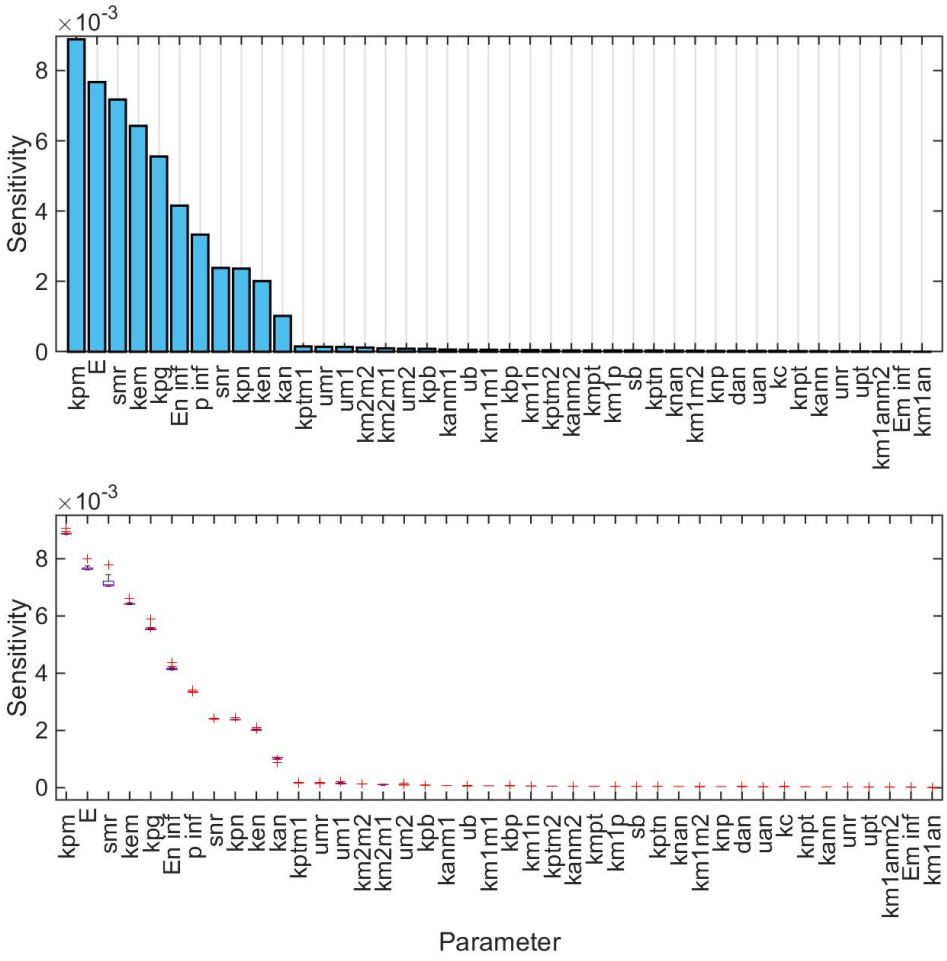

Figure 4.33: FAST global sensitivity analysis results: Mean and box plot of sensitivity for average inflammation variable density over time

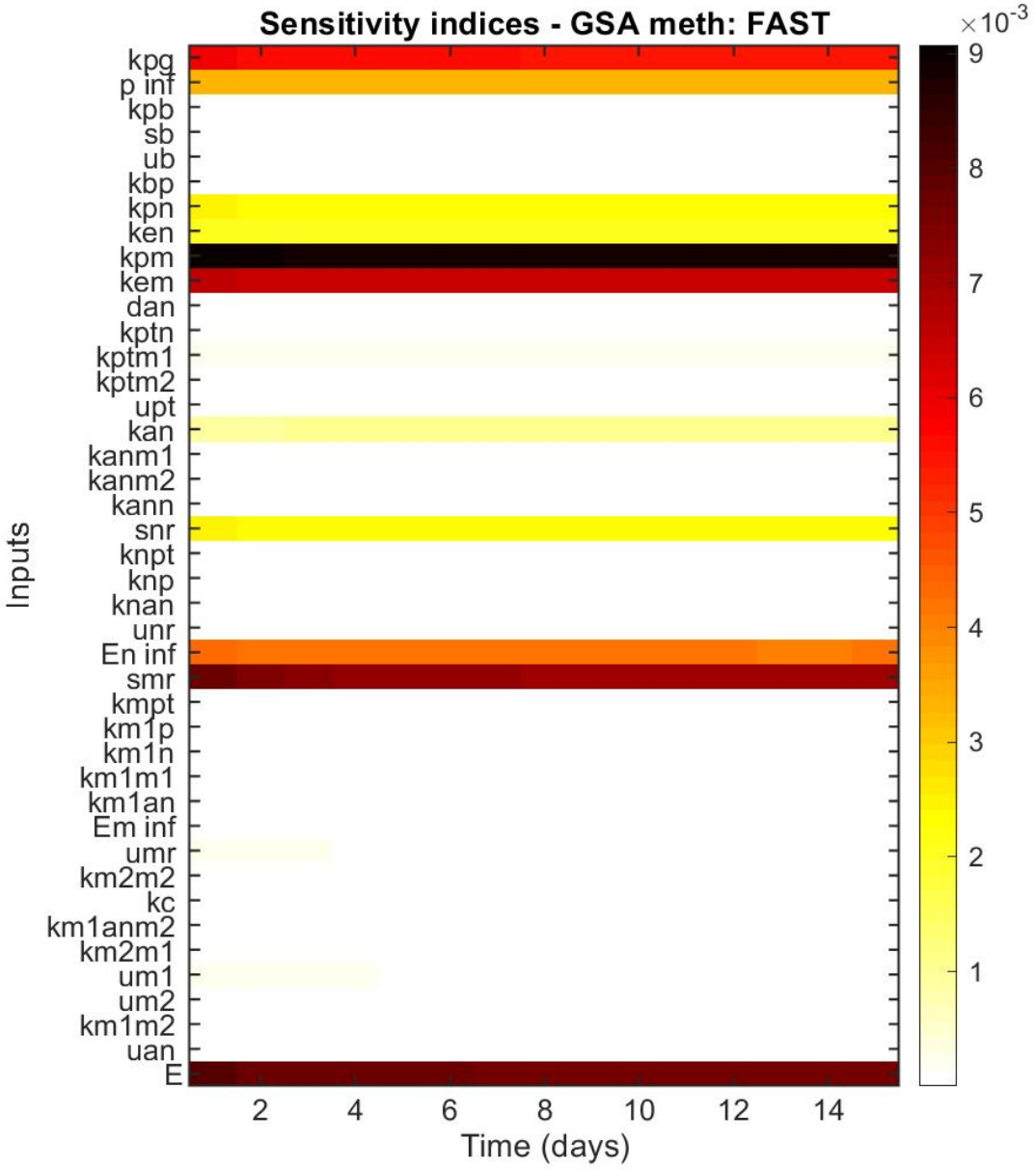

Figure 4.34: FAST global sensitivity analysis results: Sensitivity indices for the average inflammation variable density over 15 days

4.3 Stochastic Differential Equation Model

In realistic biological systems, there are underlying mechanisms that can cause erratic changes [45, 71]. These state variables in the system do not live in isolation but are changing along with underlying subsystems that can positively or negatively influence these densities. Underlying uncontrolled or erratic changes can be accounted for my incorporating white noise. The noise can be taken constant or proportional to the state variable. If they are taken proportional, the term will be of the form $\sigma S dW_S(t)$, where σ depends on the range of variation of the state variable S, and $W_S(t)$ is the random process.

Random process were implemented for each state variable equation in the inflammation system. The terms are chosen to be proportional to the state variable. The random processes are assumed to be Wiener processes. The result is a stochastic differential equation system. The random processes are defined as $W_P(t), W_P(t), W_{Pt}(t), W_{AN}(t), W_N(t), W_{M1}(t)$, and $W_{M2}(t)$, which are processes affecting the densities of pathogens, debris, apoptotic neutrophil, neutrophil, M1 macrophages, and M2 macrophages, respectively. Note that for each meets the following criteria. Let $W(t)$ be a standard Wiener process, over $[0, T]$. The Wiener process satisfies the following conditions that was described in [26] and is stated as follows:

Brownian Motion. A scalar standard Brownian motion, or standard Wiener process, over $[0, T]$ is a random variable $W(t)$ that depends continuously on $t \in [0, T]$ and satisfies the following three conditions.

1. W(0) = 0 (with probability 1).

2. For $0 \leq s < t \leq T$ the random variable given by the increment $W(t) - W(s)$ is normally distributed with mean zero and variance t − s; equivalently, W(t) − $W(s) \sim \sqrt{t-s}N(0,1)$, where N(0, 1) denotes a normally distributed random variable with zero mean and unit variance.

3. For $0 \leq s<t<u<v \leq T$ the increments W(t) − W(s) and W(v) − W(u) are independent.

Let S stand for the respective state variable. For each equation, $\sigma S dW_S(t)$ is incorporated to account for random fluctuations in the rate effected by the current density of S. σ is chosen to be a constant which characterizes the influence of the random process. Adding each respective white noise term, gives the following system:

$$
\begin{aligned}
dP &= k_{pg}P(1-\frac{P}{P_\infty})dt - \frac{k_{pb}s_bP}{\mu_b + k_{bp}P}dt - k_{pn}PN(1+k_{en}E)dt - k_{pm}P(M_1+M_2)(1+k_{em}E)dt \\
&\quad +\sigma P dW_P(t) \\
dP_t &= \mu_{an}A_N dt - k_{ptn}P_tN(1+k_{en}E)dt - k_{ptm1}P_tM_1(1+k_{em}E)dt - k_{ptm2}P_tM_2(1+k_{em}E)dt \\
&\quad -\mu_{pt}P_t dt + \sigma P_t dW_{Pt}(t) \\
dA_N &= k_{an}N dt - k_{anm1}A_NM_1(1+k_{em}E)dt - k_{anm2}A_NM_2(1+k_{em}E)dt - k_{ann}N(1+k_{en}E)dt \\
&\quad -d_{an}A_N dt - \mu_{an}A_N + \sigma A_N dW_{AN}(t) \\
dN &= R_N\frac{S_{nr}}{\mu_{nr}+R_N}\frac{1}{(1+\frac{E}{E_{ninf}})^2}dt - k_{an}N dt + \sigma N dW_N(t)dt, \quad R_N = k_{npt}P_t + k_{np}P + k_{nan}A_N \\
dM_1 &= R_{M1}\frac{s_{mr}}{\mu_{mr}+R_{M1}+R_{M2}}dt - k_{m1m2}A_NM_1dt + k_{m2m1}M_2dt - \mu_{m1}M_1dt + \sigma M_1 d_{M1}W_{M1}(t), \\
&\quad R_{M1} = k_{mpt}P_t + k_{m1p}P + k_{m1n}N + \frac{k_{m1m1}M_1}{1+(\frac{E}{E_{M\infty}})^2} + k_{m1an}A_N \\
dM_2 &= R_{M2}\frac{s_{mr}}{\mu_{mr}+R_{M1}+R_{M2}}dt + k_{m1m2}A_NM_1dt - k_{m2m1}M_2dt - \mu_{m2}M_2dt + \sigma M_2 dW_{M2}(t),
\end{aligned}
$$

$$R_{M2} = k_{m2m2}M_2 + k_c.$$

Realizations were simulated for different values of σ using Milstein method. First σ is set equal to 0.05. Figure 4.35 shows sample realizations compared to the deterministic solution. Next, a higher number of simulations were analyzed (N=5000). Then the mean and standard deviation of these simulations where calculated. Though these realizations may result in fluctuations in the wound healing process, when taking the mean, the results is comparable to the deterministic solution (Figure 4.36). The next type of analyses was implemented to describe how does the output of each state variable change for each simulation. The output was averaged over the 15 days and this average was compared as the simulations increased (Figure 4.37). This was repeated 6 times, with each time increasing the maximum number of iterations. For $\sigma = 0.1$, the average of each state variable fluctuates between a certain range.

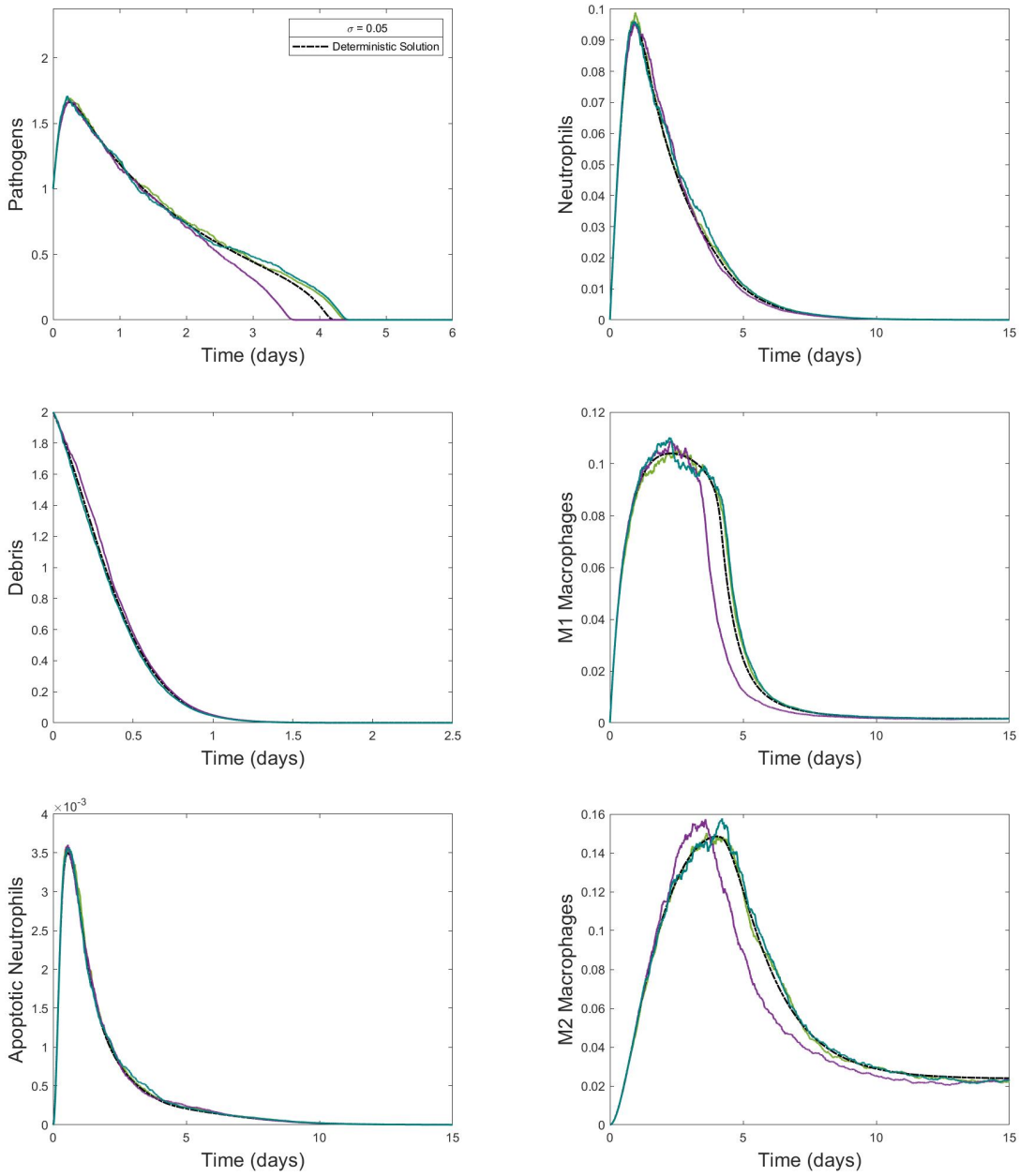

Figure 4.35: Stochastic simulations for each state variable when $\sigma = 0.05$

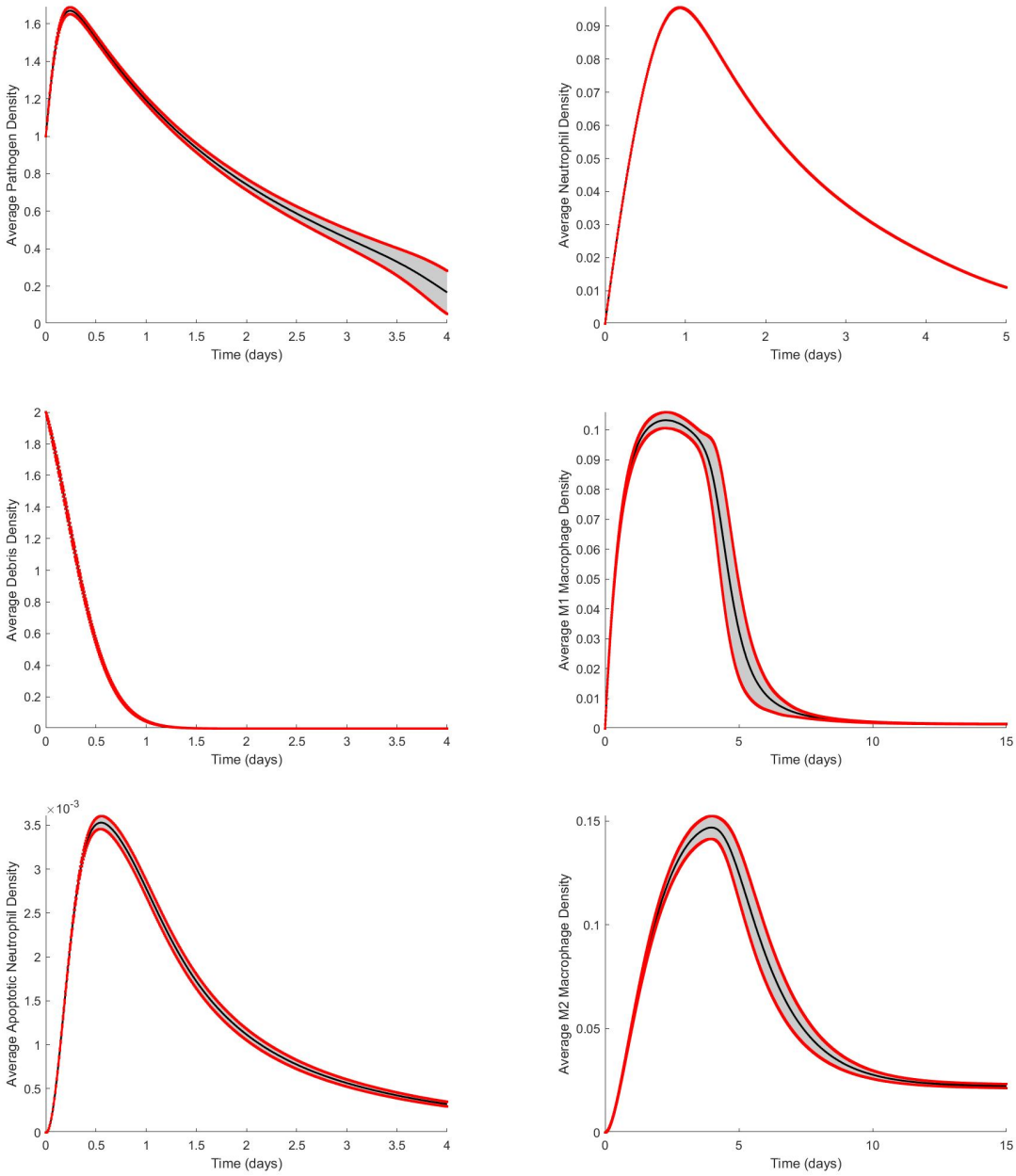

Figure 4.36: Mean and standard deviation of N=5000 simulations when $\sigma = 0.05$

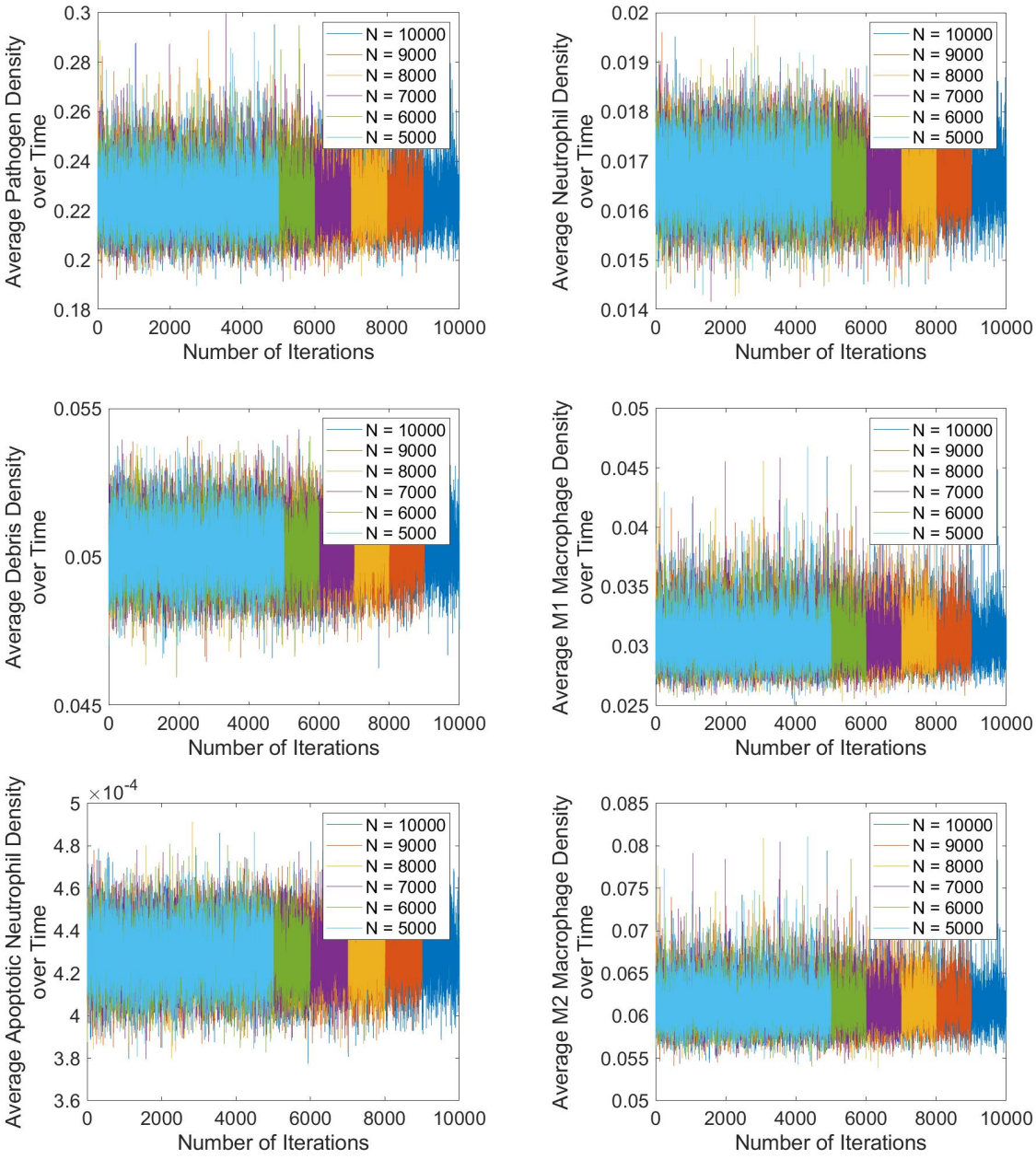

Figure 4.37: Mean of each state variable over time for different number of iterations when $\sigma = 0.05$

Next σ is increased to 0.1. Figure 4.38 shows sample realizations compared to the deterministic solution. Some realizations result in a slightly different solving

time for pathogens and when M1 macrophages peak, there are larger fluctuations. Figure 4.39 show the mean and standard deviation when N=5000 realizations were simulated. The mean is still comparable to the deterministic solution. The deviation away from the mean is increased when compared to the deviation when $\sigma = 0.01$. Figure 4.40 shows a higher range of fluctuations of the mean when compared to the range of fluctuations for $\sigma = 0.01$.

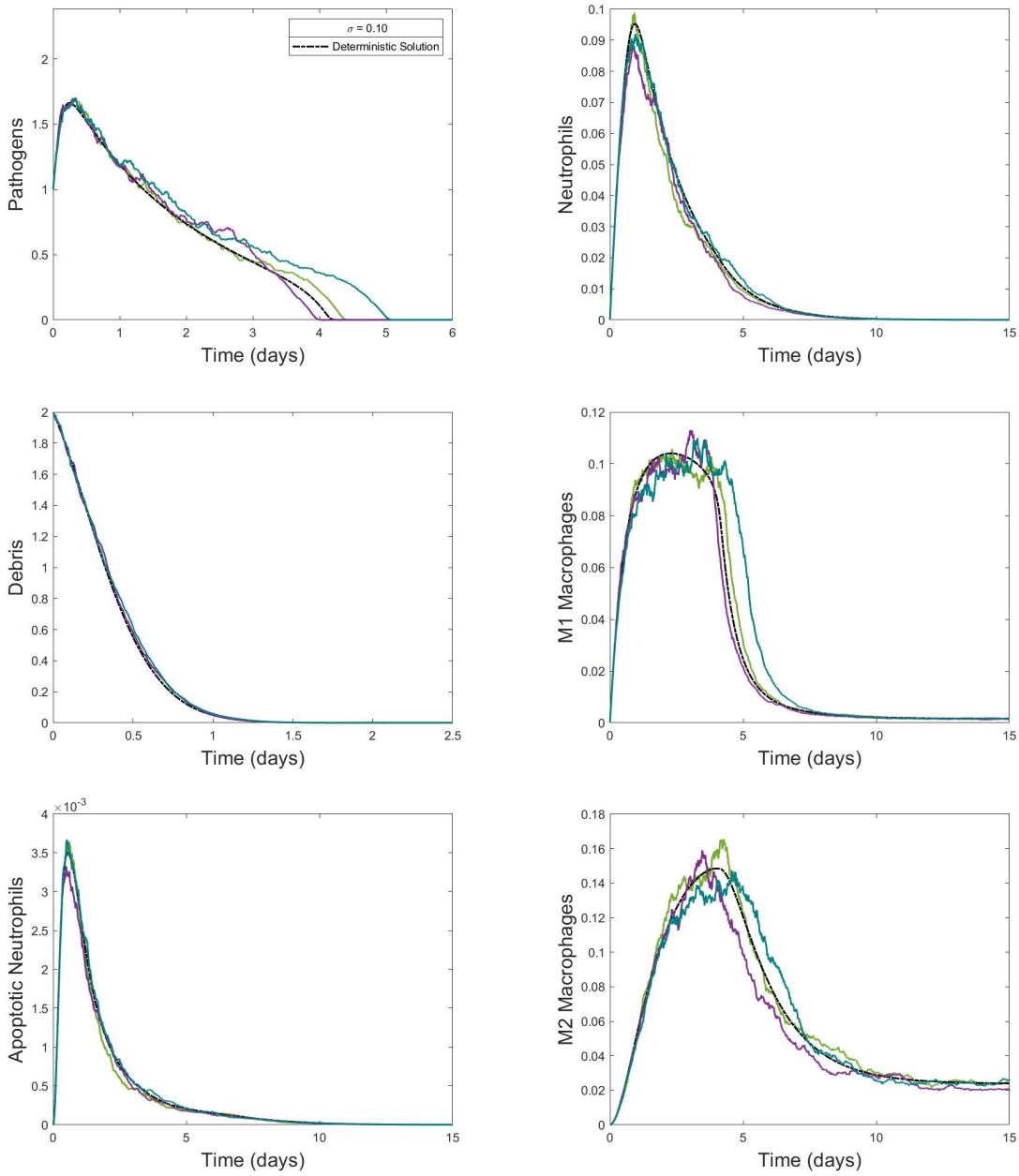

Figure 4.38: Stochastic simulations for each state variable when $\sigma = 0.1$

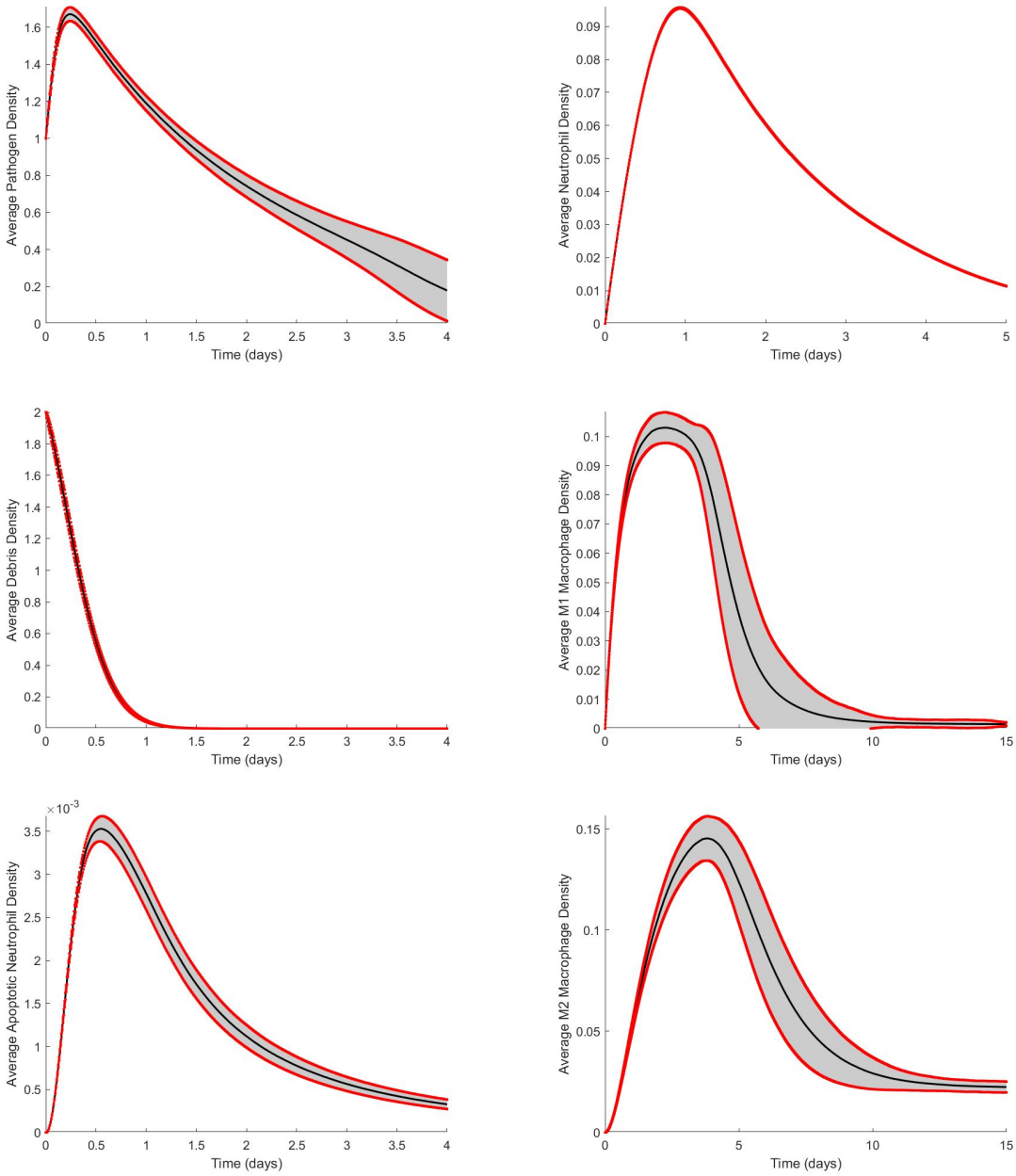

Figure 4.39: Mean and standard deviation of N=5000 simulations when $\sigma = 0.1$

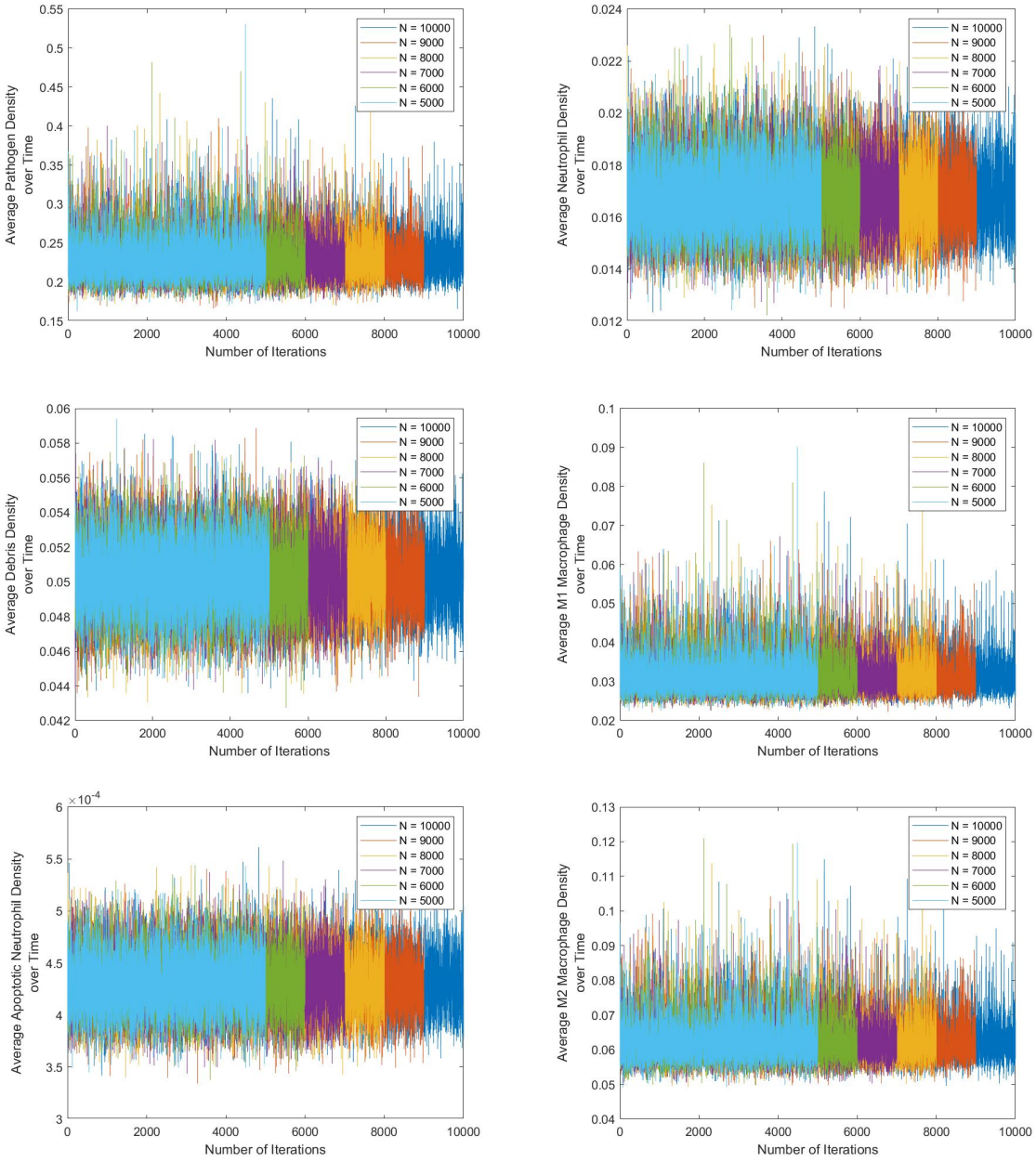

Figure 4.40: Mean of each state variable over time for different number of iterations when $\sigma = 0.1$

Considering $\sigma = 0.5$, example simulations result in different solution times for pathogens and peak values for M2 macrophages (Figure 4.41). Figure 4.39 shows

the mean and standard deviation when N=5000 realizations were simulated. These standard deviation from the mean are larger as expected due to σ being larger (Figure 4.43). Analyzing the changes over the number of simulations, the range in which the mean fluctuates is increased (Figure 4.43).

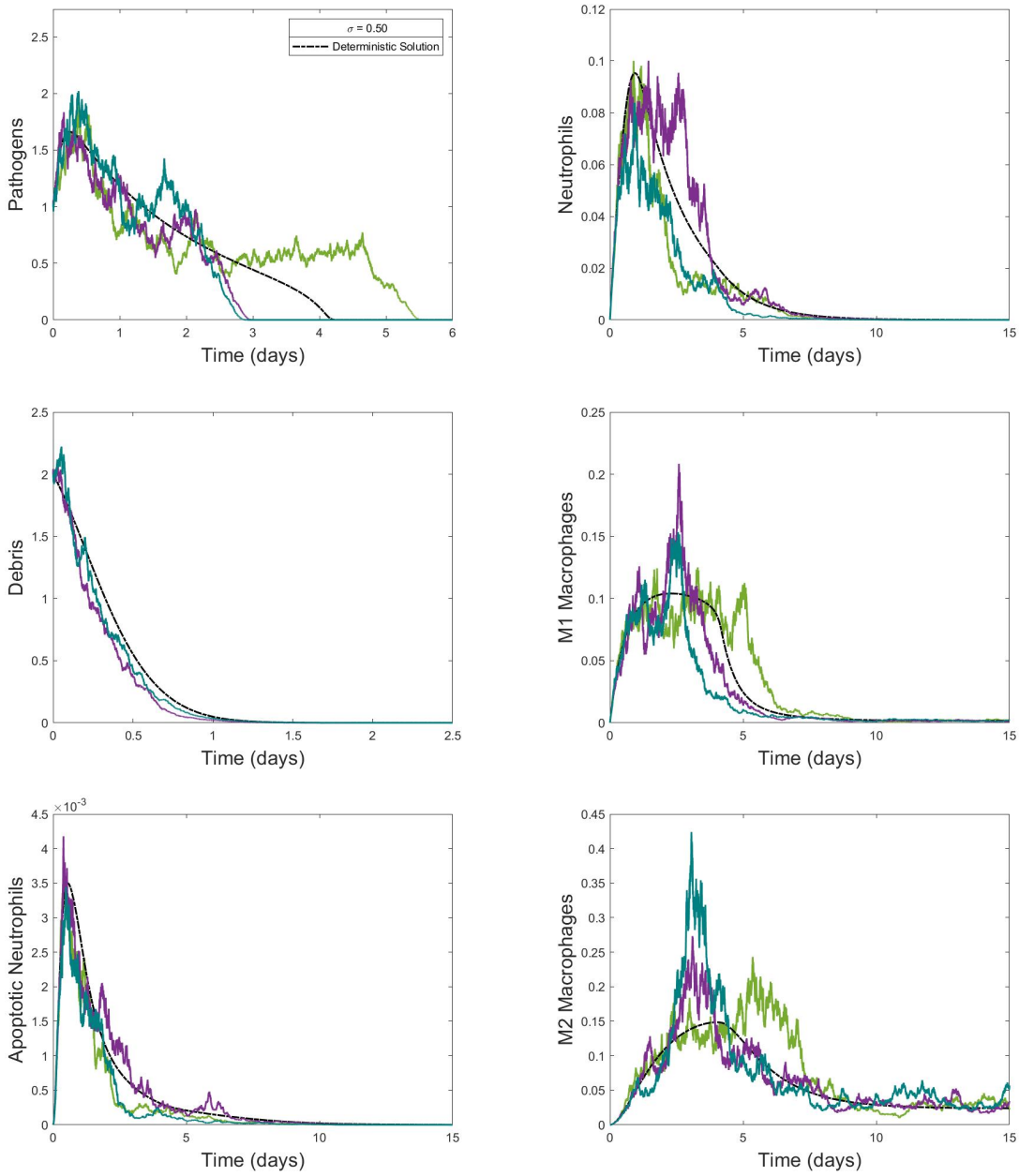

Figure 4.41: Stochastic simulations for each state variable when $\sigma = 0.5$

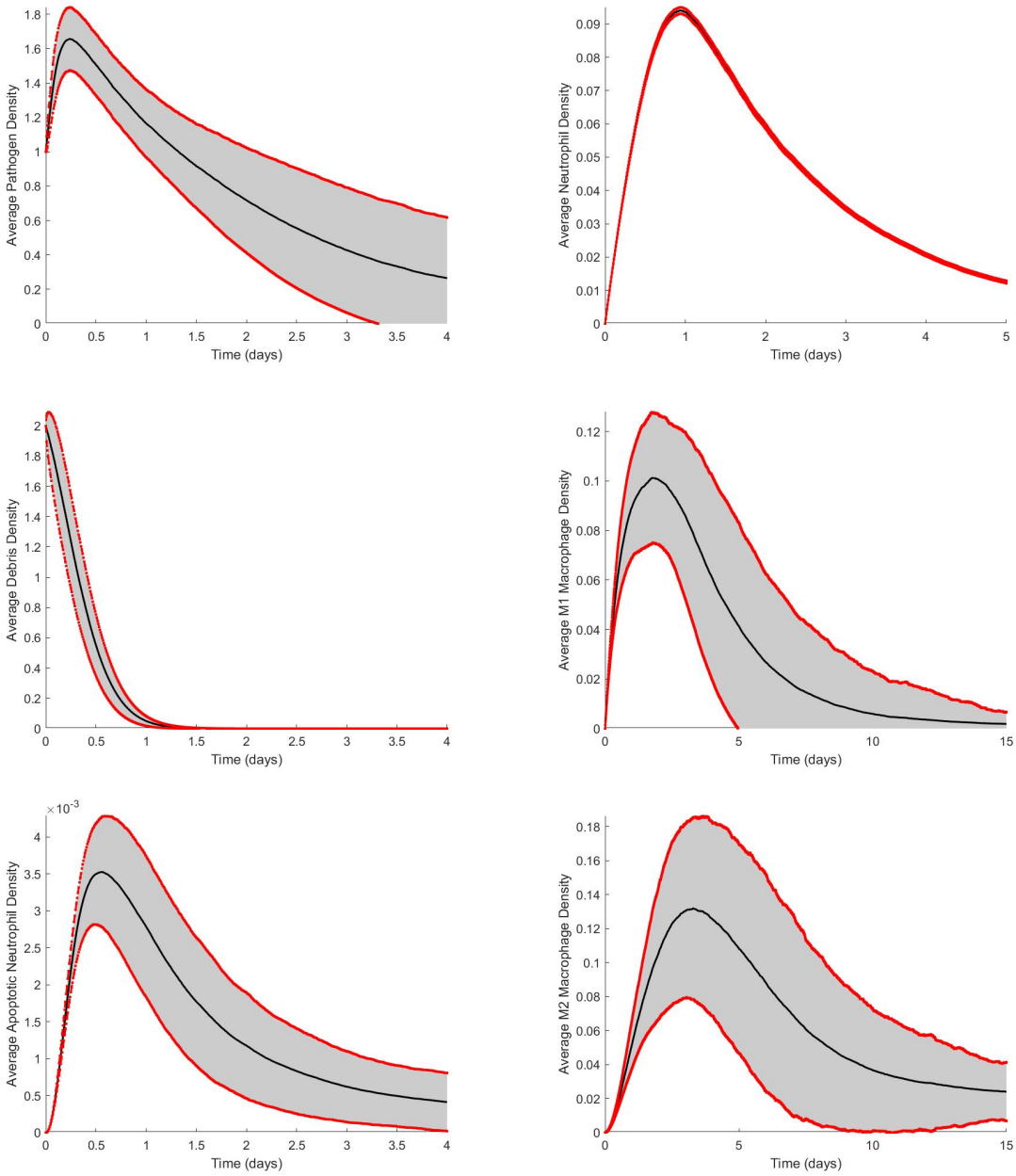

Figure 4.42: Mean and standard deviation of N=5000 simulations when $\sigma = 0.5$

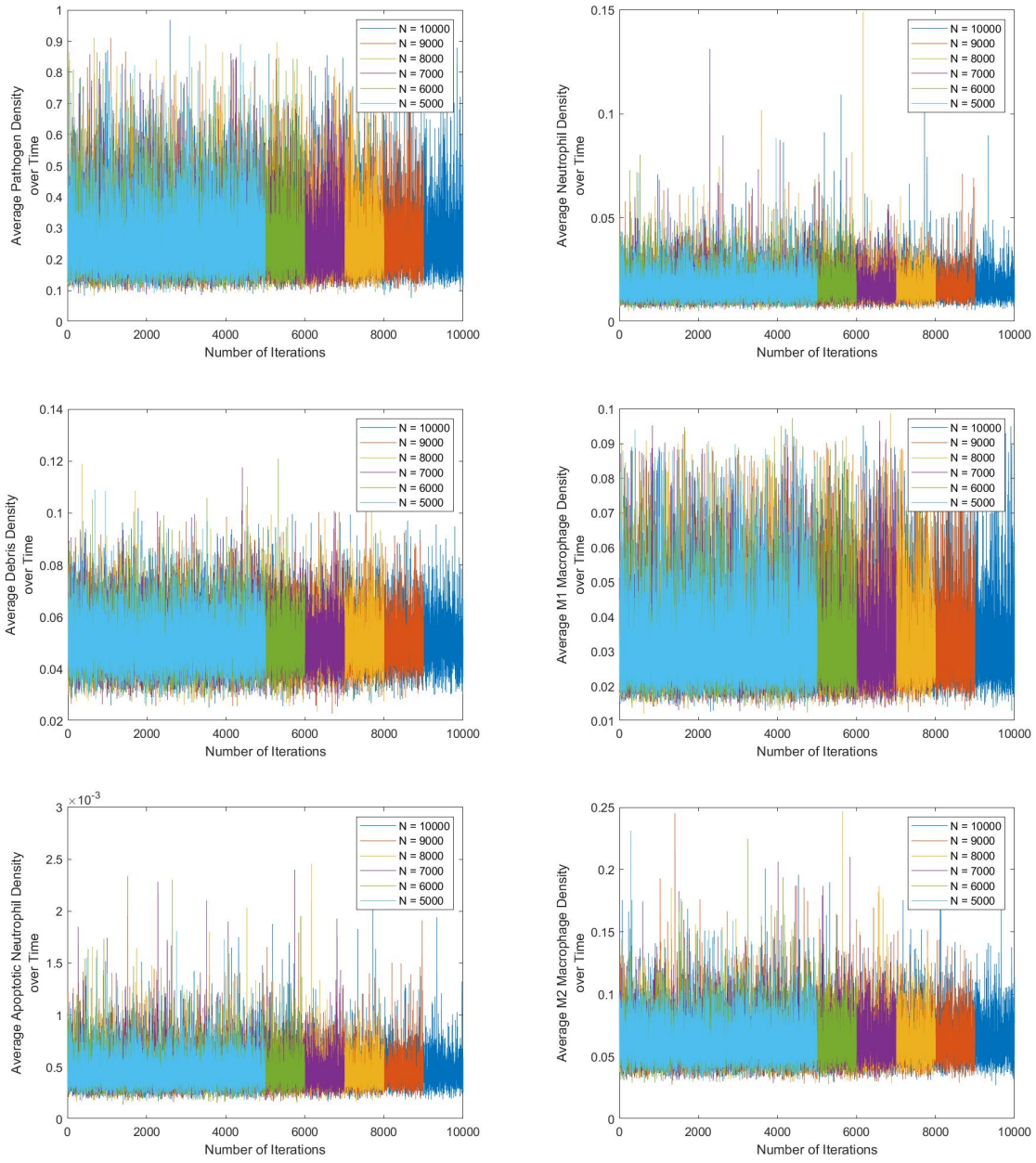

Figure 4.43: Mean of each state variable over time for different number of iterations when $\sigma = 0.5$

CHAPTER 5

PROLIFERATION AND MATURATION MODEL CONSTRUCTION

5.1 Proliferative Phase

In the proliferative phase the focus is shifted from removing debris and pathogens to rebuilding and improving the provisional matrix. An important immunoregulatory cytokine, TGF-β, causes fibroblasts to migrate to the wound by chemotaxis [59, 65]. TGF-β is produced by macrophages [34, 78], neutrophils [22], fibroblasts [10, 18, 29], myofibroblasts [5, 76]. The production of TGF-β is also enhanced by the process of efferocytosis [7, 13, 30, 38, 54, 79, 80]. These fibroblasts produce the major protein component of the ECM which is collagen. Through the influence of TGF-β, fibroblasts can differentiate into a more specialized cell known as a myofibroblast which also produces collagen but also α-smooth muscle actin which causes the edges of the wound to contract.

Proteases play another important part of the proliferative phase. More specifically, matrix metalloproteinases (MMPs) break down collagen. This contributes to the turn over of collagen as the wound heals. There are different types of MMPs such as MMP-1, MMP-3, and MMP-9. MMPs can be produced by macrophages, neutrophils, fibroblasts, and myofibroblasts. TGF-β induces the expression of tissue inhibitors of matrix metalloproteinases (TIMPS) which inhibit MMPs ability to break down collagen.

5.1.1 TGF-β Equation

Since TGF-β is a cytokine that contributes to the ant-inflammatory processes we will incorporate the production of TGF-β by M2 macrophages with the term, $k_2 M_2$. The production from efferocytosis will be represented by the mass action term, $k_{\beta ap} A_N (M_1 + M_2)$. The other terms $k_{\beta N} N$, $k_{\beta F} F k_{\beta My} M_y$, and $\mu_\beta T_\beta$ will represent the production of $TGF - \beta$ from neutrophils, production via fibroblasts, and exit rate of TGF-β, respectively. Incorporating these mechanisms we get the following differential equation

$$\frac{dT_\beta}{dt} = k_{\beta N} N + k_{\beta ap} A_N (M_1 + M_2) + k_{\beta M2} M_2 + k_{\beta F} F + k_{\beta My} M_y - \mu_\beta T_\beta.$$

Since the inflammation model incorporated estrogen, estrogen mediation effects will be also taken into consideration for the proliferative portion. According to Zhou et al. [82], presence of estrogen is associated with an increase production of TGF-β. Adding the effect of estrogen we get the updated equation:

$$\frac{dT_\beta}{dt} = [k_{\beta N} N + k_{\beta ap} A_N (M_1 + M_2) + k_{\beta M2} M_2 + k_{\beta F} F + k_{\beta My} M_y](1 + k_{\beta e} E) - \mu_\beta T_\beta.$$

5.1.2 MMP Equation

MMPs are produced by M1 and M2 macrophages [17, 23, 32, 74], neutrophils [24, 41, 49], fibroblasts [19, 28, 46, 67], and myofibroblasts [47, 68]. In addition to TGF-β's ability to influence migration of fibroblasts to produce collagen, Leivonen

et al. [44] notes that TGF-β also plays a role in down regulating the expression of MMPs. They can do this by inducing the expression of tissue inhibitors of MMPs (TIMPs). Some other sources that disscus this include [20,42,44,63]. This inhibition is incorporated into the M_{MP} equation by including the inhibition term $\frac{1}{1+(\frac{T_\beta}{T_{\beta inh}})^2}$. The production via M1, M2, N, F, and M_y is represented by $k_{MMPM1}M1$, $k_{MMPM2}M_2$, $k_{MMPN}N$, $k_{MMPF}F$, and $k_{MMPMy}M_y$, respectively. Finally the exit term for MMPs are represented by $\mu_{MMP}M_{MP}$. These give the following equation:

$$\frac{dM_{MP}}{dt} = \frac{k_{MMPM1}M1 + k_{MMPM2}M_2 + k_{MMPN}N + k_{MMPF}F + k_{MMPMy}M_y}{1 + (\frac{T_\beta}{T_{\beta inh}})^2} - \mu_{MMP}M_{MP}.$$

5.1.3 Fibroblast and Myofibroblast Equations

For the fibroblast equation the migration to the wound via chemotaxis from TGF-β is represented by the term $c_{F\beta}T_\beta$, and then after these cells migrate, they can proliferate [59,65]; this is represented by the term $p_F F$. This proliferation may be enhanced by the presence of TGF-β. This is represented by the term $k_{F\beta}T_\beta F$. Fibroblasts can then differentiate into myofibroblasts ($d_F F$) and this is a process that can also be enhanced by the presence of TGF-β [64,72] ($k_{MyF\beta}FT_\beta$). Fibroblasts that do not differentiate either leave the wound or commit apoptosis. The exit term is represented by $\mu_F F$. Taking these mechanisms into account, the differential equation for fibroblasts is constructed as the following:

$$\frac{dF}{dt} = c_{F\beta}T_\beta + p_F F + k_{F\beta}T_\beta F - d_F F - k_{MyF\beta}FT_\beta - \mu_F F.$$

For myofibroblasts, we have the differentiation of fibroblasts ($d_f F + k_{MyF\beta} F T_\beta$) and the exit term $\mu_{my} M_y$ giving the following equation:

$$\frac{dM_y}{dt} = d_F F + k_{MyF\beta} F T_\beta - \mu_{my} M_y.$$

5.1.4 Collagen Equations

Fibroblasts and myofibroblasts secrete different types of collagen including collagen type I and type III [2]. Type III collagen is a weaker form of collagen than type I. At the beginning stages of extracellular matrix reformation, type III collagen is produced, but is later replaced by stronger type I collagen [11]. The presence of TGF-β enhances the process of collagen secretion, so the secretion of type I collagen with and without the enhancement of TGF-β is represented by $k_{cwf}(F + M_y)(1 + k_{ctb} T_\beta) + k_{cmy} M_y$. Collagen is defined as a percentage where 0 indicating no collagen in the wound and 1 indicating collagen has filled the wound. Similarly to the assumption implemented in Segal et al. [66], the state of existing collagen will affect the rate at which collagen is formed and broken down. To account for this, a collagen deposition multiplier was implemented and defined as $I(C_I + C_{III}) = \frac{1}{1+e^{a(C_I + C_{III} - b)}}$ (Figure 5.1). For $a = 20$ and $b = 0.7$, when the percentage of collagen in the wound is closer to zero, the multiplier is closer to 1, hence having negligible inhibition on the deposition. As the collagen content gets closer to 100 percent, the inhibition takes more effect. A similar inhibition is also implemented for degradation by MMPs. Here the term $1 - \frac{1}{1+e^{a(C_{III} + C_I - b)}}$ is used which when When $a = 20$ and $b = 0.7$ and $C_{III} + C_I \to 1$, the inhibition gets closer to 0, allowing more MMPs to degrade collagen. However, when $C_{III} + C_I \to 0$, the inhibition takes more into affect, inhibiting the breakdown by MMPs. After collagen

type III collagen comes into contact with MMPs and is broken down, it is assumed that type III collagen will be deposited in its place by fibroblasts and myofibroblasts.

Finally, the negative effect on the ECM from by-products of neutrophils are taken into account for collagen type III by the term $d_{cn}C_{III}N$. Taking into account these mechanisms, the following is the resulting equations for collagen type I and collagen type III:

$$\frac{dC_{III}}{dt} = \frac{k_{cwf}(F + M_y)(1 + k_{ctb}T_\beta) + k_{cmy}M_y}{1 + e^{a(C_{III}+C_I-b)}} - d_{cn}C_{III}N - d_{cMmp}M_{MP}C_{III}(1 - \frac{1}{1 + e^{a(C_{III}+C_I-b)}})$$

$$\frac{dC_I}{dt} = k_{csf}\frac{M_{MP}C_{III}(F + M_y)}{1 + e^{a(C_{III}+C_I-b)}}$$

where $C_{III} + C_I \leq 1$.

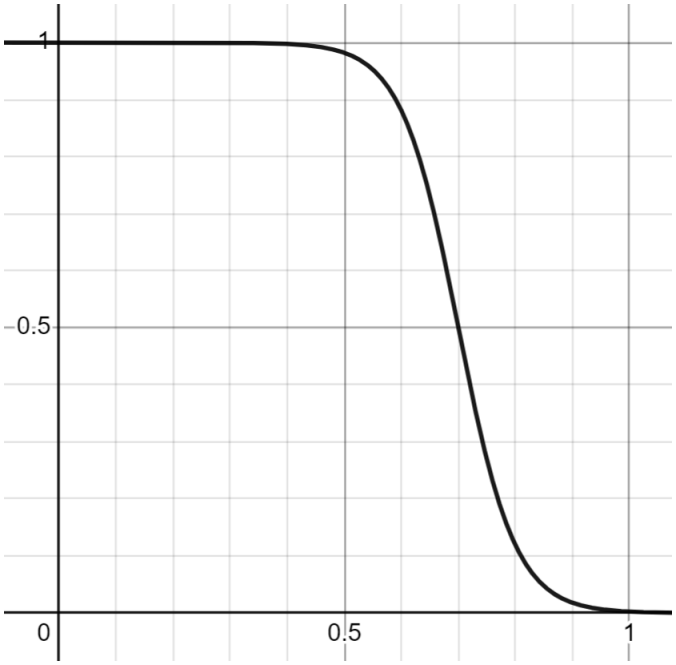

Figure 5.1: Collagen Deposition Effect = $\frac{1}{1+e^{a(Collagen-b)}}$. Depostion Effect when a = 20 and b = 0.7

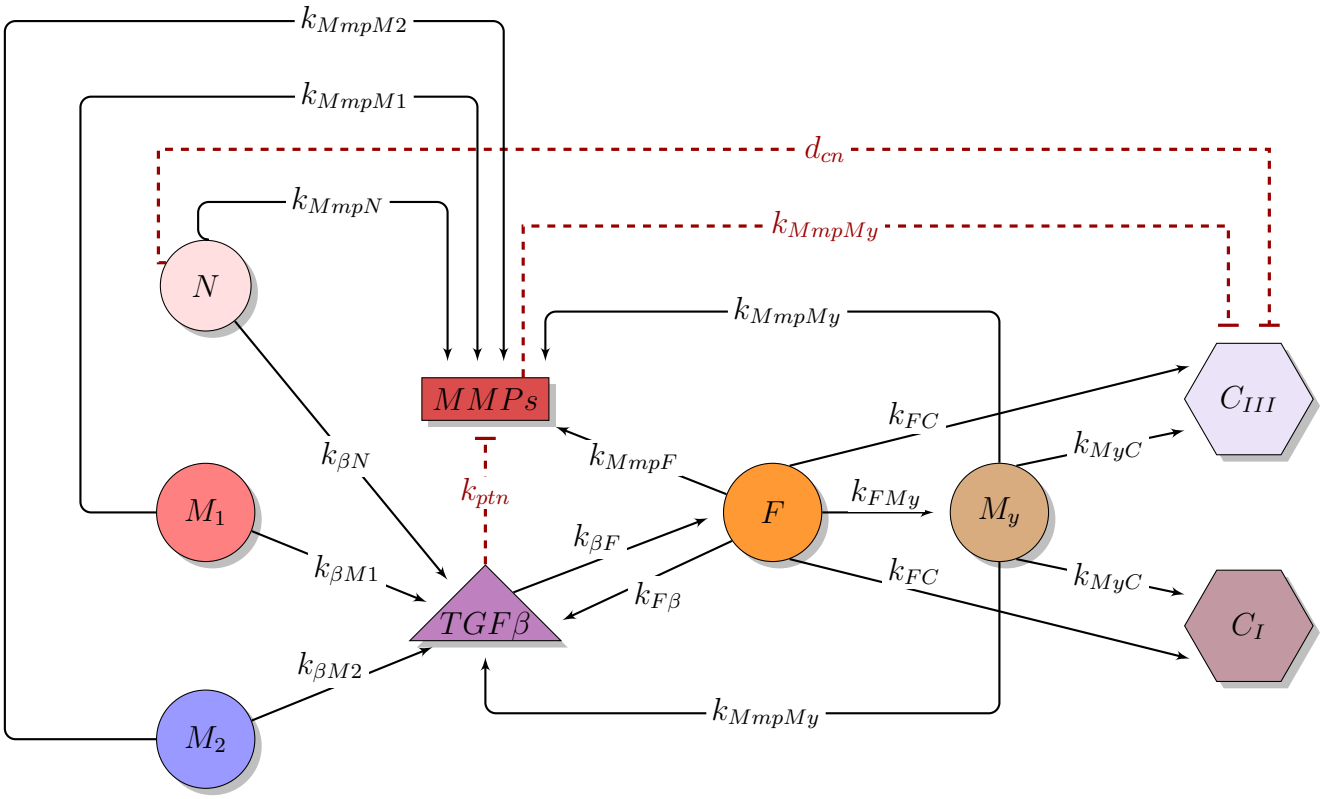

Figure 5.2: Proliferation and maturation model schematic. Dynamics of inflammatory system and parameters involved in each corresponding transition where arrows, $\rightarrow$, indicate upregulation, and bars, $\dashv$, indicate inhibition. Phenomena involved with upregulation include release of substance that promotes differentiation of a predecessor cell, proliferation of the state variable, release of substance that adds to the state variable, or the differentiation of the state variable into the following state variable. The phenomena involved with inhibition is TGF-β's association with an induced presence of TIMPs which are known to inhibit MMPs [34, 42], and the byproducts of neutrophils that cause tissue damage [75].

CHAPTER 6

PROLIFERATION AND MATURATION MODEL ANALYSES AND RESULTS

6.1 Final Equations

A schematic of the relationship between the final stages of the inflammation stage and the state variables of the proliferation and remodeling phase is provided in Figure 5.2. The final system for the proliferation and remodeling stage is the following:

$$
\begin{aligned}
\frac{dT_\beta}{dt} &= k_{\beta N}N + k_{\beta ap}A_N(M_1+M_2) + k_{\beta M2}M_2 + k_{\beta F}F + k_{\beta My}M_y - \mu_\beta T_\beta \\
\frac{dM_{MP}}{dt} &= \frac{k_{MMPM1}M1 + k_{MMPM2}M_2 + k_{MMPN}N + k_{MMPF}F + k_{MMPMy}M_y}{1+(\frac{T_\beta}{T_{\beta inh}})^2} - \mu_{MMP}M_{MP} \\
\frac{dF}{dt} &= c_{F\beta}T_\beta + p_F F + k_{F\beta}T_\beta F - d_F F - k_{MyF\beta}FT_\beta - \mu_F F \\
\frac{dM_y}{dt} &= d_F F + k_{MyF\beta}FT_\beta - \mu_{my}M_y \\
\frac{dC_{III}}{dt} &= \frac{k_{cwf}(F+M_y)(1+k_{ctb}T_\beta)+k_{cmy}M_y}{1+e^{a(C_{III}+C_I-b)}} - d_{cn}C_{III}N - d_{cMmp}M_{MP}C_{III}(1-\frac{1}{1+e^{a(C_{III}+C_I-b)}}) \\
\frac{dC_I}{dt} &= k_{csf}\frac{M_{MP}C_{III}(F+M_y)}{1+e^{a(C_{III}+C_I-b)}}
\end{aligned}
$$

6.2 Proliferation and Remodeling stage parameters

In order to estimate parameter values, the following assumption were used in addition to the data from an immunohistochemistry experiment in Kajikawa et al. [35] was used (Figure 6.1). The following are the assumption used:

1. Fibroblasts peak between day 7 and day 14 [4, 66]
2. Myofibroblasts peak after fibroblasts peak
3. Collagen finishes being deposited by day 56 [66]
4. MMPs peak around day 5 [34]

In order to use the data, the data for collagen type I and collagen type III was scaled. In a normal state a pre-wounded area has a certain amount of different type of collagen. Collagen type I encompasses a larger amount. For some type of tissue this is around 80 percent, and collagen type III encompasses 20 percent or less [12, 57]. Using the assumption that collagen finishes being deposited by day 56, the signal on the last day of the data in Kajikawa et al. [35] is scaled so that these values are 0.8 and 0.2 for collagen I and collagen III, respectively. The the rest of the values are scaled using the same factor giving the proportion value in the wound (Table 6.1). Using the assumptions and the new data a parameter set is found and is provided in Table 6.2. The corresponding simulations are in Figure 6.2.

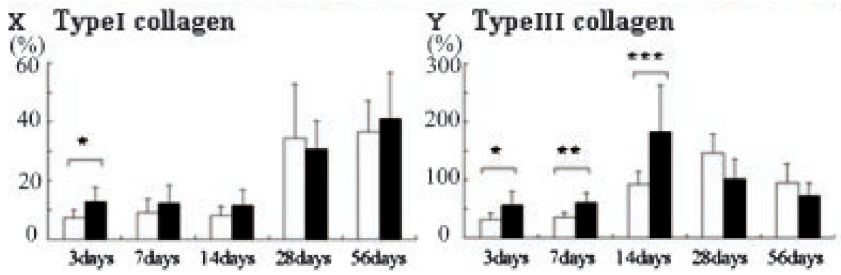

Figure 6.1: Immunoreactivity signal of type I and type III collagen over time in [35]

Table 6.1: Type I and type III collagen data from [35] and data after scaling

	Immunoreactivity Signal			Wound Percent	
	Collagen I	Collagen III		Collagen I	Collagen III
Day 3	7.183 ±4.442	33.333 ±11.111		0.156 ±0.096	0.0689 ±0.0230
Day 7	9.688 ±4.687	36.508 ±9.524		0.210 ±0.1017	0.0754 ±0.0198
Day 14	8.438 ±3.437	149.206 ±112.899	$\longrightarrow$	0.1831 ±0.0746	0.308 ±0.233
Day 28	35 ±17.813	93.651 ±86.349		0.759 ±0.386	0.193 ±0.178
Day 56	36.875 ±10.625	93.825 ±33.175		0.8 ±0.231	0.2 ±0.0685

Table 6.2: Parameter descriptions and results after optimization

TGF-β Equation			
Parameter	Description	Estimation based on general dynamics and data	Unit
$k_{\beta n}$	Production of TGF-β by neutrophils	0.679	$\frac{\frac{T\beta}{N-units}}{day}$
$k_{\beta m2}$	Production of TGF-β by M2 macrophages	1.713	$\frac{\frac{T_\beta}{M-units}}{day}$
$k_{\beta an}$	Production of TGF-β which is affected by phagocyation of apoptotic neutrophils	3.314	$\frac{\frac{T_\beta}{M-units*AN-uits}}{day}$
$k_{\beta f}$	Production of TGF-β by fibroblasts	0.124	$\frac{\frac{T_\beta}{F-units}}{day}$
$k_{\beta My}$	Production of TGF-β by myofibroblasts	0.153	$\frac{\frac{T_\beta}{My-units}}{day}$
$k_{\beta e}$	Increase in TGF-β caused by estrogen	6.067	$\frac{1}{E-units}$
μ_β	Exit rate of TGF-β	1.144	$\frac{1}{day}$

MMP Equation			
Parameter	Description	Estimation based on general dynamics and data	Unit
k_{MmpM1}	Production of MMPs by M1 macrophages	0.001	$\frac{\frac{MMP}{M-units}}{day}$
k_{MmpM2}	Production of MMPs by M2 macrophages	9.505	$\frac{\frac{MMP}{M-units}}{day}$
k_{MmpN}	Production of MMPs by neutrophils	0.001	$\frac{\frac{MMP}{N-units}}{day}$
k_{MmpF}	Production of MMPs by fibroblasts	0.212	$\frac{\frac{MMP}{F-units}}{day}$
k_{MmpMy}	Production of MMPs by Myofibroblasts	0.007	$\frac{\frac{MMP}{My-units}}{day}$
$T_{\beta Timp}$	Inhibition of MMPs by increase of TIMPs caused by TGF-β	19.999	$T_\beta - units$
μ_{Mmp}	Exit rate of MMPs	0.398	$\frac{1}{day}$
Fibroblast and Myofibroblast Equations			
Parameter	Description	Estimation based on general dynamics and data	Unit
c_{fb}	Chemeotaxis of fibroblasts stimulated by TGF-β	0.256	$\frac{\frac{F-units}{T_\beta-units}}{day}$
p_f	Proliferation rate of fibroblasts	0.704	$\frac{1}{day}$
k_{fb}	Proliferation of fibroblasts stimulated by TGF-β	0.0001	$\frac{\frac{1}{T_\beta}}{day}$
d_f	Differentiation rate of fibroblasts	0.001	$\frac{1}{day}$
$k_{myF\beta}$	Differentiation of fibroblasts influenced by TGF-β	1.012	$\frac{1}{day}$
μ_f	Exit rate of fibroblasts	0.0001	$\frac{\frac{1}{T_\beta-units}}{day}$
μ_{my}	Exit rate of myofibroblasts	0.943	$\frac{1}{day}$

Collagen Equations			
Parameter	Description	Estimation based on general dynamics and data	Unit
k_{cwf}	Production rate of type III collagen by fibroblasts and myofibroblasts	4.777	$\frac{\frac{C_{III}-units}{F-units}}{day}$
k_{ctb}	Influence of production rate of type III collagen by TGF-β	0.001	$\frac{1}{T_\beta - units}$
k_{cmy}	Increased production rate of type III collagen by myofibroblasts not influenced by TGF-β where $k_{cwf} + k_{cmy}$ is the total production rate	0.018	$\frac{\frac{C_{III}-units}{My-units}}{day}$
d_{cn}	Destruction of type III collagen by byproducts of neutrophils	0.001	$\frac{\frac{1}{N-units}}{day}$
d_{cmmp}	Destruction of type III collagen by MMPs	22.359	$\frac{\frac{1}{M-units}}{day}$
k_{csf}	Replacement of type III collagen by type I collagen by fibroblasts and myofibroblasts after degradation from MMPs	0.414	$\frac{\frac{1}{A_N-units}}{day}$
a	Parameter that controls production and destruction of collagen type I and type III	0.001	
b	Parameter that controls production and destruction of collagen type I and type III	0.7	

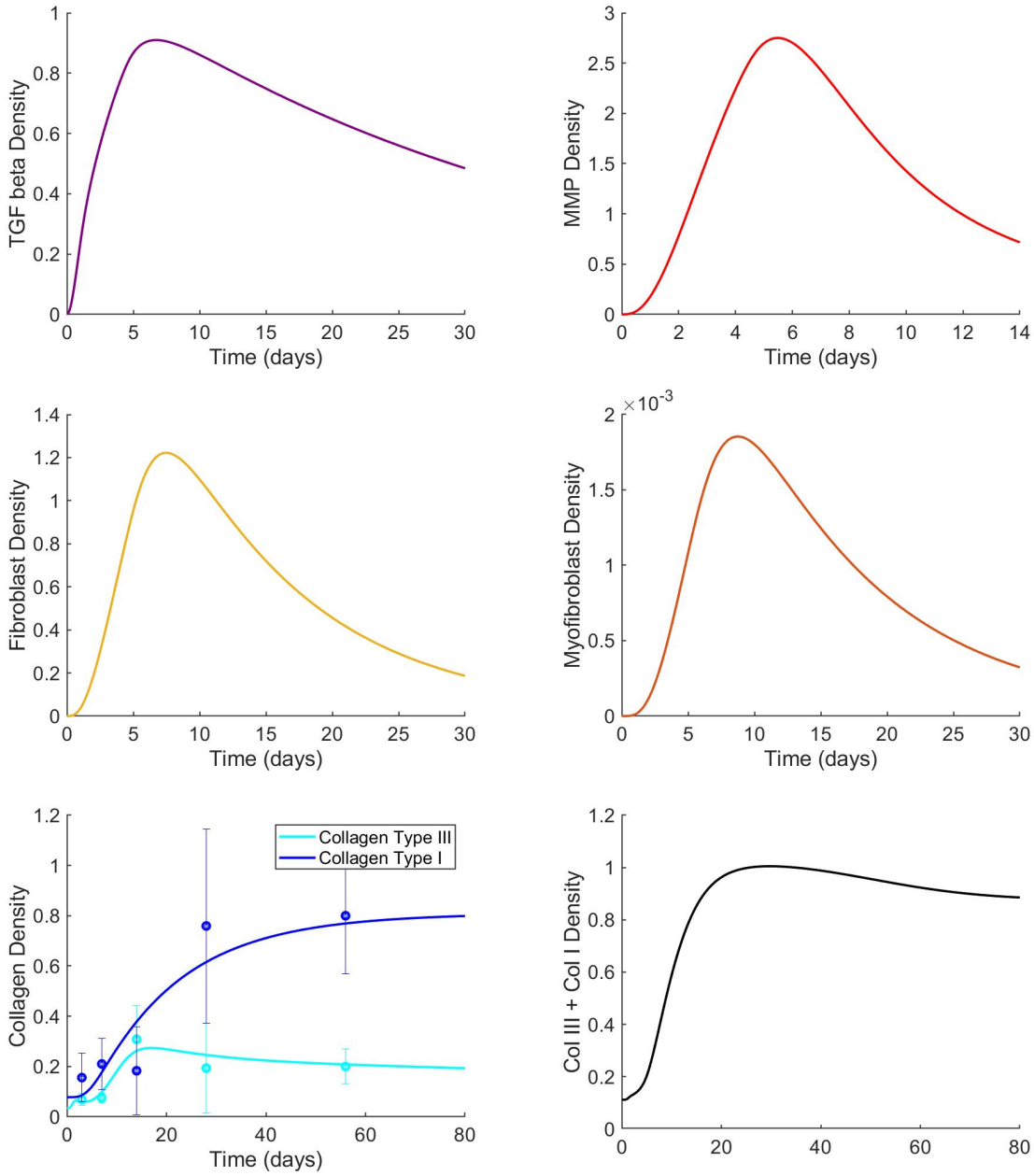

Figure 6.2: Transients resulting from assumptions based on literature with $P_0 = 1$ and $P_{t0} = 2$

6.3 Global sensitivity analysis for proliferation and remodeling stage

Global senstivity analysis for for the whole model was conducted with respect to total collagen, that is, $C_I + C_{III}$. In order to help reduce the sampling space, the parameters associated with the smallest sensitivity indices for total inflammation variable average where left out (see Figure 4.33). For the parameters associated with higher indices, the same range that was used is used for the inflammation sensitivity analysis was used again here. For the proliferation and remodeling parameters, a set range around the parameter set in Table 6.2 was used.

For total collagen the standard deviation away from the mean increases at a high rate (Figure 6.3). Parameters that resulted in a higher sensitivity index were kmmpn (production of MMPs by neutrophils), kpg (growth rate of pathogens), ummp (decay rate of MMPs), dcn (destruction of type III collagen by byproducts of neutrophils) , sb (source of background immune response), kem (estrogen increase in the phagocytic abilities of macrophages), and kmmpm2 (production of MMPs by M2 macrophages) (Figure 6.4 and 6.5).

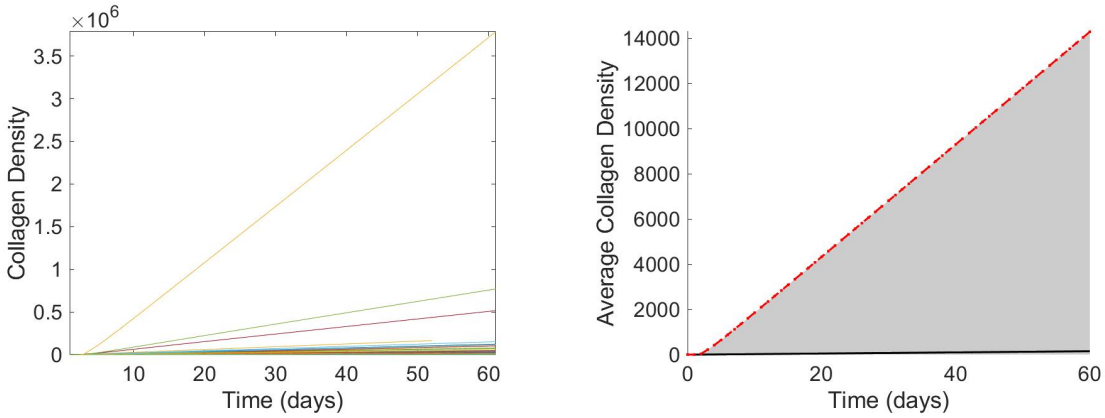

(a) Simulations (b) Mean and Standard Deviation

Figure 6.3: Simulations of Total Collagen Density after Sampling and the Average Pathogen Density of the Simulations

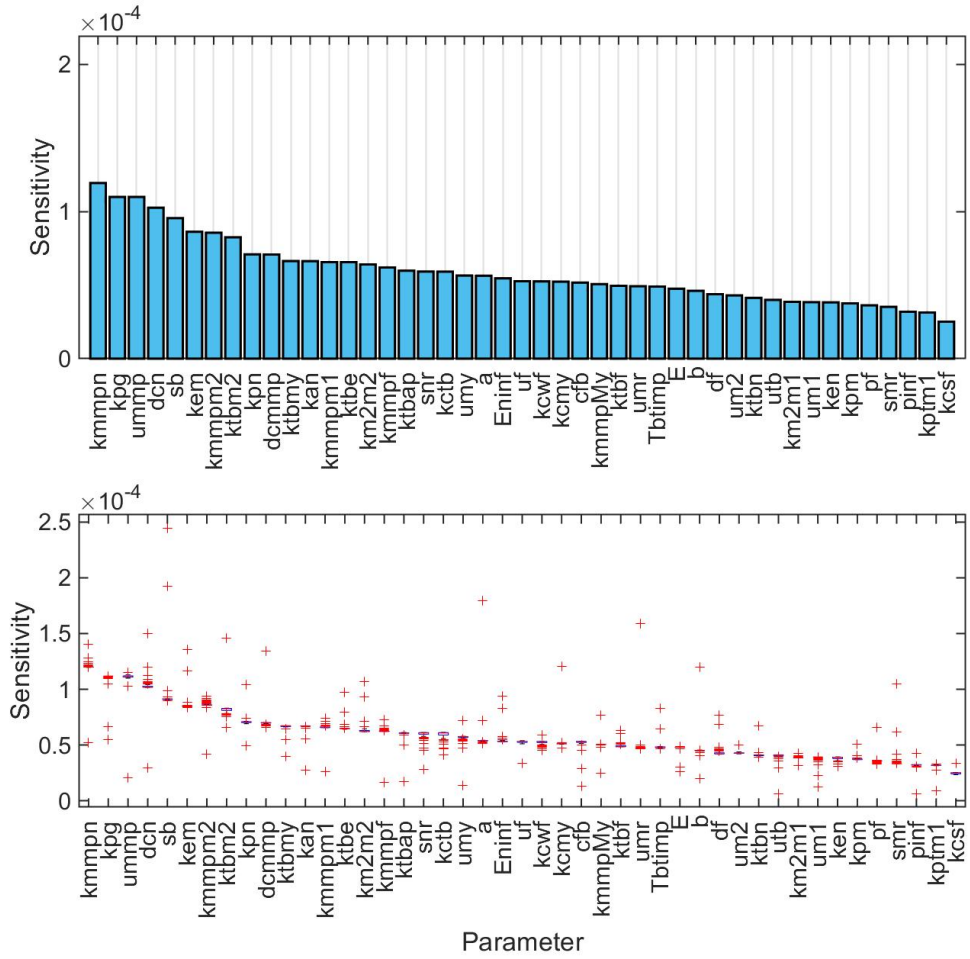

Figure 6.4: FAST global sensitivity analysis results: Mean and box plot of sensitivity for total collagen density over time

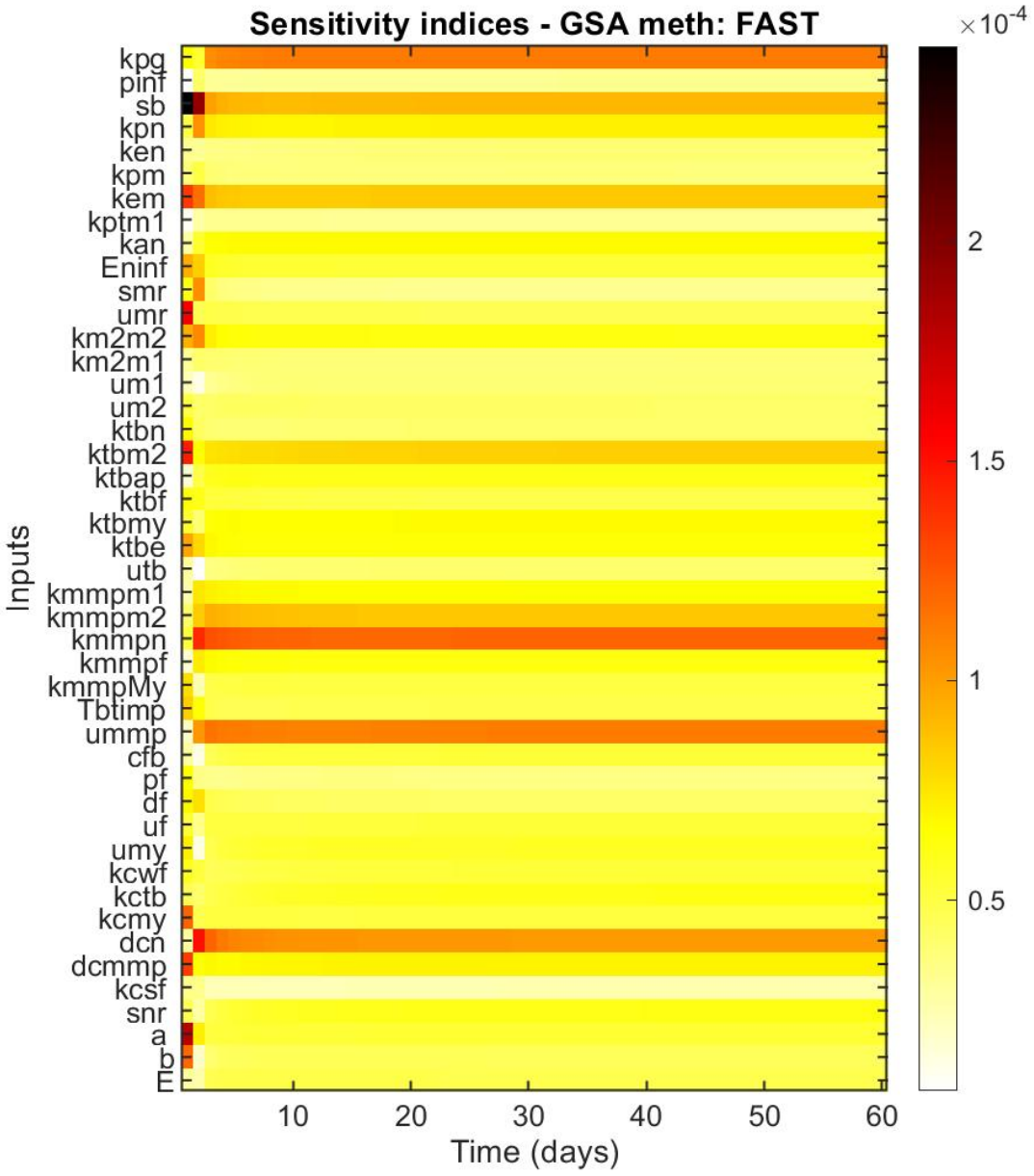

Figure 6.5: FAST global sensitivity analysis results: Sensitivity for total collagen over 15 days

6.3.1 Stochastic Differential Equation System

Next a random process was implemented for each state variable equation as before, giving a stochastic differential equation system. Let the random processes $W_{T\beta}(t), W_{mmp}(t), W_F(t), W_{My}(t), W_{C3}(t)$, and $W_{C1}(t)$ be independent standard Brownian motions affecting the densities of $T_\beta, M_{MP}, F, M_y, C_{III}$, and C_I, respectively. Similarly to the inflammation system, the white noise terms proportional to the state variable are implemented for each equation. The stochastic differential equation system for the proliferation and remodeling variables is as follows:

$$
\begin{aligned}
dT_\beta &= [\ k_{\beta N}N + k_{\beta ap}A_N(M_1+M_2) + k_{\beta M2}M_2 + k_{\beta F}F + k_{\beta My}M_y - \mu_\beta T_\beta\ ]\ dt + \sigma T_\beta dW_{T\beta}(t) \\
dM_{MP} &= [\ \frac{k_{MMPM1}M1 + k_{MMPM2}M_2 + k_{MMPN}N + k_{MMPF}F + k_{MMPMy}M_y}{1+(\frac{T_\beta}{T_{\beta inh}})^2} \\
&\quad -\mu_{MMP}M_{MP}\ ]\ dt + \sigma M_{MP} dW_{mmp}(t) \\
dF &= [\ c_{F\beta}T_\beta + p_F F + k_{F\beta}T_\beta F - d_F F - k_{MyF\beta}FT_\beta - \mu_F F\ ]\ dt + \sigma F d_F W_F(t) \\
dM_y &= [\ d_F F + k_{MyF\beta}FT_\beta - \mu_{my}M_y\ ]\ dt + \sigma M_y dW_{My}(t) \\
dC_{III} &= [\ \frac{k_{cwf}(F+M_y)(1+k_{ctb}T_\beta) + k_{cmy}M_y}{1+e^{a(C_{III}+C_I-b)}} - d_{cn}C_{III}N \\
&\quad -d_{cMmp}M_{MP}C_{III}(1-\frac{1}{1+e^{a(C_{III}+C_I-b)}})\ ]\ dt + \sigma C_{III} dW_{C3}(t) \\
dC_I &= [\ k_{csf}\frac{M_{MP}C_{III}(F+M_y)}{1+e^{a(C_{III}+C_I-b)}}\ ]\ dt + \sigma C_I dW_{C1}(t)
\end{aligned}
$$

Realizations were simulated for $\sigma = 0.1$ using Milstein method. Some realizations were simulated showing fluctuations in the peak of M1 macrophages and resulting low and high values for collagen type I (Figure 6.6 and Figure 6.7). The mean of 50,

1000, and 5000 simulations of each variable was analyzed (Figure 6.8 - 6.13) . These means are identical to the deterministic solution (Figure 6.12 and Figure 6.13). Then the result of taking the mean over 60 days for each iteration is analyzed, the mean for each variable is bounded between a certain range indicted in (Figure 6.14 and Figure 6.15).

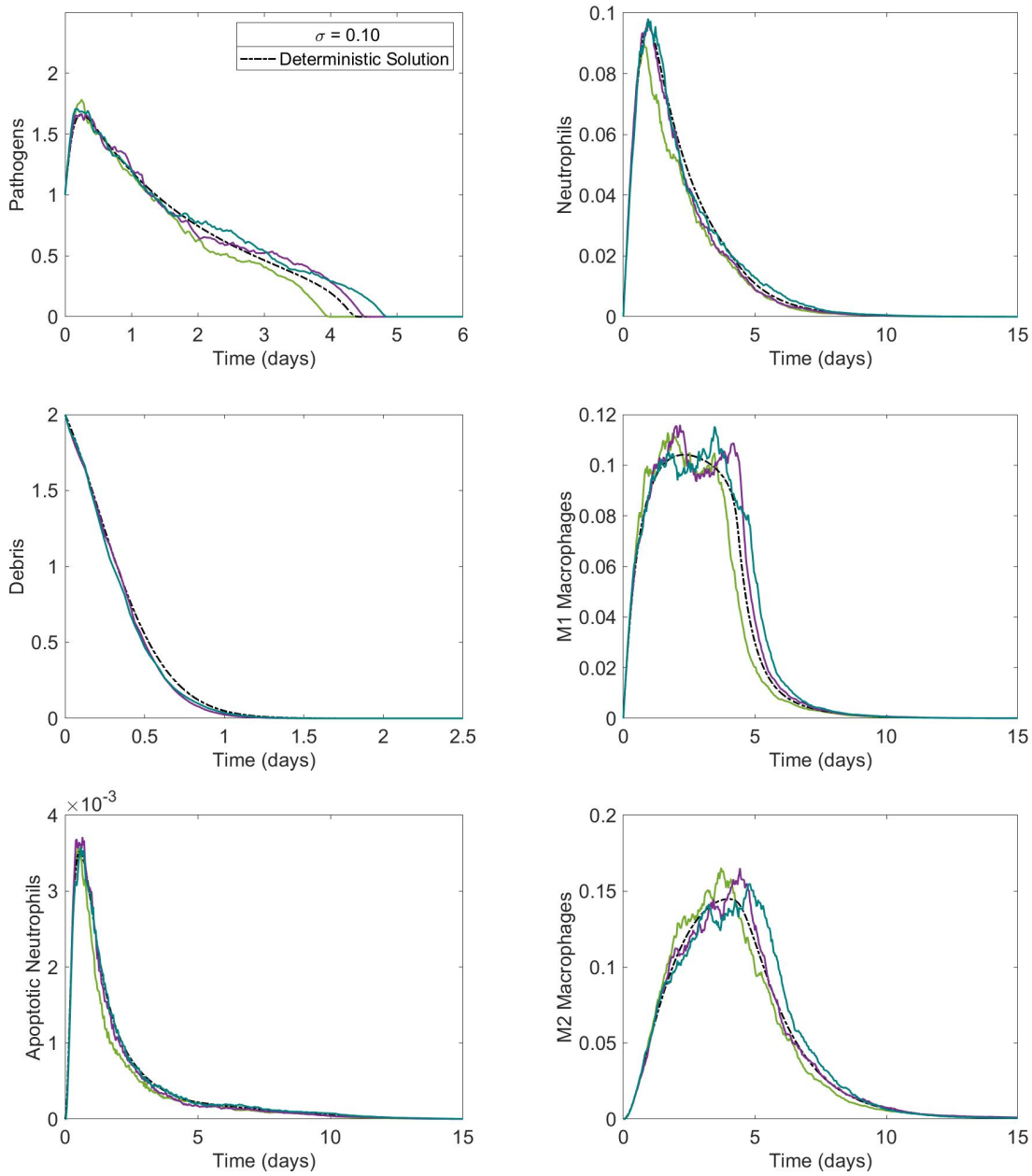

Figure 6.6: Stochastic Simulations for each State Variable of the Inflammation Stage when $\sigma = 0.1$

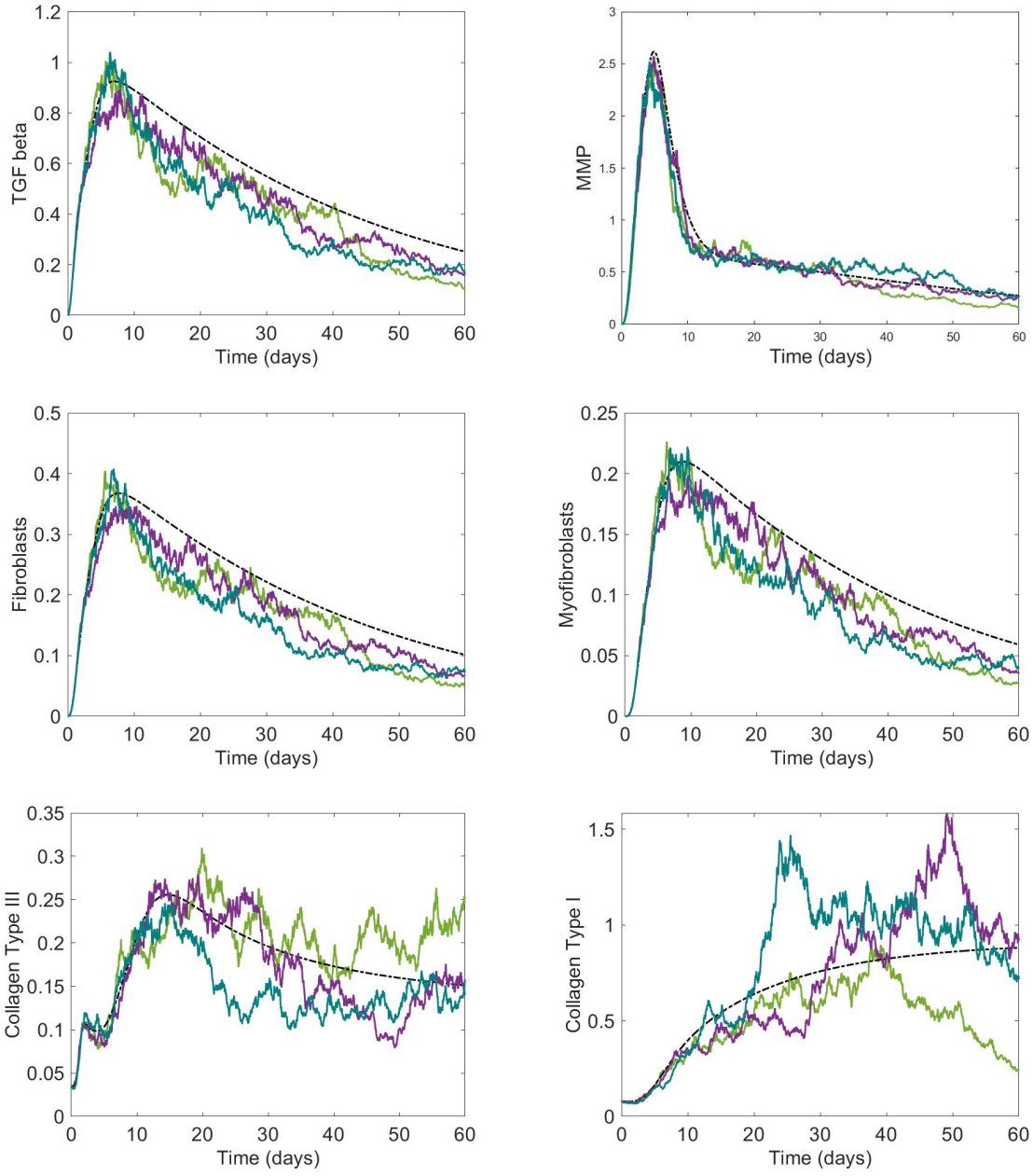

Figure 6.7: Stochastic simulations for each state variable of the proliferation and remodeling stage when $\sigma = 0.1$

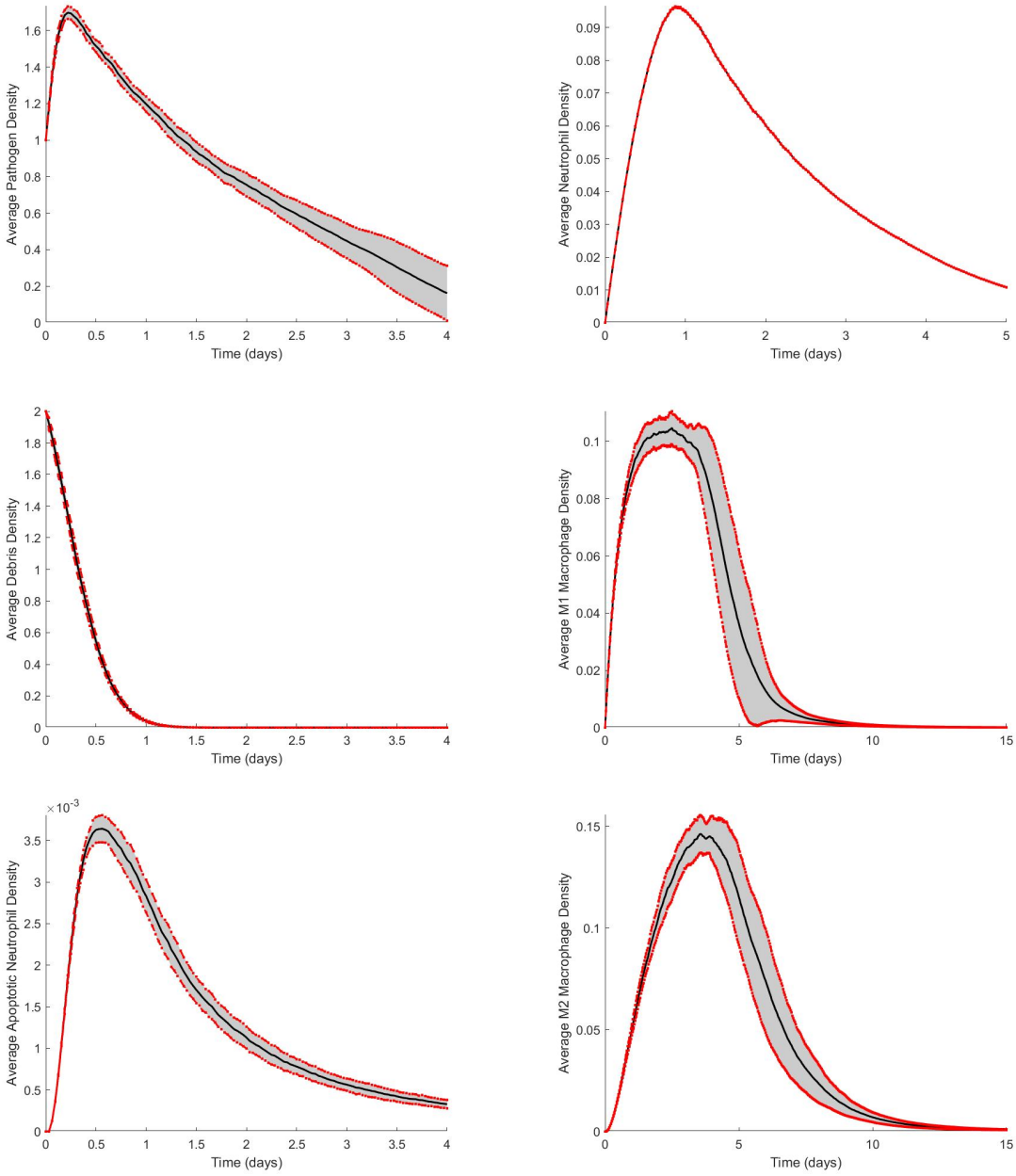

Figure 6.8: Mean and standard deviation of N=50 simulations of the inflammation variables when $\sigma = 0.1$

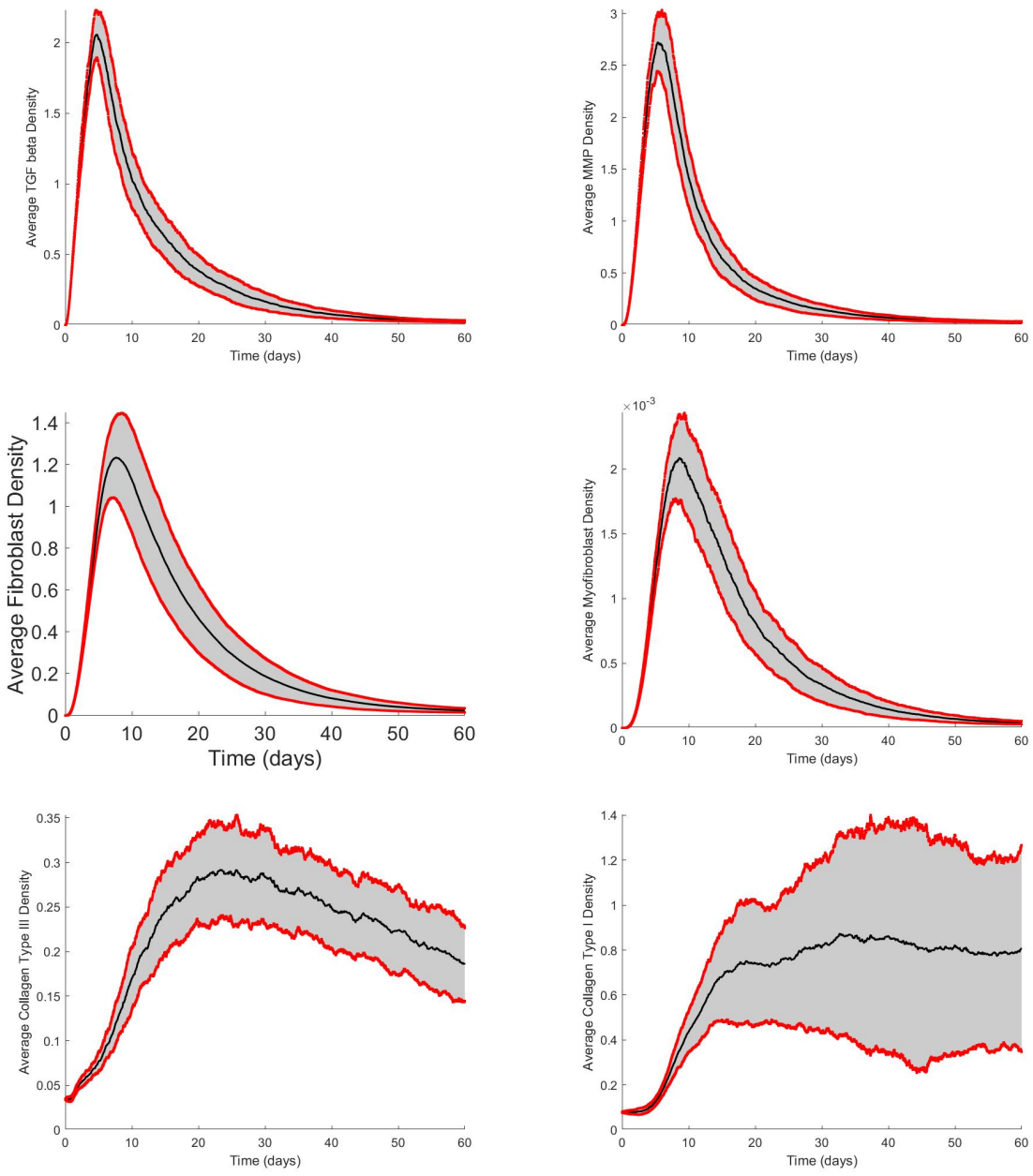

Figure 6.9: Mean and standard deviation of N=50 simulations of the proliferation and remodeling variables when $\sigma = 0.1$

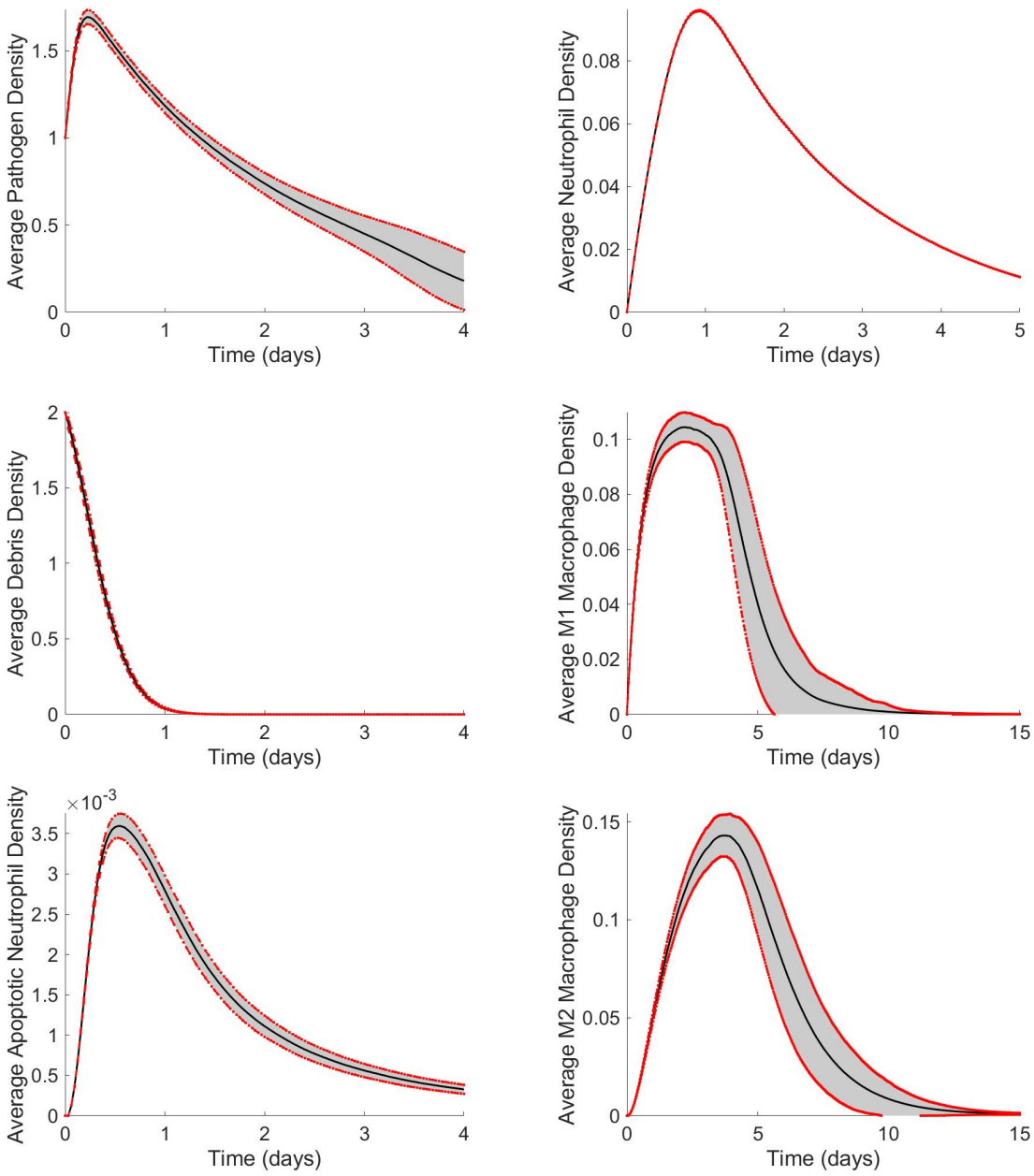

Figure 6.10: Mean and standard deviation of N=1000 simulations of the inflammation variables when $\sigma = 0.1$

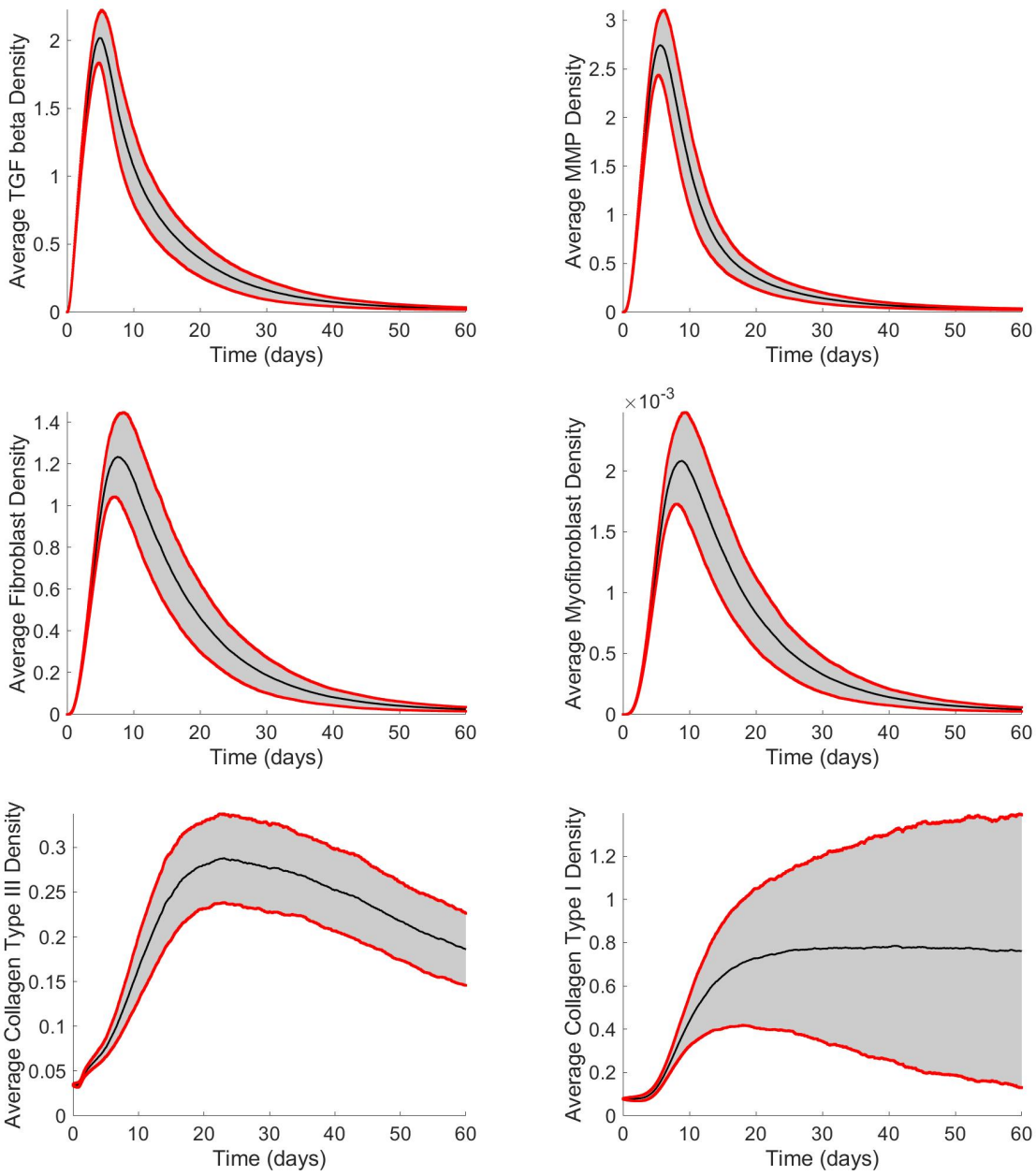

Figure 6.11: Mean and standard deviation of N=1000 simulations of the proliferation and remodeling variables when $\sigma = 0.1$

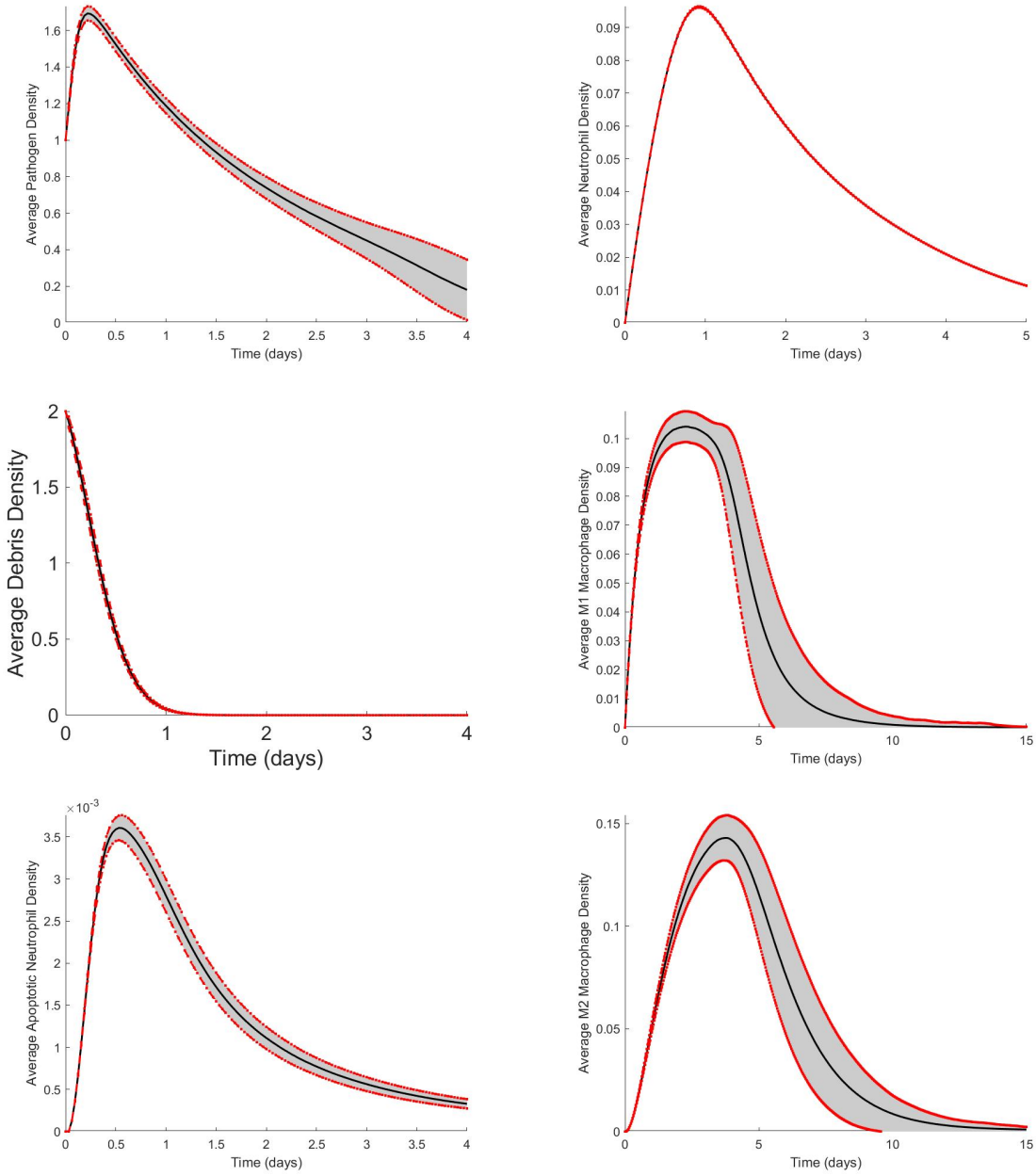

Figure 6.12: Mean and standard deviation of N=5000 simulations of the inflammation variables when $\sigma = 0.1$

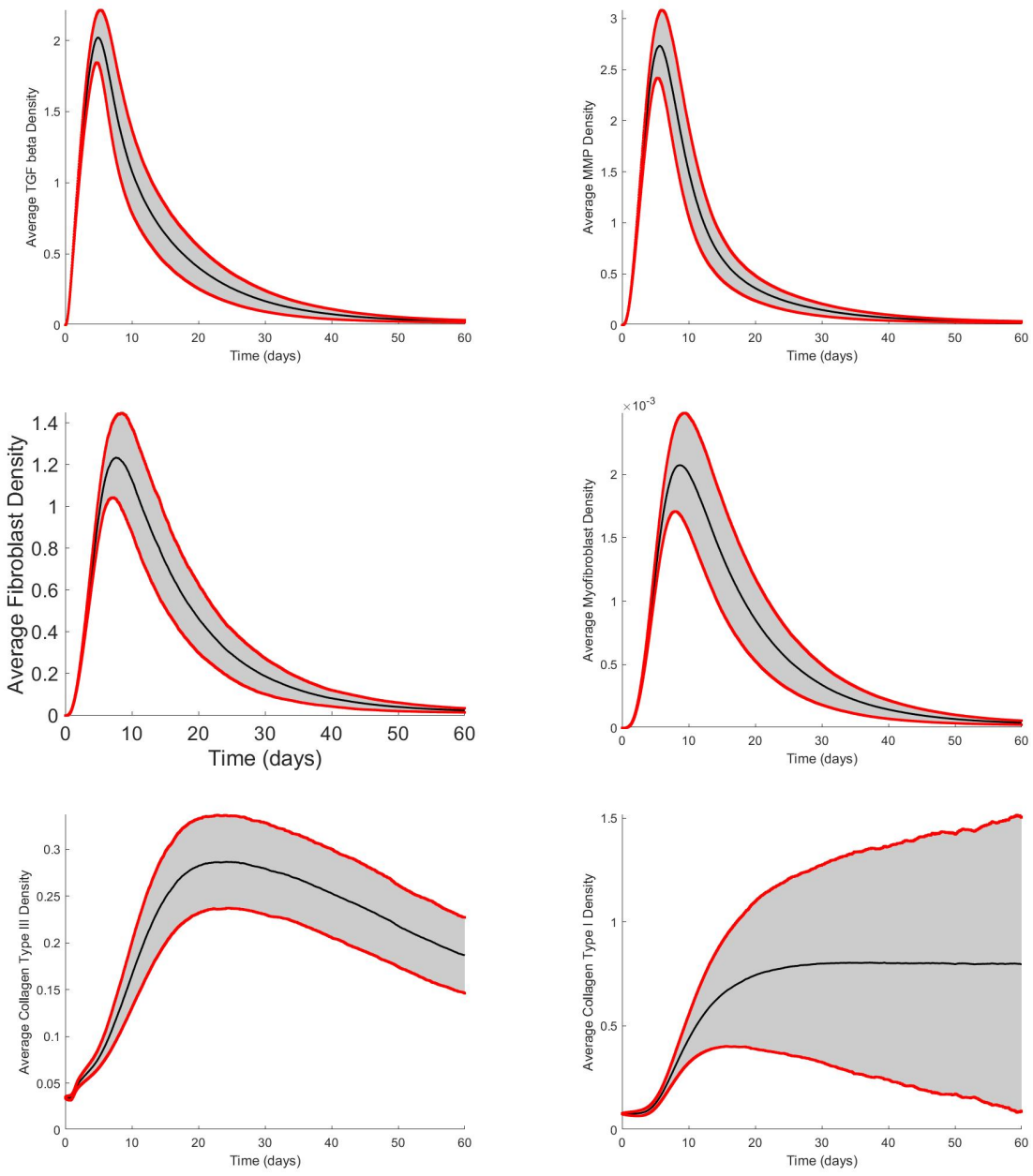

Figure 6.13: Mean and standard deviation of N=5000 simulations of the proliferation and remodeling variables when $\sigma = 0.1$

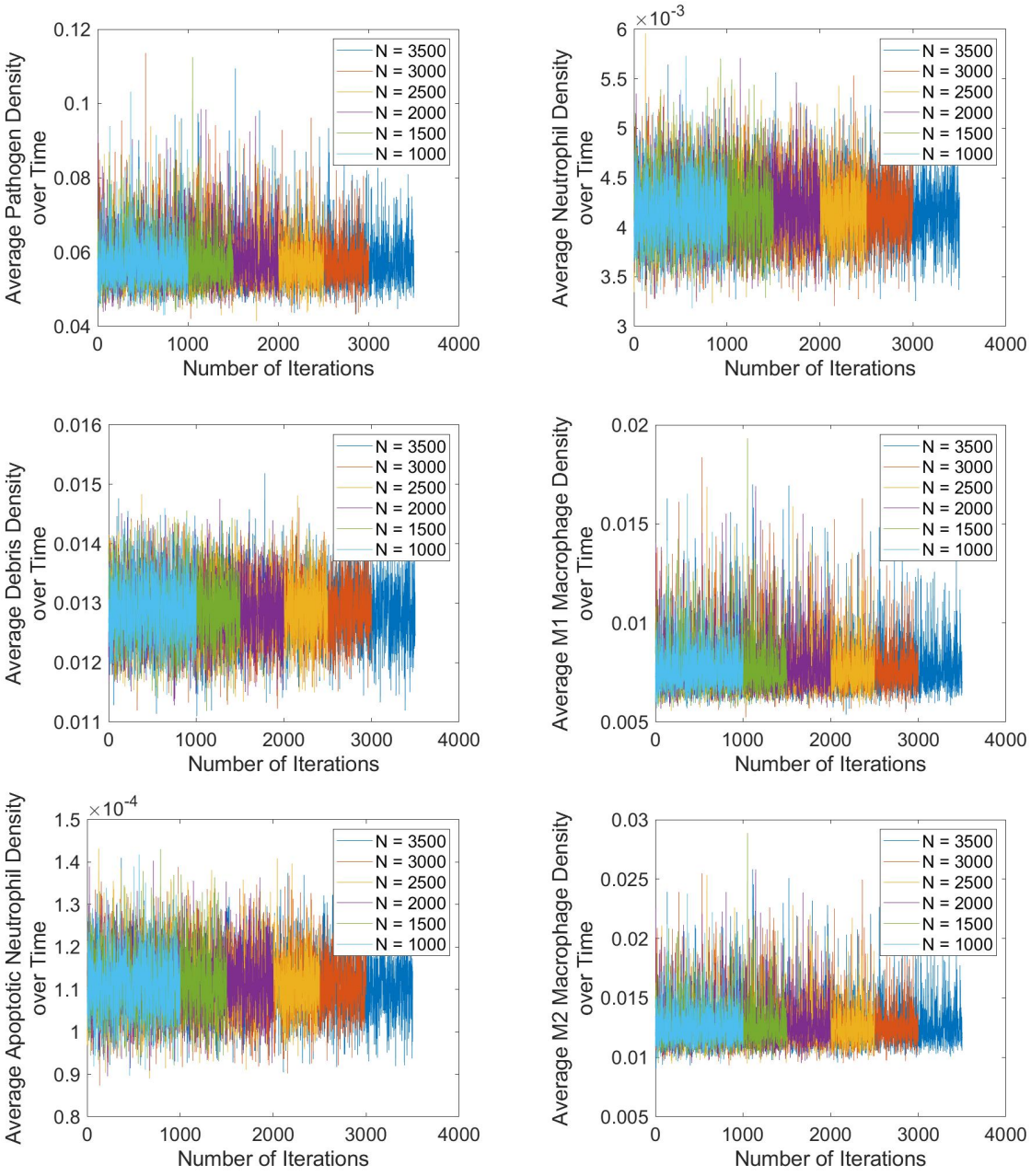

Figure 6.14: Mean of each state variable over time for different number of iterations when $\sigma = 0.1$

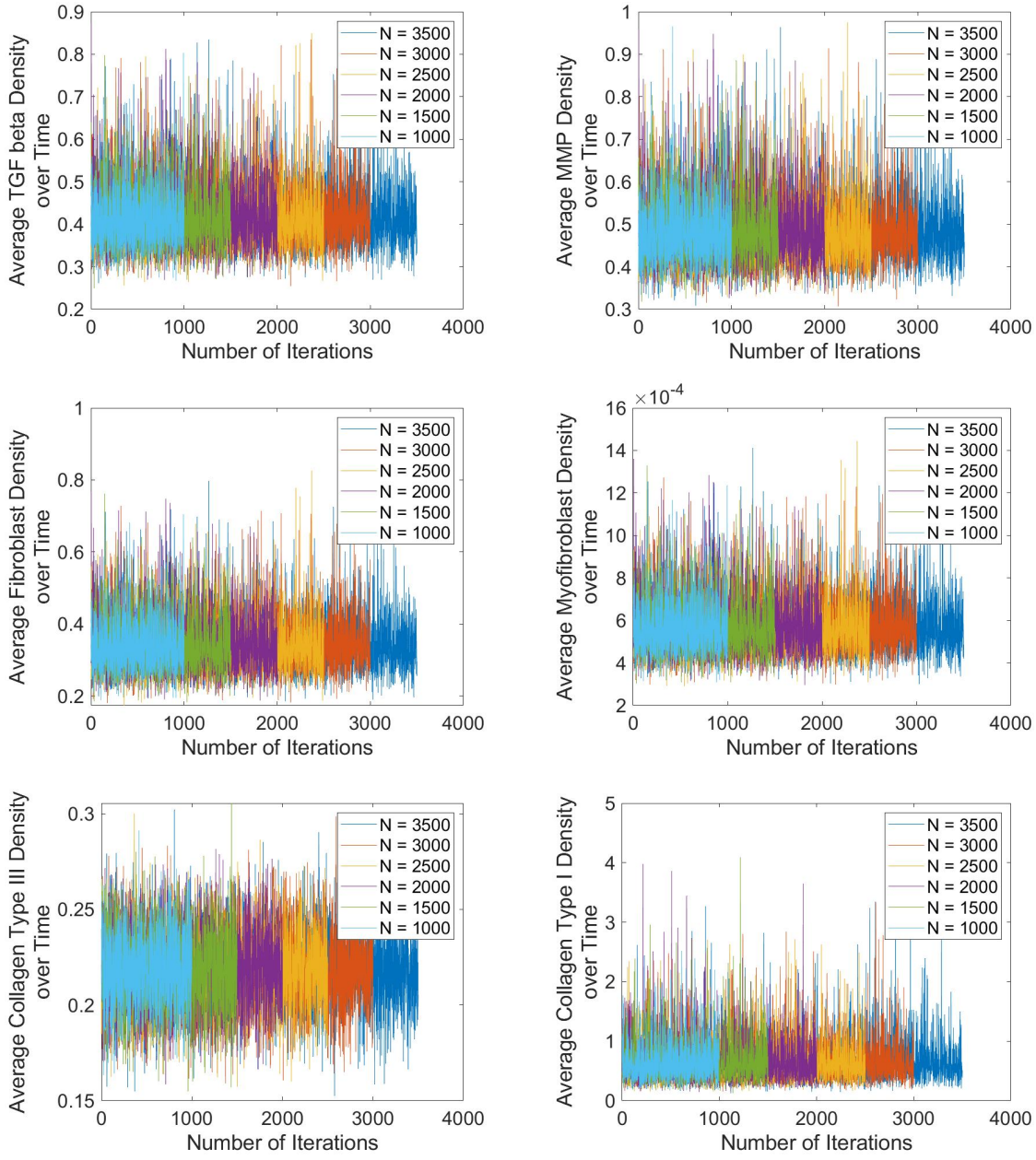

Figure 6.15: Mean of each state variable over time for different number of iterations when $\sigma = 0.1$

CHAPTER 7

DISCUSSION

7.1 Model Construction and Parameter Estimates

There were some elements that were in Cooper et al. [9] and Torres et al. [70] that were not incorporated into this model. For example, the assumption that neutrophils inhibit phagocytation by the increase of oxygen in the environment. Some factors may be noted regarding this assumption. Neutrophils release reactive oxygen species, but also require oxygen intake from the environment [16]. In addition, after a wound occurs, due to the obstruction of blood vessels, the means to distribute oxygen to the tissue is not reconstituted until the process of angiogenesis is finished [27].

There is literature to suggest that neutrophils contribute to the inhibition of healing. Dovi et al. [15] found that the presence of neutrophils in mice on days 2 and 3 had an effect on re-epitheliatiozation. The effect of neutrophil presence on collagen content was tested for day 3 and day 5. The effect on collagen content were not found to be statistically significant. For this model where neutrophil by-products inhibiting collagen deposition was considered, the effect was smaller than the other factors taken into account, that is $d_{cn} = 0.001$, which supports that the inhibition effects from neutrophils on collagen may not be a mechanism that causes as high of collagen degradation as other factors (e.g., degradation by MMPs) though according to the FAST indices found, relative to other parameters, a change in this parameter can result in a significant change in the resulting total collagen density.

Another outcome in proliferation model was that $k_{MmpM1} = 0.001 < k_{MmpM2} = 9.505$ which suggests that M1 macrophages do not secrete as many MMPs as M2 macrophages. This outcome corroborates research by Jager et al. [31]. In this study the expression of MMPs from different macrophages subtypes. In this *in vitro* experiment they found that M2 macrophages had higher expression of MMP-1, MMP-9, MMP-12 than the expressions found in M1 macrophages.

7.2 Sensitivity Analysis

Parameters corresponding to the largest sensitivity indices are the ones that need to be measured with more care. These parameters are indicated to have more influence on the output. Accordingly, it would be expected that treatments that target these parameters would be the most effective.

Due to the high parameter space, the cumulative computation time was considerable. Under other sensitivity analysis methods such as VBSA we would expect the same group of parameters being associated with high sensitivity indices, but the order of parameters with regard to which results in the higher sensitivity index might change.

Overall, according to the FAST method, for the first 15 days the source of monocytes were determined to be one of the parameters associated with high sensitivity indices for all six state variables in the inflammation model. This is corroborated when doing the sensitivity analysis again with respect to the average density of all six state variables (Figure 4.33).

To summarize, according to the FAST GSA method the parameters associated with higher sensitivity in regards to pathogens for the first 15 days of wound healing are:

1. growth rate of monocytes, 2. phagocytation rate of pathogens by macrophages, 3. growth rate of pathogens, 4. the source of background local response, and 5. destruction of pathogens by neutrophils. Taken under consideration of estrogen parameters, some of parameters that were indicated to result in relatively high sensitive output are 1. the estrogen increase in the phagocytic ability of macrophages and 2. estrogen concentration.

The parameters associated with higher sensitivity in regards to debris for the first 15 days of wound healing are: 1. source of monocytes, 2. apoptotic rate of neutrophils, 3. exit rate of neutrophils that resulted in addition to debris, 4. destruction of debris by neutrophils, and 5. intrinsic decay of apoptotic neutrophils not adding to debris. Taken under consideration of estrogen parameters, some of parameters that were indicated to result in relatively high sensitive output are 1. estrogen concentration, 2. estrogen increase in the phagocytic abilities of neutrophils, and 3. estrogen increase in the phagocytic ability of macrophages.

For apoptotic neutrophils we have 1. source of monocytes, 2. source of resting neutrophils, 3. apoptotic rate of neutrophils, 4. intrinsic decay of apoptotic neutrophils, and 5. destruction of apoptotic neutrophils by neutrophils. With regards to estrogen we have 1. estrogen concentration and 2. estrogen increase in the phagocytic ability of macrophages.

For neutrophils we have 1. exit rate of monocytes, 2. source of monocytes, 3. apoptotic rate of neutrophils, 4. intrinsic decay of apoptotic neutrophils, and 5. growth rate of resting neutrophils. With regards to estrogen we have 1. estrogen concentration and 2. estrogen increase in the phagocytic ability of neutrophils.

For M1 macrophages we have 1. exit rate of M1 macrophages, 2. source of monocytes, 3. exit rate of monocytes, 4. exit rate of M2 macrophages, and 5. transition rate between M1 macrophages to M2 macrophages With regards to estrogen we have 1. estrogen concentration and 2. estrogen's effect of he inhibition off M1 macrophages production by other M1 macrophages

For M2 macrophages we have 1. exit rate of M2 macrophages, 2. source of monocytes, 3.transition from M2 Macrophages to M1 macrophages, 4. exit rate of monocytes, and 5. exit rate of M1 macrophages. In regard to estrogen we have 1. estrogen concentration and 2. estrogen's effect of he inhibition off M1 macrophages production by other M1 macrophages.

For total collagen we have 1. kmmpn (production of MMPs by neutrophils) 2. kpg (growth rate of pathogens) 3. ummp (decay rate of MMPs) 4. dcn (destruction of type III collagen by byproducts of neutrophils), and 5. sb (source of background immune response). In regard to estrogen, we have kem (estrogen increase in the phagocytic abilities of macrophages).

In comparison to the local sensitivity analysis conducted in Torres et al [70] we see that source of monocytes were determined to be associated with a higher sensitivity indice when considering the change in the peak (i.e., amplitude and peak time) of M1 macrophages and when considering the M2 macrophage peak time (see smr in Figure 7.1). Overall, for the Torres model, snr was the parameter associated with the highest sensitivity calculations for all three criteria for M1 macrophages. In contrast, the FAST index for snr was not that high (Figure 4.28), though this parameter was determined to be one of the relatively more sensitive parameters in regard to neutrophil output, apoptotic neutrophil output, and the average output.

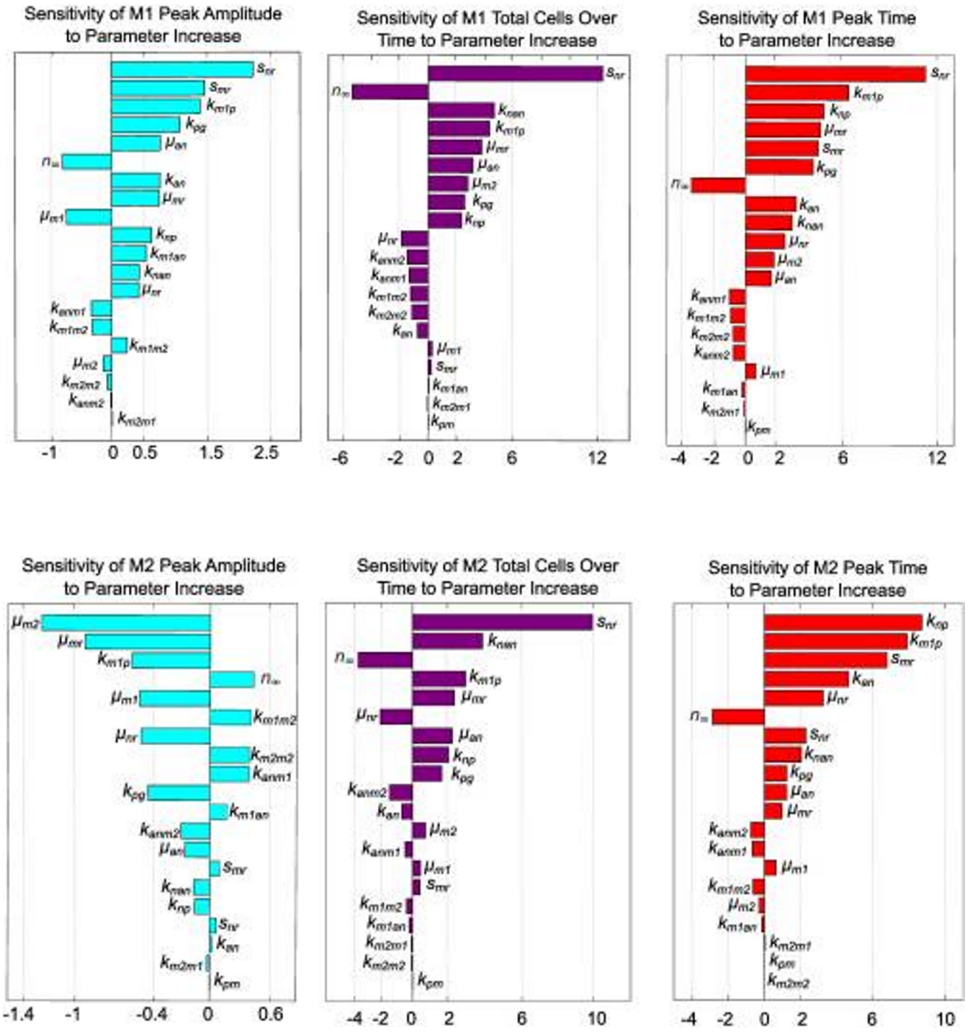

Figure 7.1: Local sensitivity analysis conducted in Torres et al [70]

7.3 Future Work

Karavitis and Kovacs [36] discuss effects of environmental pollutants, ethanol consumption, and cigarette smoking on macrophages phagocytosis and efferocytosis. Futher expansion of this model could include incorporating ethanol or pollutants such as ozone. Such applications may be of interest in investigating etiologies of health factors for certain occupations or certain groups of people.

Phagocytic ability of macrophages can be altered by factors including exposure to environmental pollutants, cigarette smoke, consumption of alcohol, cigarettes [36], and current medical conditions such as HIV [1]. Hence, depending on the mechanistic pathway that results in decrease phagocytic ability, certain rates of phagocytic ability would be decreased, and the dynamic change in this state would be important to elucidate.

Models can capture multifaceted elements that control outcomes, but these models are a tool that apply results based on current knowledge. As the experimental literature on these topics expand, the more accurate these scientific models will be as the assumptions are updated. Moreover, the use of the model is dependent on the specifications the model was built upon.

Model analysis is important in analyzing the behavior under a set of specified assumptions and circumstances. Sensitivity analysis is useful for identifying which factors are important. These findings can be used to help factor in consideration for experimental design. For example, the analyses of this model supports that the influx of monocytes when compared to other factors have a high sensitivity to the different dynamics of inflammation stage. Experimental investigations of changes in the expected inflammation output may consider monocyte recruitment. Models are

supplemental in providing a means to elucidate outcomes and effects and can help build integrity in the experimental literature where unavoidable limitations such as those in *in vivo* vs *in vitro*, animal vs human research, and also the consideration that immune response from a wound in a controlled environment may not be the same as in a specimen that is exposed to different environments.

REFERENCES

[1] Kentaro Akata, Janice M Leung, Kei Yamasaki, Fernando S Leitao Filho, Julia Yang, Chen Xi Yang, Hiroto Takiguchi, Tawimas Shaipanich, Basak Sahin, Beth A Whalen, Cheng Wei Tony Yang, Don D Sin, and Stephan F van Eeden. Altered Polarization and Impaired Phagocytic Activity of Lung Macrophages in People With Human Immunodeficiency Virus and Chronic Obstructive Pulmonary Disease. *The Journal of Infectious Diseases*, 225(5):862–867, March 2022.

[2] Bruce Alberts, Alexander Johnson, Julian Lewis, Martin C. Raff, Keith Roberts, and Peter Walter. Fibroblasts and Their Transformations: The Connective-Tissue Cell Family. 2002.

[3] Amiram Ariel and Charles Serhan. New Lives Given by Cell Death: Macrophage Differentiation Following Their Encounter with Apoptotic Leukocytes during the Resolution of Inflammation. *Frontiers in immunology*, 3:4, January 2012.

[4] Shahzad Ather, K.G. Harding, and S.J. Tate. 1 - Wound management and dressings. In S. Rajendran, editor, *Advanced Textiles for Wound Care (Second Edition)*, pages 1–22. Woodhead Publishing, January 2019.

[5] Jennifer Baum and Heather S Duffy. Fibroblasts and Myofibroblasts: What Are We Talking About? *Journal of Cardiovascular Pharmacology*, 57(4), 2011.

[6] Donna L. Bratton and Peter M. Henson. Neutrophil clearance: when the party is over, clean-up begins. *Trends in Immunology*, 32(8):350–357, August 2011.

[7] Hua Chen, Shimpei Kasagi, Cheryl Chia, Dunfang Zhang, Eric tu, Ruiqing Wu, Peter Zanvit, Nathan Goldberg, Wenwen Jin, and WanJun Chen. Extracellular Vesicles from Apoptotic Cells Promote TGF Production in Macrophages and Suppress Experimental Colitis. *Scientific Reports*, 9, April 2019.

[8] Christina Cobbold and J.a Sherratt. Mathematical Modelling of Nitric Oxide Activity in Wound Healing can explain Keloid and Hypertrophic Scarring. *Journal of theoretical biology*, 204:257–88, June 2000.

[9] Racheal L Cooper, Rebecca A Segal, Robert F Diegelmann, and Angela M Reynolds. Modeling the effects of systemic mediators on the inflammatory phase of wound healing. *Journal of theoretical biology*, 367, February 2015. Place: London : Publisher: Academic Press.

[10] MF Cordeiro, SS Bhattacharya, GS Schultz, and PT Khaw. TGF-beta 1, -beta 2, and -beta 3 in vitro: Biphasic effects on Tenon's fibroblast contraction, proliferation, and migration. *INVESTIGATIVE OPHTHALMOLOGY & VISUAL SCIENCE*, 41(3):756–763, March 2000.

[11] Michael Czubryt. Common threads in cardiac fibrosis, infarct scar formation, and wound healing. *Fibrogenesis & tissue repair*, 5:19, November 2012.

[12] Evan Davison-Kotler, William S. Marshall, and Elena García-Gareta. Sources of Collagen for Biomaterials in Skin Wound Healing. *Bioengineering*, 6(3), 2019.

[13] de Oliveira Fulco Tatiana, Andrade Priscila Ribeiro, de Mattos Barbosa Mayara Garcia, Pinto Thiago Gomes Toledo, Ferreira Paula Fernandez, Ferreira Helen, da Costa Nery José Augusto, Real Suzana Côrte, Borges Valéria Matos, Moraes Milton Ozório, Sarno Euzenir Nunes, Sampaio Elizabeth Pereira, Pin-

heiro Roberta Olmo, and Flynn J. L. Effect of Apoptotic Cell Recognition on Macrophage Polarization and Mycobacterial Persistence. *Infection and Immunity*, 82(9):3968–3978, September 2014. Publisher: American Society for Microbiology.

[14] Amanda Doran, Arif Yurdagul, and Ira Tabas. Efferocytosis in health and disease. *Nature Reviews Immunology*, 20:1–14, December 2019.

[15] J. Dovi, Li-Ke He, and L. DiPietro. Accelerated wound closure in neutrophi[U+FFFD] depleted mice. *Journal of Leukocyte Biology*, 73, 2003.

[16] Julia V. Dovi, Anna M. Szpaderska, and Luisa A. DiPietro. Neutrophil function in the healing wound: adding insult to injury? *Thrombosis and haemostasis*, 92 2:275–80, 2004.

[17] Paul Elkington, Justin Green, and Jon Friedland. Analysis of Matrix Metalloproteinase Secretion by Macrophages. *Methods in molecular biology (Clifton, N.J.)*, 531:253–65, February 2009.

[18] Nikolaos G. Frangogiannis. Transforming growth factor– in tissue fibrosis. *Journal of Experimental Medicine*, 217(3):e20190103, February 2020.

[19] Carolina García-de Alba, Carina Becerril, Víctor Ruiz, Yolanda González, Silvia Reyes, Jorge García-Alvarez, Moisés Selman, and Annie Pardo. Expression of matrix metalloproteases by fibrocytes: possible role in migration and homing. *Am J Respir Crit Care Med*, 182(9):1144–1152, November 2010.

[20] Luciana R. Gomes, Letícia F. Terra, Rosângela AM Wailemann, Leticia Labriola, and Mari C. Sogayar. TGF-1 modulates the homeostasis between MMPs and

MMP inhibitors through p38 MAPK and ERK1/2 in highly invasive breast cancer cells. *BMC Cancer*, 12(1):26, January 2012.

[21] Mallary C. Greenlee-Wacker. Clearance of apoptotic neutrophils and resolution of inflammation. *Immunological Reviews*, 273(1):357–370, September 2016. Publisher: John Wiley & Sons, Ltd.

[22] Gary R. Grotendorst, Georgeann Smale, and Dobromir Pencev. Production of transforming growth factor beta by human peripheral blood monocytes and neutrophils. *Journal of Cellular Physiology*, 140(2):396–402, August 1989. Publisher: John Wiley & Sons, Ltd.

[23] Elaine Hayes, Aikaterini Tsaousi, Karina Di Gregoli, S Jenkinson, Andrew Bond, Jason Johnson, Laura Bevan, Anita Thomas, and Andrew Newby. Classical and alternative activation and metalloproteinase expression occurs in foam cell macrophages in male and female ApoE null mice in the absence of T- and B-lymphocytes. *Frontiers in Immunology*, 5, 2014.

[24] Beate Heissig, Chiemi Nishida, Yoshihiko Tashiro, Yayoi Sato, Makoto Ishihara, Makiko Ohki, Ismael Gritli, Jeanette Rosenkvist, and Koichi Hattori. Role of neutrophil-derived matrix metalloproteinase-9 in tissue regeneration. *Histology and histopathology*, 25 6:765–70, 2010.

[25] Andrés Hidalgo, Edwin R. Chilvers, Charlotte Summers, and Leo Koenderman. The Neutrophil Life Cycle. *Special Issue: New Advances in Neutrophil Immunity*, 40(7):584–597, July 2019.

[26] Desmond Higham. An Algorithmic Introduction to Numerical Simulation of Stochastic Differential Equations. *SIAM Review*, 43:525–546, September 2001.

[27] Wan Hong, Michael Hu, Mikaela Esquivel, Grace Liang, Robert Rennert, Adrian McArdle, Kevin Paik, Dominik Duscher, Geoffrey Gurtner, H Lorenz, and Michael Longaker. The Role of Hypoxia-Inducible Factor in Wound Healing. *Advances in wound care*, 3:390–399, May 2014.

[28] Eric Howard, Beverly Crider, Dawn Updike, Elizabeth Bullen, Eileen Parks, Carol Haaksma, David Sherry, and James Tomasek. MMP-2 expression by fibroblasts is suppressed by the myofibroblast phenotype. *Experimental cell research*, 318:1542–53, March 2012.

[29] Min Huang, Sherven Sharma, Li Zhu, Michael Keane, Jie Luo, Ling Zhang, Marie Burdick, Ying Lin, Mariam Dohadwala, Brian Gardner, Raj Batra, Robert Strieter, and Steven Dubinett. IL-7 inhibits fibroblast TGF- production and signaling in pulmonary fibrosis. *The Journal of clinical investigation*, 109:931–7, May 2002.

[30] Mai-Lan Huynh, Valerie Fadok, and Peter Henson. Phosphatidylserine-dependent ingestion of apoptotic cells promotes TGF-1 secretion and the resolution of inflammation. *Journal of Clinical Investigation*, 109:41–50, January 2002.

[31] Nynke Jager, Bastiaan Vries, Jan-Luuk Hillebrands, Niels Harlaar, Rene Tio, Riemer Slart, Gooitzen Dam, Hendrikus Boersma, and Clark Zeebregts. Distribution of Matrix Metalloproteinases in Human Atherosclerotic Carotid Plaques and Their Production by Smooth Muscle Cells and Macrophage Subsets. *Molecular imaging and biology : MIB : the official publication of the Academy of Molecular Imaging*, 18, September 2015.

[32] Bergin Philip James, Wen Sicheng, Pan-Hammarström Qiang, and Quiding-Järbrink Marianne. Secretion of matrix metalloproteinase-9 by macrophages, in vitro, in response to Helicobacter pylori. *FEMS Immunology & Medical Microbiology*, 45(2):159–169, August 2005.

[33] Charles. Janeway. *Immunobiology : The immune system in health and disease*. Garland Pub., New York, 2001.

[34] Yufang Jin, Hai-Chao Han, J. Berger, Qiuxia Dai, and M. Lindsey. Combining experimental and mathematical modeling to reveal mechanisms of macrophage-dependent left ventricular remodeling. *BMC Systems Biology*, 5:60 – 60, 2010.

[35] Yoshiteru Kajikawa, Toru Morihara, Hirotaka Sakamoto, Ken-ichi Matsuda, Yasushi Oshima, Atsuhiko Yoshida, Masateru Nagae, Yuji Arai, Mitsuhiro Kawata, and Toshikazu Kubo. Platelet-rich plasma enhances the initial mobilization of circulation-derived cells for tendon healing. *Journal of Cellular Physiology*, 215(3):837–845, June 2008. Publisher: John Wiley & Sons, Ltd.

[36] John Karavitis and E. Kovacs. Macrophage phagocytosis: Effects of environmental pollutants, alcohol, cigarette smoke, and other external factors. *Journal of leukocyte biology*, 90:1065–78, August 2011.

[37] Sang Yong Kim and Meera Nair. Macrophages in wound healing: activation and plasticity. *Immunology and Cell Biology*, 97, February 2019.

[38] Yoko Kojima, Irving L. Weissman, and Nicholas J. Leeper. The Role of Efferocytosis in Atherosclerosis. *Circulation*, 135(5):476–489, January 2017. Publisher: American Heart Association.

[39] Ioannis Kourtzelis, George Hajishengallis, and Triantafyllos Chavakis. Phagocytosis of Apoptotic Cells in Resolution of Inflammation. *Frontiers in Immunology*, 11, March 2020.

[40] Paulina Krzyszczyk, Rene Schloss, Andre Palmer, and François Berthiaume. The Role of Macrophages in Acute and Chronic Wound Healing and Interventions to Promote Pro-wound Healing Phenotypes. *Frontiers in physiology*, 9(Journal Article):419–419, 2018. Place: Switzerland Publisher: Frontiers Research Foundation.

[41] Tomohiro Kurihara, Ryoko Shimizu-Hirota, Masayuki Shimoda, Takeshi Adachi, Hideyuki Shimizu, Stephen J. Weiss, Hiroshi Itoh, Shingo Hori, Naoki Aikawa, and Yasunori Okada. Neutrophil-Derived Matrix Metalloproteinase 9 Triggers Acute Aortic Dissection. *Circulation*, 126(25):3070–3080, December 2012. Publisher: American Heart Association.

[42] Hee-Jin Kwak, Myung-Jin Park, Hyeyoung Cho, Chang-Min Park, Sang-Ik Moon, Hyung-Chan Lee, In-Chul Park, Mi-Suk Kim, Chang Hun Rhee, and Seok-Il Hong. Transforming Growth Factor-1 Induces Tissue Inhibitor of Metalloproteinase-1 Expression via Activation of Extracellular Signal-Regulated Kinase and Sp1 in Human Fibrosarcoma Cells. *Molecular Cancer Research*, 4(3):209–220, March 2006.

[43] Hyo-Bum Kwak. Aging, exercise, and extracellular matrix in the heart. *Journal of exercise rehabilitation*, 9:338–347, June 2013.

[44] Suvi-Katri Leivonen, Konstantinos Lazaridis, Julie Decock, Andrew Chantry, Dylan Edwards, and Veli-Matti Kähäri. TGF–Elicited Induction of Tissue

Inhibitor of Metalloproteinases (TIMP)-3 Expression in Fibroblasts Involves Complex Interplay between Smad3, p38, and ERK1/2. *PloS one*, 8:e57474, February 2013.

[45] Erel Levine and Terence Hwa. Stochastic fluctuations in metabolic pathways. *Proceedings of the National Academy of Sciences of the United States of America*, 104:9224–9, June 2007.

[46] Diana Lindner, Christin Zietsch, P. Moritz Becher, Karsten Schulze, Heinz-Peter Schultheiss, Carsten Tschöpe, and Dirk Westermann. Differential Expression of Matrix Metalloproteases in Human Fibroblasts with Different Origins. *Biochemistry Research International*, 2012:875742, March 2012. Publisher: Hindawi Publishing Corporation.

[47] Chunfeng Ma and Nasser Chegini. Regulation of matrix metalloproteinases (MMPs) and their tissue inhibitors in human myometrial smooth muscle cells by TGF-1. *Molecular Human Reproduction*, 5(10):950–954, October 1999.

[48] Fernando Martinez and Siamon Gordon. Martinez, FO & Gordon, S. The M1 and M2 paradigm of macrophage activation: time for reassessment. F1000Prime Rep. 6, 13. *F1000prime reports*, 6:13, March 2014.

[49] Nayara Medeiros, Rafaelle Fares Gusmao, Eliza Franco, Giovane Sousa, Rafael Mattos, Ana Chaves, Maria Nunes, Walderez Dutra, Rodrigo Correa-Oliveira, and Manoel Rocha. Differential Expression of Matrix Metalloproteinases 2, 9 and Cytokines by Neutrophils and Monocytes in the Clinical Forms of Chagas Disease. *PLoS Neglected Tropical Diseases*, 11, January 2017.

[50] Nathan B. Menke, John W. Cain, Angela Reynolds, David M. Chan, Rebecca A. Segal, Tarynn M. Witten, Danail G. Bonchev, Robert F. Diegelmann, Kevin R. Ward, and Engineering Shock Center Virginia Commonwealth University Reanimation, The Wound Healing Group. An in silico approach to the analysis of acute wound healing. *Wound Repair and Regeneration*, 18(1):105–113, January 2010. Publisher: John Wiley & Sons, Ltd.

[51] David Mosser and Justin Edwards. Exploring the full spectrum of macrophage activation. *Nat Rev Immunol*, 18:958–969, January 2008.

[52] David M Mosser and Justin P Edwards. Exploring the full spectrum of macrophage activation. *Nature Reviews. Immunology*, 10(6):460, June 2010. Place: London Publisher: Nature Publishing Group.

[53] Kelly E. Murphy, Cameron L. Hall, Scott W. McCue, and D.L. Sean McElwain. A two-compartment mechanochemical model of the roles of transforming growth factor and tissue tension in dermal wound healing. *Journal of Theoretical Biology*, 272(1):145–159, March 2011.

[54] Natalia Nacu, Irina G Luzina, Kendrick Highsmith, Virginia Lockatell, Kerill Pochetuhen, Zachary A Cooper, Michael P Gillmeister, Nevins W Todd, and Sergei P Atamas. Macrophages produce TGF-beta-induced (beta-ig-h3) following ingestion of apoptotic cells and regulate MMP14 levels and collagen turnover in fibroblasts. *J Immunol*, 180(7):5036–5044, April 2008.

[55] Samuel R. Nussbaum, Marissa J. Carter, Caroline E. Fife, Joan DaVanzo, Randall Haught, Marcia Nusgart, and Donna Cartwright. An Economic Evaluation of the

Impact, Cost, and Medicare Policy Implications of Chronic Nonhealing Wounds. *Value in Health*, 21(1):27–32, January 2018. Publisher: Elsevier.

[56] Adrian F Ochsenbein and Rolf M Zinkernagel. Natural antibodies and complement link innate and acquired immunity. *Immunology Today*, 21(12):624–630, December 2000.

[57] Matthias Pauschinger, Andrea Doerner, Andrew Remppis, Roman Tannhäuser, Uwe Kühl, and Heinz-Peter Schultheiss. Differential myocardial abundance of collagen type I and type III mRNA in dilated cardiomyopathy: effects of myocardial inflammation. *Cardiovascular Research*, 37(1):123–129, January 1998.

[58] Janesh Pillay, Ineke den Braber, Nienke Vrisekoop, Lydia M. Kwast, Rob J. de Boer, José A. M. Borghans, Kiki Tesselaar, and Leo Koenderman. In vivo labeling with 2H2O reveals a human neutrophil lifespan of 5.4 days. *Blood*, 116(4):625–627, July 2010.

[59] A E Postlethwaite, J Keski-Oja, H L Moses, and A H Kang. Stimulation of the chemotactic migration of human fibroblasts by transforming growth factor beta. *Journal of Experimental Medicine*, 165(1):251–256, January 1987.

[60] Periathamby Antony Raj and Andrew R Dentino. Current status of defensins and their role in innate and adaptive immunity. *FEMS Microbiology Letters*, 206(1):9–18, January 2002.

[61] Angela Reynolds, Jonathan Rubin, Gilles Clermont, Judy Day, Yoram Vodovotz, and G Bard Ermentrout. A reduced mathematical model of the acute inflamma-

tory response: I. Derivation of model and analysis of anti-inflammation. *Journal of theoretical biology*, 242(1):220–236, September 2006.

[62] Elke Roeb. Matrix metalloproteinases and liver fibrosis (translational aspects). *SI : Fibrosis – Mechanisms and Translational Aspects*, 68-69:463–473, August 2018.

[63] Juan F. Santibanez, Hristina Obradović, Tamara Kukolj, and Jelena Krstić. Transforming growth factor-, matrix metalloproteinases, and urokinase-type plasminogen activator interaction in the cancer epithelial to mesenchymal transition. *Developmental Dynamics*, 247(3):382–395, March 2018. Publisher: John Wiley & Sons, Ltd.

[64] Matthias A. Scharenberg, Benjamin E. Pippenger, Ragna Sack, Dominik Zingg, Jacqueline Ferralli, Susanne Schenk, Ivan Martin, and Ruth Chiquet-Ehrismann. TGF–induced differentiation into myofibroblasts involves specific regulation of two MKL1 isoforms. *Journal of Cell Science*, 127(5):1079–1091, March 2014.

[65] T SCHREIER, E DEGEN, and W BASCHONG. FIBROBLAST MIGRATION AND PROLIFERATION DURING IN-VITRO WOUND-HEALING - A QUANTITATIVE COMPARISON BETWEEN VARIOUS GROWTH-FACTORS AND A LOW-MOLECULAR-WEIGHT BLOOD DIALYSATE USED IN THE CLINIC TO NORMALIZE IMPAIRED WOUND-HEALING. *RESEARCH IN EXPERIMENTAL MEDICINE*, 193(4):195–205, August 1993.

[66] Rebecca Segal, Robert Diegelmann, Kevin Ward, and Angela Reynolds. A Differential Equation Model of Collagen Accumulation in a Healing Wound. *Bulletin of mathematical biology*, 74:2165–82, July 2012.

[67] Jung-Won Shin, Soon-Hyo Kwon, Ji-Young Choi, Jung-Im Na, Chang-Hun Huh, Hye-Ryung Choi, and Kyung-Chan Park. Molecular Mechanisms of Dermal Aging and Antiaging Approaches. *International Journal of Molecular Sciences*, 20(9), 2019.

[68] Savita Singh and Michael Torzewski. Fibroblasts and Their Pathological Functions in the Fibrosis of Aortic Valve Sclerosis and Atherosclerosis. *Biomolecules*, 9(9), 2019.

[69] N. Strydom and S.M. Rankin. Regulation of Circulating Neutrophil Numbers under Homeostasis and in Disease. *Journal of Innate Immunity*, 5(4):304–314, 2013.

[70] Marcella Torres, Jing Wang, Paul J Yannie, Shobha Ghosh, Rebecca A Segal, and Angela M Reynolds. Identifying important parameters in the inflammatory process with a mathematical model of immune cell influx and macrophage polarization. *PLoS Computational Biology*, 15(7), July 2019. Place: San Francisco Publisher: Public Library of Science.

[71] Katarina Trajkovic, Clarissa Valdez, Daniel Ysselstein, and Dimitri Krainc. Fluctuations in cell density alter protein markers of multiple cellular compartments, confounding experimental outcomes. *PLOS ONE*, 14(2):e0211727, February 2019. Publisher: Public Library of Science.

[72] Alexandre Vallée and Yves Lecarpentier. TGF-[beta] in fibrosis by acting as a conductor for contractile properties of myofibroblasts. *Cell & Bioscience*, 9(1):NA, December 2019. NA.

[73] Sibylle von Vietinghoff and Klaus Ley. Homeostatic Regulation of Blood Neutrophil Counts. *The Journal of Immunology*, 181(8):5183–5188, 2008. Publisher: American Association of Immunologists _eprint: https://www.jimmunol.org/content/181/8/5183.full.pdf.

[74] Nicole L. Webster and Suzanne M. Crowe. Matrix metalloproteinases, their production by monocytes and macrophages and their potential role in HIV-related diseases. *Journal of Leukocyte Biology*, 80(5):1052–1066, November 2006. Publisher: John Wiley & Sons, Ltd.

[75] Traci A. Wilgus, Sashwati Roy, and Jodi C. McDaniel. Neutrophils and Wound Repair: Positive Actions and Negative Reactions. *Advances in Wound Care*, 2(7):379–388, September 2013. Publisher: Mary Ann Liebert, Inc., publishers.

[76] P. Wipff, Daniel Rifkin, Jean-Jacques Meister, and Boris Hinz. Myofibroblast contraction activates latent TGF-1 from the extracellular matrix. *The Journal of Cell Biology*, 179:1311 – 1323, 2007.

[77] Helen Wright, Robert Moots, Roger Bucknall, and Steven Edwards. Neutrophil function in inflammation and inflammatory diseases. *Rheumatology (Oxford, England)*, 49:1618–31, March 2010.

[78] Thomas A. Wynn and Kevin M. Vannella. Macrophages in Tissue Repair, Regeneration, and Fibrosis. *Immunity*, 44(3):450–462, March 2016.

[79] Yi Qun Xiao, Celio G. Freire-de Lima, William P. Schiemann, Donna L. Bratton, R. William Vandivier, and Peter M. Henson. Transcriptional and Translational Regulation of TGF- Production in Response to Apoptotic Cells. *The Journal of Immunology*, 181(5):3575, September 2008.

[80] Weipeng Xiong, S. Courtney Frasch, Stacey M. Thomas, Donna L. Bratton, and Peter M. Henson. Induction of TGF-1 Synthesis by Macrophages in Response to Apoptotic Cells Requires Activation of the Scavenger Receptor CD36. *PLOS ONE*, 8(8):e72772, August 2013. Publisher: Public Library of Science.

[81] Chonggang Xu and George Gertner. Understanding and comparisons of different sampling approaches for the Fourier Amplitudes Sensitivity Test (FAST). *Computational Statistics & Data Analysis*, 55:184–198, January 2011.

[82] T. Zhou, Z. Yang, Y. Chen, Y. Chen, Z. Huang, B. You, Y. Peng, and J. Chen. Estrogen Accelerates Cutaneous Wound Healing by Promoting Proliferation of Epidermal Keratinocytes via Erk/Akt Signaling Pathway. *Cellular Physiology and Biochemistry*, 38(3):959–968, 2016.

[83] Ltd Zouali. *Antibodies*. Major Reference Works. John Wiley & Sons Incorporated,, New York :, 1 edition, 2001. ISSN: 9780470016176 Publication Title: Encyclopedia of life sciences.

BIOGRAPHICAL STATEMENT

Amanda Patrick grew up in East Texas, and moved to Arlington, TX where she attended the University of Texas at Arlington for her undergraduate studies in mathematics and additional concentrations in criminal justice and biology. She completed Bachelor of Science in Mathematics with Honors and subsequently, she pursued a Master of Science in Forensic Science at Texas Tech University in 2018. She continued her graduate studies by pursuing her doctorate in Mathematics at the University of Texas at Arlington where she concentrated her research in mathematical applications in immunology and wound healing. Her research interests encompasses areas in mathematical topics such as dynamical systems, statistics, probability, and optimization.